

University of Nevada, Reno

**Using Fiber - Optic Distributed Temperature Sensing to Assess Soil
Temperature, Bulk Soil Thermal Properties, and Soil Moisture within
the Shallow Subsurface**

A thesis submitted in partial fulfillment of the
requirements for the degree of Master of Science in Hydrogeology

by

Lucas M. Williamson

Dr. Scott W. Tyler / Thesis Advisor

August, 2012



University of Nevada, Reno
Statewide • Worldwide

THE GRADUATE SCHOOL

We recommend that the thesis
prepared under our supervision by

LUCAS M. WILLIAMSON

entitled

**Using Fiber-Optic Distributed Temperature Sensing To Assess Soil Temperature,
Bulk Soil Thermal Properties, And Soil Moisture Within The Shallow Subsurface**

be accepted in partial fulfillment of the
requirements for the degree of

MASTER OF SCIENCE

Scott W. Tyler, Advisor

Christine E. Hatch, Committee Member

Wally W. Miller, Graduate School Representative

Marsha H. Read, Ph. D., Dean, Graduate School

August, 2012

Abstract

There currently exists a gap in the field scale measurement of many soil properties. Particularly, efficient measurement of soil moisture over the field scale at depths below the top few centimeters of the soil column has proven elusive. Distributed temperature sensing (DTS) allows for the nearly continuous measurement of temperature over both a spatial and temporal scale by use of standard fiber optic cables. Measurement of temperature progression throughout a soil column can lead to estimates of bulk soil thermal properties. Theoretically, these estimated thermal properties used in conjunction with determined soil characteristics can then provide soil moisture estimates. At an experimental field site in Smith Valley, three fiber optic cables were installed into the shallow subsurface in a vertical profile at depths of 5, 10, and 15 centimeters. Cables were placed within plots of various crop types and varying irrigation schedules. The effect of both surface crop type and irrigation on subsurface soil temperature is analyzed and presented. Through inversion of the conduction equation, spatial and temporal results of thermal diffusivity across the field are assessed. Thermal response of the soil changes in accordance with wetting due to irrigation, as well as subsequent drying up of the soil.

In terms of soil moisture, it continues to be difficult to accurately provide quantitative estimates, although drier soils provide much better estimates than do wet soils. Soil moisture estimates were in general agreement with observed values, but prior knowledge of the general wetness of the soil is necessary to improve the estimate. In a non-irrigated plot of tef (*eragrostis tef*), observed volumetric moisture values from the top 5 centimeters of soil ranged from $0.02 \text{ m}^3/\text{m}^3$ to $0.18 \text{ m}^3/\text{m}^3$, while the estimated soil moisture contents integrated over a depth of 5 to 15 centimeters stayed fairly consistent around $0.12 \text{ m}^3/\text{m}^3$ throughout the 25-day period. The effects of irrigation and cloudy conditions were clearly discernible, as were the relative differences between those plots receiving significant irrigation and those that remained drier throughout the study. The use of DTS in such an application can provide highly detailed pictures of temporally changing soil temperature, but progression to soil moisture estimation still remains challenging due to the non-uniqueness of the relation between soil thermal diffusivity and soil moisture content.

Acknowledgements

Funding of this project was provided by the Walker Basin Project, a comprehensive, research-based project sponsored by the University of Nevada, Reno Academy for the Environment and the Desert Research Institute. In addition, DTS instrumentation crucial to this study was provided by the Center for Transformative Environmental Monitoring Programs (CTEMPS).

Many people from various affiliations played a large role in this project, and without their time, effort, and ideas, much of this work would not have been possible. Jop Jansen, Philip Stive, Chris Sladek, Jazmin Aravena, Erin Carroll-Moore, Dr. Jim Trexler and Dr. John McCormack were invaluable for various components of this research.

Special thanks to Mark Hausner and Dr. Francisco Suarez for their assistance and patience throughout this entire project. Special thanks also to Dr. Christine Hatch, who was instrumental in the early stages of this project and provided guidance along the way. Also to Dr. Susan Steele-Dunne who was incredibly helpful and generous with both ideas and the use of her conduction model.

Finally, I would like to thank my committee members, Dr. Christine Hatch and Dr. Wally Miller, for support and help during this project. I'd especially like to thank my advisor, Dr. Scott Tyler, for his guidance and support every step of the way.

Table of Contents

Section 1. Introduction

Section 2. Soil Moisture Measurement Review

2.1. Soil Thermal Properties

2.2. Point Scale Measurements

2.3. Large Scale Measurements

2.4. COSMOS

Section 3. DTS Theory and Previous Studies

3.1. Theory

3.2. Previous Studies

Section 4. Problem Statement and Specific Objectives

4.1. Problem Statement and Project Goals

4.2. Specific Objectives

Section 5. Field Site Description

Section 6. Methods

6.1. Fieldwork

6.1.1. Plow Design

6.1.2. Cable Installation and DTS System Setup

6.1.3. Weather Stations

6.1.4. Core Samples

6.2. Laboratory Work

6.2.1. Bulk Density and Gravimetric Moisture Content

6.2.2. Organic Matter Content

6.2.3. Quartz Fraction

6.2.4. Thermal Conductivity – Soil Moisture Relationship

6.3. Modeling

6.3.1. Excel Finite Difference Mesh

6.3.2. MATLAB Diffusion Model

6.3.3. Soil Moisture Estimation

Section 7. Results

7.1. Field Work Results

7.2. Laboratory Results

7.2.1. Soil Core Results

7.2.2. Organic Matter Content Results

7.2.3. Quartz Content Results

7.2.4. Thermal Conductivity – Soil Moisture Relationship Results

7.3. Temperature Analysis

7.4. Modeling Results

7.4.1. Excel Finite Difference Mesh compared to Diffusion Model

7.4.2. Estimated Thermal Diffusivity

7.4.3. Estimated Soil Moisture

Section 8. Discussion

8.1. Temperature Analysis

8.1.1. Irrigation Effects

8.1.2. Crop Type Effects

8.2. Estimated Thermal Diffusivity Analysis

8.2.1. Estimated Thermal Diffusivity on Point Scale

8.2.2. Estimated Thermal Diffusivity on the Field Scale

8.3. Estimated Soil Moisture Analysis

8.3.1. Estimated Soil Moisture on Point Scale

8.3.2. Estimated Soil Moisture on the Field Scale

Section 9. Conclusions

9.1. Concluding Remarks and Recommendations

9.2. Future Study

Section 10. References

List of Tables

7.2.1a. Soil cores from August 10 th , 2010	74
7.2.1b. Soil cores from September 10 th , 2010	75
7.2.1c. Irrigation schedule	78
7.2.2. Organic matter content determination	80
7.2.3. Volume fraction of quartz determination	85
7.2.4. Measured thermal properties and moisture contents	90
7.3.1. Plot number descriptions	95
7.3.2. Irrigation schedule for September	104
8.1.2. Average crop heights	133
8.5.2. Moisture estimates using both sides of thermal diffusivity – soil moisture curve	158

List of Figures

2.1.1. Example thermal conductivity – soil moisture relationship	6
2.1.2. Example thermal diffusivity – soil moisture relationship	8
2.1.3. Temperature statistics from Mohanty <i>et al.</i> (1995)	12
3.1.1. Rayleigh, Brillouin, and Raman scattering	29
5.1.1. Aerial view showing location of 5C Cottonwood Ranch	38
6.1.1. Plow design	40
6.1.2a. Typical Kaiphone fiber optic cable	42
6.1.2b. Aerial photo of field site with cable path marked out	43
6.2.3a. Quartz soil thin section	51
6.2.3b. Blue component of quartz thin section	51
6.2.3c. Quartz crystals outlined in soil thin section	52
6.3.3. Example thermal diffusivity – soil moisture relationship	66
7.1.1. Air temperatures and net radiation recorded in the field	68
7.1.2. Soil moisture measurements from wireless meteorological stations	69
7.1.3. Raw temperature data from Oryx	72
7.2.1. Gravimetric moisture results compared to EC-5 moisture results	76
7.2.3. Quartz crystals outlined in soil thin section	84
7.2.4a. Campbell curve relating thermal conductivity to soil moisture	87
7.2.4b. Campbell curve relating thermal diffusivity to soil moisture	89
7.2.4c. Campbell curve compared to measured curve of thermal conductivity	91
7.2.4d. Campbell curve compared to measured curve of thermal diffusivity	91
7.3.1. Diurnal temperature signals at three depths	93
7.3.2. Daily maximum soil temperature at depth of 5 cm for each plot	97
7.3.3. Mean daily maxi soil temperature at depth of 5 cm for each crop type	98
7.3.4. Temperature difference between daily max and min at depth of 5 cm	101

7.3.5. Temperature difference between daily max and min at depth of 10 cm	102
7.3.6. Temperature difference between daily max and min at depth of 15 cm	103
7.4.1a. Thermal diffusivity results from Excel finite-difference mesh	106
7.4.1b. Diffusivity results of finite-difference mesh and conduction model	108
7.4.2a. Predicted versus observed temperatures in irrigated alfalfa plot	110
7.4.2b. Predicted versus observed temperatures in non-irrigated tefB plot	110
7.4.2c. Estimated thermal diffusivity in an alfalfa plot	111
7.4.2d. Estimated thermal diffusivity in an irrigated prairie sandreed plot	112
7.4.2e. Estimated thermal diffusivity in a non-irrigated tefB plot	112
7.4.2f. Thermal diffusivity results over space and time	114
7.4.3a. Campbell curve compared to measured curve of thermal diffusivity	115
7.4.3b. Campbell curve shifted to match measured curve	117
7.4.3c. Thermal diffusivity trend lines	118
7.4.3d. Estimated soil moisture results in irrigated alfalfa plot	120
7.4.3e. Moisture contents in irrigated prairie sandreed plot	121
7.4.3f. Moisture contents in irrigated tefB plot	121
7.4.3g. Soil moisture results over space and time	123
7.4.3h. Average soil moisture per plot	125
8.1.1a. Air temperatures and net radiation on September 8 th , 2010	127
8.1.1b. Soil temperatures and measured soil moistures in irrigated plot	129
8.1.1c. Soil temperatures and measured soil moistures in non-irrigated plot	130
8.1.2. Temperature and soil moisture data from Al-Kayssi <i>et al.</i> (1990)	136
8.2.1a. Diurnal temperature signals at three depths	141
8.2.1b. Estimated thermal diffusivity with 6 hour windows – non-irrigated	144
8.2.1c. Estimated thermal diffusivity with 6 hour windows – irrigated	144
8.2.1d. Estimated thermal diffusivity with 10 hour windows – non-irrigated	145

8.2.1e. Estimated thermal diffusivity with 10 hour windows – irrigated	146
8.3.1a. Estimated soil moisture in irrigated tefB plot	152
8.3.1b. Estimated soil moisture in irrigated basin wild rye plot	153
8.3.1c. Estimated soil moisture in non-irrigated basin wild rye plot	153
8.3.2a. Thermal diffusivity results over space and time	156
8.3.2b. Soil moisture results over space and time	157

SECTION 1. INTRODUCTION

Environmental sensing technology has seen rapid developments in the past few decades. In today's world, measurement and observation of hydrologic reservoirs and processes is becoming increasingly important, as access to and use of fresh water is growing more critical. This holds particularly true for arid, agricultural regions, as they generally require the most water use. It is not only important to simply monitor water use in these areas, but also to study the interactions between crops and all factors affecting their root zone and ultimate growth. Thus, environmental sensing in the shallow subsurface yields much potential towards maximizing effective crop growth while still minimizing the overuse of water in the form of irrigation.

Within the shallow subsurface, soil temperature, thermal properties, and soil moisture are all interrelated. It is difficult to study the occurrence and distribution of one property over time, without also studying the other two properties. In addition, the inherent heterogeneity in soil and temporal variance of soil moisture across a field requires an ability to measure such parameters on the small watershed scale. There are currently many methods to measure temperature and soil moisture on point scales, effectively measuring over a domain of only a few centimeters. At the other extreme, advancements have been achieved in remote sensing allowing for measurement of these properties over much larger scales, but at low spatial resolution and only measuring the top few centimeters of the ground surface. To most effectively study soil temperature,

thermal properties, and soil moisture within the subsurface, the currently existing field scale gap in measurement of these properties must be filled.

This study attempts to fill that gap in field scale soil measurement via the use of distributed temperature sensing technology (DTS). Three fiber optic cables were buried in the shallow subsurface under varying crop types and different irrigation regimes. Buried at depths of 5, 10, and 15 centimeters, the DTS system allows for temperature measurements every 5 minutes, over 1 meter spatial resolution at these various depths. This then allows for soil temperature to be assessed throughout the field, across various crop types. Knowledge of soil temperatures at various depths through time provides information necessary for thermal property estimation, namely thermal conductivity and thermal diffusivity. Specifically, thermal diffusivity in the soil can be estimated through inversion of the conduction equation. Using these thermal diffusivity estimates in conjunction with measured soil properties, soil moisture over time and space can be assessed.

SECTION 2. SOIL MOISTURE MEASUREMENT REVIEW

Although an important component to the global hydrologic cycle, soil moisture remains difficult to observe and quantify. The need to accurately predict soil moisture in the shallow subsurface is becoming more urgent throughout the world, as increasingly serious shortages of water continue to occur, especially in agricultural regions. These water issues make it imperative to improve efficiency of irrigation and other water use practices. To significantly improve water use efficiency, a thorough understanding including both the processes involving soil moisture as well as quantification of soil moisture within the vadose zone is necessary.

The recognition that accurate measurements of soil moisture are essential in environmental and agricultural fields is nothing new. Within the past several decades, numerous techniques have been developed to address the issue of obtaining robust, accurate measurements of soil moisture (Walker *et al.*, 2004; Robinson *et al.*, 2008; Evett and Parkin, 2005). Several of these techniques will be discussed in the following sections.

2.1 SOIL THERMAL PROPERTIES

Before discussing techniques used to measure soil moisture, it is first necessary to introduce and define soil thermal properties. The following discussion will include volumetric heat capacity C , thermal conductivity λ , and thermal diffusivity D , all of which are a function of several soil properties including soil moisture.

A soil's volumetric heat capacity C , is defined as the change of a unit volume's heat content per unit change in temperature (Hillel, 2004). In other words, the volumetric heat capacity defines the amount of heat that can be stored in the soil. It is generally presented in units of Joules per cubic meter per degree, or $\text{J m}^{-3} \text{K}^{-1}$. The volumetric heat capacity of soil can be calculated by adding the heat capacities of the individual soil constituents,

$$C_{soil} = X_a C_a + X_w C_w + \sum_{j=1}^N X_{sj} C_{sj}, \quad \text{Equation 2.1.1}$$

where X refers to volume fraction, C to volumetric heat capacity, and the subscripts a , w , and sj to air, water, and solid constituent j (out of a total of N different solid materials in the soil) (Jury and Horton, 2004). In addition, the volumetric heat capacity C of a pure substance is equal to density of that substance ρ multiplied by the specific heat c of that substance (Jury and Horton, 2004),

$$C = \rho c. \quad \text{Equation 2.1.2}$$

Specific heat c differs from volumetric heat capacity C in that it refers to heat capacity per unit mass of a pure substance, as opposed to the bulk volumetric heat capacity.

Thermal conductivity λ is defined as the quantity of heat transferred through a unit area of the conducting body in unit time under a unit temperature gradient (Hillel, 2004). Simply put, thermal conductivity provides a measure of how well a substance can conduct heat. Common units in which thermal conductivity is presented are watts per meter per degree, $\text{W m}^{-1} \text{K}^{-1}$. Much like volumetric heat capacity, soil thermal

conductivity depends on the volumetric proportions of various soil constituents, as well as size and arrangement of particles, and the physical contact between solids and liquids. Jury and Horton (2004) provide thermal conductivity values of quartz, water, organic matter and air as 8.5, 0.59, 0.25 and 0.026 $\text{W m}^{-1} \text{K}^{-1}$, respectively, a ratio of roughly 327:23:10:1. These huge differences in thermal conductivity illustrate the effect that connectivity between particles and air displacement by water has on the bulk thermal conductivity of a soil. Another value worth noting is the thermal conductivity of feldspar, which is roughly 1.67 $\text{W m}^{-1} \text{K}^{-1}$ (Jury and Horton, 2004). Feldspar is used here as a representative of other common minerals found in soil. It is clear that the conductivity of quartz is much greater than feldspar (and other common soil solids), and therefore the volume fraction of quartz in particular will greatly affect the bulk soil thermal conductivity. Explanation of this difference in thermal conductivity between quartz and other soil minerals lies in the chemical structure of each mineral. Silicates easily constitute the largest fraction of the earth's crust and mantle, and so most soil minerals are silicates of some form. This is the case for quartz and also for the example provided, feldspar. Quartz is the purest silica since it is composed of only silicon and oxygen, with a chemical formula of SiO_2 . Feldspar however, just like all silicates other than quartz, contains additional metal ions. Feldspar has a chemical formula of $\text{KAl}[\text{Si}_3\text{O}_8]$ (Horai and Simmons, 1969). Horai and Simmons (1969) explained that the covalent bonding between silicon and oxygen is much stronger than the bonds between other atoms within silicate crystals. Therefore, vibrational motions (heat energy) within the structure are transmitted most effectively through the silicon-oxygen connections. In

minerals other than quartz, metallic ions are found in the empty spaces of the silicon-oxygen network, and serve to effectively reduce the propagation of vibrational motions throughout the lattice. In other words, as the molecular makeup becomes more complicated, the thermal conductivity decreases (Horai and Simmons, 1969).

The relation between thermal conductivity and volumetric soil moisture is specific to each soil type at each location. The basic trend though is of an initial rapid increase of conductivity as water content begins to increase, followed by a much slower and steadier increase as the water content continues to increase towards saturation.

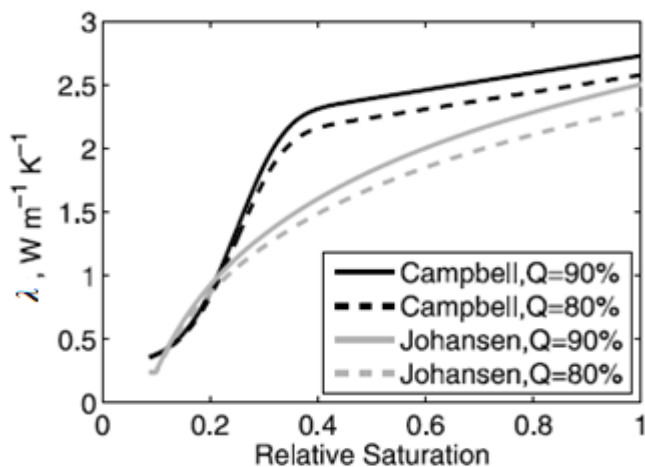


Figure 2.1.1. Basic relation between thermal conductivity and soil moisture for Campbell and Johansen models considering both 90 and 80 percent volume fraction of quartz (Steele-Dunne *et al.*, 2009).

When a soil is dry, there is minimal contact between the solid mineral grains. During this dry phase, air, which acts as a very poor thermal conductor, fills all pores and acts as the connecting medium between grains. Because of this, the bulk thermal conductivity is low. However, as soon as water is introduced to the system, the water

displaces air in the wedges immediately surrounding points of grain contact. This greatly increases the cross sectional area through which heat can be conducted. Not only does the addition of water increase the contact area, but it also displaces the poorly conducting air phase. This explains the rapid increase in thermal conductivity as soil moisture initially increases. As more water is added to the system, the films surrounding the solid particles become thicker, and the increase in conduction area is less drastic per unit of water added. Therefore, after the initial wetting period the thermal conductivity continues to increase, but at a much slower rate than when drier conditions persisted. There are many general relationships that have been developed between thermal conductivity and soil moisture. The various relationships are generally similar, but utilize slightly different soil properties. Several of the better known relationships are introduced in de Vries (1963), Campbell (1985), Chung and Horton (1987), and Johansen (1977). It is worth noting that these are basic relationships that were mostly derived empirically. Depending on needs, it is important to create a unique relation between soil thermal conductivity and volumetric water content for a soil of interest.

Thermal diffusivity is defined as the change in temperature produced in a unit volume by the quantity of heat flowing through the volume in unit time under a unit temperature gradient (Hillel, 2004). In a sense, thermal diffusivity can be thought of as a measure of thermal inertia. It is a measure of the rate at which a temperature disturbance at one point in the soil travels to another point. Therefore, its units are length squared per time, usually presented as $\text{m}^2 \text{sec}^{-1}$. Thermal diffusivity, thermal conductivity, and volumetric heat capacity are all very closely related:

$$D = \lambda / C, \quad \text{Equation 2.1.3}$$

where D is thermal diffusivity, λ is thermal conductivity, and C is volumetric heat capacity (Jury and Horton, 2004). In a soil with high thermal diffusivity, heat will move rapidly through the system because the bulk soil conducts heat quickly relative to the soil's volumetric heat capacity. Similar to thermal conductivity, the relationship between thermal diffusivity and soil moisture content is unique for each soil. However, the relationship always displays a common trend. Thermal diffusivity increases very rapidly with an initial increase in water content until a maximum is reached. At this point, thermal diffusivity decreases with further increases in water content.

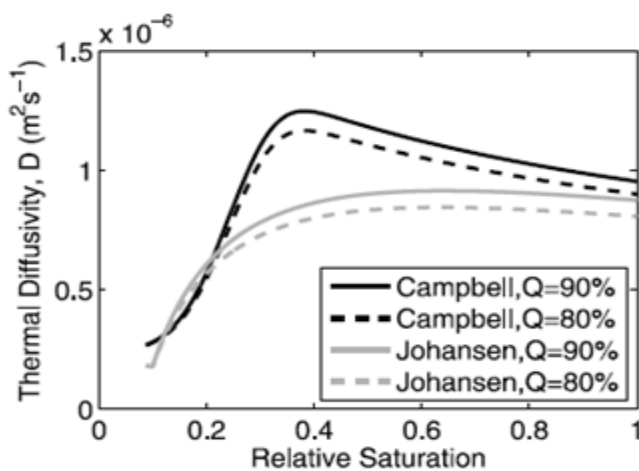


Figure 2.1.2. Basic relation between thermal diffusivity and soil moisture for Campbell and Johansen models considering both 90 and 80 percent volume fraction of quartz (Steele-Dunne *et al.*, 2009).

This pattern in the relation between thermal diffusivity and moisture content is explained by the ratio of thermal conductivity to volumetric heat capacity. Heat capacity rises linearly with water content, whereas thermal conductivity experiences its quickest

rise at low soil moisture contents (Jury and Horton, 2004). This results in a maximum in the curve between thermal diffusivity and soil moisture content.

When discussing thermal properties and heat transfer within soil, it is very important to mention the basic laws for both steady, homogeneous situations as well as unsteady, transient conditions. Of specific importance are the basic laws of conduction. The first law is commonly referred to as Fourier's Law, and simply states that in a homogeneous body under steady conditions, the heat flux is directly proportional to the temperature gradient and is in the direction of high to low temperature. Presented in its one-dimensional, vertical form:

$$q_z = -\lambda_z \frac{\partial T}{\partial z}, \quad \text{Equation 2.1.4}$$

where q_z is the heat flux in the vertical direction, λ_z is the thermal conductivity in the vertical direction, and dT/dz is the vertical temperature gradient (Hillel, 2004). However, in real-world soil conditions, temperature and many soil properties are dependent on time (i.e. under transient or unsteady conditions). Therefore, temperature changes in time need to be considered. In order to account for this time factor, the principle of energy conservation is used. This principle states that when considering an elemental volume without any internal sources or sinks of heat, the change in temperature with time must equal the change in heat flux with distance. Presented in one dimension:

$$C\left(\frac{\partial T}{\partial t}\right) = -\frac{\partial q_z}{\partial z}, \quad \text{Equation 2.1.5}$$

where C is volumetric heat capacity (Mills, 1999; Hillel, 2004).

By combining the previous two equations, the second law of heat conduction is derived:

$$C\left(\frac{\partial T}{\partial t}\right) = \lambda\left(\frac{\partial^2 T}{\partial z^2}\right). \quad \text{Equation 2.1.6}$$

When the above expression is expressed such that thermal diffusivity is the variable of interest, the equation is sometimes referred to as the thermal diffusion equation or the heat equation:

$$\frac{\partial T}{\partial t} = D(\theta) \frac{\partial^2 T}{\partial z^2} = \frac{\lambda(\theta)}{C(\theta)} \frac{\partial^2 T}{\partial z^2}, \quad \text{Equation 2.1.7}$$

where T is temperature, t is time, θ is volumetric moisture content, and z is depth (Behaegel *et al.*, 2007; Mills, 1999). When considering heat transfer in soil, thermal conduction and diffusion of heat are analogous. Since temperature is essentially a measure of the kinetic energy within a substance (i.e. heat energy), a temperature gradient will therefore cause heat exchange via collisions of molecules as they move from high to low temperatures. Just as diffusion results in movement towards equilibrium in composition within a mixture, conduction will also result in equilibrium of temperature within a substance (Hillel, 2004). From this point forward, heat conduction will be used to describe this phenomenon, and the above equation will be referred to as the conduction equation.

The previous conduction equation shows just how related all of the thermal properties are to each other, and how much they depend on soil moisture content. In

addition, it becomes apparent that soil temperature measurements can potentially be used to recover these soil parameters. Temperature serves as the basis for all thermal measurements, and as such, cannot be overlooked. Soil temperatures are dependent on many factors. When considering a particular location, key factors include net radiation at the surface, soil moisture content, soil texture, ground cover, and other surface weather conditions (Arya, 2001). Both soil moisture content and soil temperature are key factors affecting crop growth. Because of this fact, it is important to understand the variability of temperature both laterally and vertically within the shallow subsurface.

A study by Mohanty *et al.* (1995) looked at the spatio-temporal variability of soil temperature within three land areas exposed to different tillage systems. The goal of the research was to further the understanding of the spatial variations in soil temperature in plots that were exposed to various management practices. The management practices being investigated were three differing tillages: fall moldboard plowing followed by spring disking and planter operation (MP), fall chisel plowing followed by spring disking and planter operation (CP), and ridge tillage slot planting (RN) (Mohanty *et al.*, 1995). Different tillage practices result in differing degrees of surface disturbance and residue, which has a significant effect on both soil temperature and soil conductivity. Thermocouples were placed at 1 and 10 centimeter depths, forming a 7 meter by 7 meter grid in each of the three tillage plots, each consisting of 49 measurement sites. All plots were kept as bare soil, and temperature measurements were then analyzed over one diurnal cycle. Because the data were not collected concurrently across the plots, the data were analyzed for variability within the individual tillage system, rather than for

comparison between tillage systems (Mohanty *et al.*, 1995). For each plot, Mohanty *et al.* (1995) investigated basic statistics for the temperatures recorded at both the 1 centimeter and 10 centimeter depths.

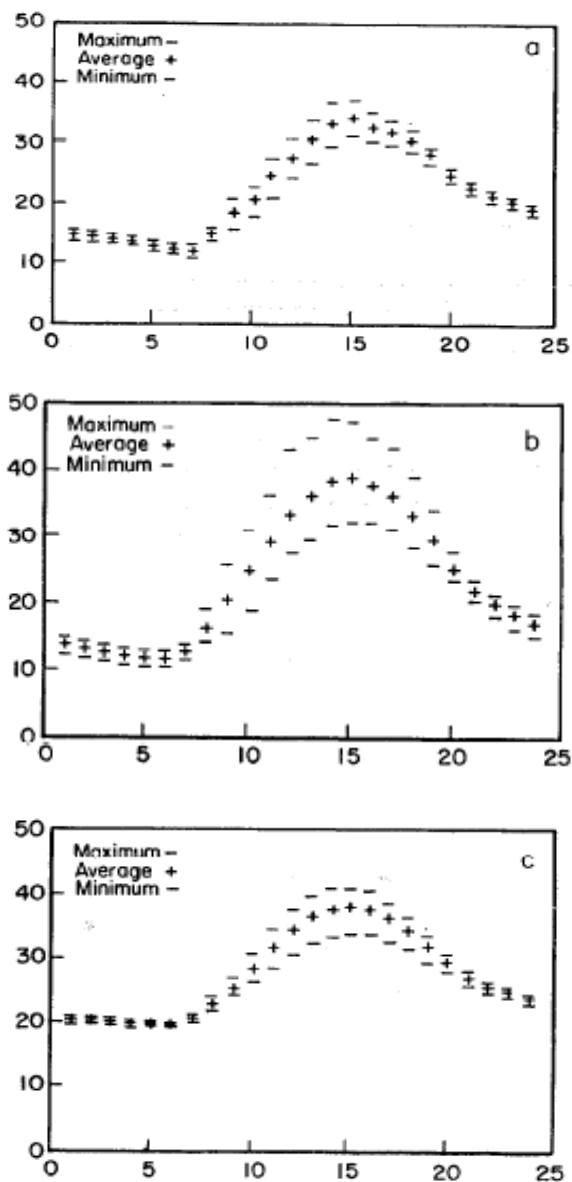


Figure 2.1.3. Mean and extreme hourly temperature values at 1-cm depth in each tillage type. Plot A is moldboard tillage, Plot B is chisel plow tillage, and Plot C is ridge till. X-axis is Time (Hours). Y-axis is Soil Temperature (°C). (Mohanty *et al.*, 1995)

The difference between the hourly extremes was very clearly time dependent. Measurements from early afternoon during the diurnal maximum showed the largest range in temperatures, while those recorded closer to diurnal minimums showed very little difference in extremes. Although this pattern was persistent across tillage systems, the degree to which the range showed temporal dependence varied for each tillage. For example, the CP plot experienced much larger variance in hourly temperature extremes than the other two tillage plots. Because of the tillage management, the CP plot had a more random distribution of surface residue cover than the other plots, implying that more of the thermocouples could have been affected by such cover (Mohanty *et al.*, 1995). It becomes apparent that varying surface features play a large role in soil temperature, even as shallow as 1 centimeter in depth. In an agricultural setting, surface vegetation should have the same effect as the surface residue mentioned here from tillage, except to a much larger degree.

2.2 POINT SCALE MEASUREMENTS

There are many soil moisture measurement techniques that measure a very small volume of soil. These are considered here as point scale measurements, because they provide no spatial resolution as standalone techniques. This section will discuss a few such techniques, as well as provide the necessary background on several soil thermal properties.

The standard gravimetric method for determining soil moisture content is still a widely used field method, even though many more sophisticated techniques have been developed. To perform this basic method, a soil core is physically taken from the site of interest, weighed in the lab, oven-dried at 105 °C for 24 hours, and then reweighed. Baking for 24 hours at 105 °C is sufficient to remove the inter-porous soil moisture within the sample, while still retaining the organic matter. Therefore, the difference in weight before and after oven-drying is the weight of water within the sample, generally then expressed as a percentage of the oven-dried weight of soil. S.G. Reynolds (1970) examines the gravimetric method in great detail, as well as relaying some of the potential sources of error with the technique. If bulk density of the soil is known, the gravimetric water content can easily be converted to volumetric water content in which soil moisture is calculated as a percentage of the total soil volume

$$\theta = w\rho_b / \rho_w. \quad \text{Equation 2.2.1}$$

θ is volumetric moisture content, w is gravimetric moisture content, ρ_b is soil bulk density and ρ_w is water density (Hillel, 2004). Presenting moisture content as a volumetric measurement is often much more intuitive, since at saturation the volumetric moisture content equals the soil porosity. The principle fault of this method is that physically removing cores from within the soil column is fairly time intensive and invasive. That being said, the gravimetric method for determining soil moisture content is commonly used as the comparison for other soil moisture measurement techniques. This method is by the far the most reliable of any measurement technique that is used, because it is the

only method to measure soil moisture content directly. The other techniques are all indirect methods, in which they measure some surrogate soil property that is then related to water content.

There are numerous other field methods developed for measuring soil moisture on the point scale. The neutron thermalization method takes advantage of the atomic makeup of a water molecule, and specifically, the small mass associated with hydrogen atoms. Neutrons carry no charge and are completely unaffected by electromagnetic fields. The only effect on the direction and speed of an emitted neutron is therefore a direct collision with the nucleus of an atom. Because the nucleus of a hydrogen atom is similar in size to a neutron, a direct collision between the two greatly reduces the neutron's energy, eventually thermalizing the neutron after several such collisions (Robinson *et al.*, 2008). The most common atoms in soil, aluminum, silicon and iron, scatter neutrons with very little energy loss because their respective masses are much larger than the neutron's mass. By utilizing a radioactive source of fast neutrons, as well as a detector of slow (thermalized) neutrons, an accurate estimate of soil moisture can be made. The high energy neutrons emitted from the source (about 1 trillion per second at an average energy of 5 megaelectron volts) are either slowed or absorbed by nuclei of atoms in the soil (Evelt, 2003). A small fraction of the emitted neutrons are scattered back to the sensor. Of the neutrons scattered back to the sensor, a smaller fraction are thermalized (average energy of about 0.025 electron volts) and therefore detectable. The count of detected, thermalized neutrons is then accurately related to moisture content through empirical calibration using independently measured water contents. The neutron thermalization

method is nondestructive, works at depths not easily attainable by other measurement methods, yields highly repeatable results and works well in rocky soils where other methods tend to fail (Evet, 2003). Although there are many apparent benefits to this technique, the main reason it has fallen out of favor is because of the inherent safety risks associated with the use of radiation.

Time-Domain Reflectometry, or TDR, is another point scale technique for measuring soil moisture in the field. TDR takes advantage of the dielectric properties of water within the soil matrix. A water molecule has a much higher dielectric constant, K_a , than other natural components of the soil. The dielectric constant of water is approximately 81, while the dielectric constant of air is 1, and is 3 to 5 for most soil grains (Ledieu, 1986). This high dielectric constant is due to the permanent dipole of each water molecule, caused by the separation of positive and negative charges due to the relative positions of the hydrogen and oxygen atoms (Robinson *et al.*, 2008). Ledieu (1986) states that the propagation velocity of an electromagnetic wave through the soil matrix is related to the proportions of the different components within the soil (i.e. air, soil grains, water, and organic matter) and each component's respective dielectric constant. Because the dielectric constant of water is so much greater than the other components, the velocity of an emitted electromagnetic wave is greatly increased and the presence of water can be easily observed and related to soil moisture content. The following equation shows how the velocity of the wave determines the dielectric constant:

$$K_a = (ct/2L)^2, \quad \text{Equation 2.2.2}$$

in which c is the speed of light in a vacuum, t is the travel time of the wave signal, and L is the length of the probe within the soil (Ren *et al.*, 2003). By using the widely-accepted empirical relationship between water content and the dielectric constant developed by Topp *et al.* (1980), moisture content can be calculated:

$$\theta = -5.3 \times 10^{-2} + (2.92 \times 10^{-2})K_a - (5.5 \times 10^{-4})K_a^2 + (4.3 \times 10^{-6})K_a^3 \quad \text{Equation 2.2.3}$$

TDR devices allow for the measurement of small but rapid changes in soil moisture content, and provide nondestructive and accurate measurements of soil moisture on the point scale (Greenwood *et al.*, 2009). It has been shown that measurement results using TDR are highly repeatable and that measurement is only slightly influenced by soil type and bulk density (Ledieu, 1986). Probe design and alignment are important considerations given that these are the variables that determine the sampling volume (Robinson *et al.*, 2003). It should be noted that semi-permanent TDR devices are commonly attached to dataloggers to provide a temporal scale to moisture measurements.

Heat pulse probes utilize heat transport to estimate soil thermal properties, and in turn can be used to indirectly estimate volumetric moisture contents. In general, a short duration heat pulse is induced in one sensor needle and the temperature response is then recorded by one or more additional thermistor needles (Robinson *et al.*, 2008). In effect, this technique measures the rate of heat dissipation through the soil medium. Most dual-probe, heat-pulse (DPHP) sensors consist of two needles, typically 3 cm long and 6 mm apart (Young *et al.*, 2008). The result is a very small volume of soil that is being measured. The heat pulse method to estimate soil thermal properties makes use of the

heat conduction equation, assuming the heat source is an infinite line and that the soil is homogeneous, isotropic, and initially at a uniform temperature. For a heat pulse of duration t_0 , the solution for the temperature change ΔT at distance r from the infinite line heat source is given by

$$\Delta T(r, t) = \frac{q'}{4\pi CD} \left[Ei\left(\frac{-r^2}{4D(t-t_0)}\right) - Ei\left(\frac{-r^2}{4Dt}\right) \right], \text{ for } t > t_0, \quad \text{Equation 2.2.4}$$

where q' is the energy input per unit length per unit time (W m^{-1}), C is volumetric heat capacity, D is thermal diffusivity, and Ei is the exponential integral function (de Vries, 1952; Mori *et al.*, 2003; Mori *et al.*, 2005; Young *et al.*, 2008). Once the volumetric heat capacity C is estimated, the volumetric moisture content can then be estimated.

$$\theta = (C - \rho_b c_s) / C_w, \quad \text{Equation 2.2.5}$$

where C is the soil's volumetric heat capacity, ρ_b is the soil bulk density, c_s is the soil specific heat, and C_w is the volumetric heat capacity of water (Knight *et al.*, 2007; Mori *et al.*, 2003; Young *et al.*, 2008). This assumes that the specific heat values of both the solid phase and water are available, and also that the specific heat of air can be ignored. A major issue for consideration surrounding the use of heat pulse probes for measuring water content is the temperature dependence of thermal properties. One such example found in Heitman *et al.* (2003) showed that a positive relationship between water contents and ambient temperatures existed. Therefore, there is a need to correct the measurements of heat pulse probes for changes in ambient temperature, especially in cases where temperature fluctuations close to the measurement volume are significant. Young *et al.*

(2008) should be referenced for descriptions of several methods to compensate for ambient temperature variations

By no means are the above mentioned point scale measurement tools all that exist or all that are employed. The previous techniques do, however, offer a reasonable summary of the different theory utilized to achieve soil moisture at one point in space.

2.3 LARGE SCALE MEASUREMENTS

Many soil moisture measurement techniques have been developed that provide a spatial resolution unachievable with point scale techniques. This section will include brief discussion of both geophysical and remote sensing methods.

Geophysical methods include ground penetrating radar, electromagnetic induction, direct current resistivity, and electrical resistivity tomography (ERT) (Bradford, 2008; Daily *et al.*, 1992; Kachanoski *et al.*, 1988; Kizito *et al.*, 2008; Michot *et al.*, 2003; Robinson *et al.*, 2008; Zhou *et al.*, 2001).

Ground penetrating radar (GPR) is similar to time domain reflectometry in that both take advantage of the high dielectric constant of water compared to the other soil constituents. Within the GPR frequency range (10 megahertz to 1 gigahertz) there exists a very strong relationship between dielectric permittivities and bulk water contents (Bradford, 2008; Michot *et al.*, 2003). Though there exist a variety of specific methods that can be used with ground penetrating radar, the basic principle is the same. A

transmission device emits electromagnetic waves that travel through a portion of the subsurface and are then received by some sort of reception antenna. Presented in a slightly different form than in equation 3.1.2, electromagnetic wave velocity is related to dielectric permittivity by the following:

$$v = c\sqrt{\varepsilon_0/\varepsilon} , \quad \text{Equation 2.3.1}$$

where v is the wave velocity, c is the speed of light in a vacuum, ε_0 is the permittivity of free space, and ε is the dielectric permittivity of the bulk material of interest (Bradford, 2008). The dielectric constant, K_a , found in section 3.1.1 is equal to $\varepsilon/\varepsilon_0$. By knowing the distance between the wave transmitter and the reception antenna, measurement of the travel time provides information about the permittivity of the subsurface materials. With calibration, this information can then be related to water content in the soil. A number of setups have been used when using ground penetrating radar to achieve estimates of soil moisture on spatial scales. Both the transmitter and receiver antennas can be positioned and moved around on the ground surface. Also, a crosshole system can be used, in which the antennas are placed into boreholes within the subsurface (Michot *et al.*, 2003; Robinson *et al.*, 2008). Ground penetrating radar provides a high resolution and non-invasive means to provide estimates of the variation in dielectric properties across the surface and subsurface. With calibration, this then provides estimates of the spatial distribution of soil moisture over those same spatial scales. A major disadvantage of the use of GPR to get at soil moisture is the amount of user knowledge that is required to accurately use and interpret the results. Also, this method encounters technical limitations

when used in saline or clay soils due to high bulk electrical conductivities (Robinson *et al.*, 2008).

Electromagnetic induction can be used as an indirect measure of soil moisture through the direct measurement of ground electrical conductivity. An energized transmitter creates magnetic field loops. These magnetic field loops produce electrical field loops, which in turn create a secondary magnetic field. Combined, the primary and secondary magnetic fields recorded in the receiver provide a measure of ground conductivity (Robinson *et al.*, 2008). By varying the instrumentation and distance between transmitter and receiver, the spacing of the initial magnetic field loops can be altered. Both an increase in the spacing of the loops and in the orientation of the loops result in greater depth of measurement (Kachanoski *et al.*, 1988; Robinson *et al.*, 2008). A relation between the bulk soil electrical conductivity and soil water content is as follows:

$$EC_A = a \theta^2 (EC_W) + b \theta (EC_W) + EC_C. \quad \text{Equation 2.3.2}$$

EC_A is the bulk soil electrical conductivity, EC_W is the electrical conductivity of the soil moisture solution, EC_C is the surface electrical conductivity of the solid phase, a and b are regression constants related to soil texture, and θ is again volumetric moisture content (Kachanoski *et al.*, 1988). According to Kachanoski *et al.* (1988), EC_C is related to the number of ions adsorbed on clay surfaces, and thus is dependent solely on the type and amount of clay in the soil. Generally, EC_A is used to estimate values of EC_W , which is a measure of soil salinity. When the study area of interest is under the same management

(i.e. the same cultivated field), it is assumed that soil texture is homogeneous and thus EC_W is dependent on soil water content (Kachanoski *et al.*, 1988; Robinson *et al.*, 2008; Scanlon *et al.*, 1999). It is therefore plausible to assume that spatial variations in measured bulk soil electrical conductivity, EC_A , can be used to determine spatial variations in soil water content. As with other geophysical methods, extensive training is required to not only set up and collect measurements, but also to effectively interpret the signal response for the desired result. Combining the efforts of electromagnetic induction with known point scale measurements could be used for more accurate estimates of the spatial distribution of soil water content.

Direct current resistivity and electrical resistivity tomography (ERT) are very similar methods. Direct current resistivity is usually defined as imaging from the ground surface, while electrical resistivity tomography refers to imaging conducted in boreholes (Robinson *et al.*, 2008). Both of these techniques utilize an array of electrodes including two or more source electrodes and two or more receiving electrodes. An electrical gradient is created between the source electrodes and the resultant potential distribution is measured at the various receiving electrodes. Many electrodes in various linear configurations can be measured in relatively short time periods, providing spatial data along transects (Michot *et al.*, 2003; Robinson *et al.*, 2008; Singha *et al.*, 2007; Zhou *et al.*, 2001). The resistivity measurements can then be used to infer information about various soil properties including soil texture, water chemistry, and soil moisture changes. The following equation shows a relation between soil moisture and the resistivity that would be measured using these techniques:

$$\rho = \rho_0 S^{-\beta}, \quad \text{Equation 2.3.3}$$

where

$$S = (\theta - \theta_r) / (\theta_s - \theta_r) \quad \text{Equation 2.3.4}$$

is the effective saturation (Zhou *et al.*, 2001). ρ is the resistivity of the porous medium ($\Omega \text{ m}$), ρ_0 is the resistivity of the porous medium when $S = 1$, β is a fitting parameter related to the properties of the porous medium, θ is the volumetric water content, θ_s is the saturated water content, and θ_r is the residual water content (Zhou *et al.*, 2001).

Resistivity imaging is possible at submeter to tens of meter scales in the field. However, it has been used mostly as a means to monitor qualitative changes in soil moisture (Robinson *et al.*, 2008). Because resistivity measurements have proven to be dependent on various soil properties and not just soil moisture, the amount of use seen by these techniques does not compare to the other geophysical methods previously described.

In addition to the use of geophysical methods to investigate soil moisture, advancements have been made in the measurement of soil moisture via remote sensing. There are three main remote sensing methods currently in use to measure soil moisture, each with its own advantages and disadvantages. The first method is passive remote sensing, in which the electromagnetic radiation naturally emitted by the site of interest is observed. Active remote sensing is the second technique, in which electromagnetic radiation is actively emitted onto the site of interest, and then the scatter is observed. The final remote sensing method observes changes in the gravity potential field. Changes in

the gravity potential field are related to changes in soil density, which in turn yields a measurement of soil moisture content (Robinson *et al.*, 2008).

Remotely sensed measurements of soil moisture content are conducted with instruments that are not in direct contact with the soil. Soil emits radiation, and the dielectric properties of the soil and the soil surface roughness determine how close the soil surface is to being a perfect emitter, or blackbody. The fraction of the total possible radiation that is emitted is called the emissivity of the soil, and varies between 0 and 1. In the longer wavelength portion of the electromagnetic spectrum, soil emissivity is a strong function of volumetric soil moisture content (Robinson *et al.*, 2008). The product of the soil temperature T , and emissivity e , is the brightness temperature T_B (Engman and Chauhan, 1995; Robinson *et al.*, 2008)

$$T_B = eT. \quad \text{Equation 2.3.5}$$

At microwave frequencies, the brightness temperature T_B is directly proportional to the emitted radiation power, which is directly measured by a radiometer (Robinson *et al.*, 2008). Therefore, T_B is easily determined through measurement. If the soil temperature is known, then the resulting quotient of brightness temperature to soil temperature provides soil emissivity estimates. Because emissivity is such a strong function of water content, this then provides an estimate of soil moisture.

Remote sensing can be conducted at various wavelengths of the electromagnetic spectrum. Depending on the result desired, either infrared or microwave radiometry can be used. When concerned with obtaining soil moisture estimates, the preferred

radiometry to use is that of microwave wavelengths. There are several key reasons why the use of larger wavelengths (i.e. microwave frequencies) is better suited for soil moisture estimation. Larger wavelengths decrease the attenuation caused by vegetation (Engman and Chauhan, 1995; Jackson, 1993). Vegetation is a key problem for remote sensing, as it can effectively mask the sensor from the soil. The use of shorter wavelengths that occur with visible or infrared sensing require additional vegetation information for correction and modeling purposes before soil moisture can be reliably observed. This is because as the wavelength decreases, scattering increases, providing more influence by vegetation structure (Jackson, 1993; Jackson *et al.*, 1996). Also, clouds and precipitation are effectively transparent at microwave frequencies, whereas infrared radiometers cannot view the soil surface through such obstacles (Engman and Chauhan, 1995; Robinson *et al.*, 2008). In addition to the above mentioned reasons, possibly the most critical reason why longer wavelengths are beneficial over shorter, infrared wavelengths is that the depth of the soil layer that contributes to the measured brightness temperature increases with wavelength (Engman and Chauhan, 1995; Jackson, 1993; Jackson *et al.*, 1996; Robinson *et al.*, 2008). At a frequency of 1.4 GHz (wavelength of 21 cm) the contributing soil layer is typically the upper 3 to 5 cm, while at 19 GHz (wavelength of 1.6 cm) the contributing soil layer to radiation is only the upper few millimeters (Robinson *et al.*, 2008). Spatial resolution using microwave frequencies varies depending upon whether originating from aircraft or satellite. Using radiometers mounted on aircraft, spatial resolution of soil moisture estimates can be on the scale of tens to hundreds of meters, but as mentioned earlier, only for the top 5 centimeters of

soil. Originating from satellite measurements, spatial resolution typically is on the order of tens of kilometers (Robinson *et al.*, 2008).

The above mentioned large scale measurement techniques for estimating soil moisture all provide a means to create some sort of spatial aspect to soil moisture observation. Although all techniques at least partially fill the gap in field scale measurement of soil moisture, each comes with its inherent problems. Geophysical methods require intensive training for both setup and accurate interpretation of results. In addition, although these methods provide more of a spatial aspect than point measurements, they do not necessarily provide an easy method to cover an entire field or small watershed scale. Remote sensing methods, on the other hand, provide very large spatial coverage of soil moisture estimation, but fine resolution cannot be achieved. In addition, remote sensing only provides a moisture estimate from within the top few centimeters of the land surface.

2.4 COSMOS

A very promising technique for measuring soil moisture on a small watershed scale also with a temporal aspect is with the measurement of ambient neutron fluxes above the soil surface (Desilets *et al.*, 2010). This method is very similar in theory to the previously discussed neutron thermalization method, except that it does not require an active emission of neutrons. Cosmic rays, which are mostly protons, collide with atmospheric nuclei resulting in the production of secondary neutrons. These secondary

neutrons can then penetrate to the earth's surface and collide with nuclei within the shallow subsurface (Zreda *et al.*, 2008). Within the soil, the intensity of these neutrons is controlled by the scattering and adsorption properties of the soil elements. Just as with neutron thermalization, the presence of hydrogen within the soil is the dominant factor contributing to the "slowing down" of the secondary neutrons (Zreda *et al.*, 2008). Therefore, the more soil moisture (and thus hydrogen) in the subsurface, the lower the ambient neutron flux above the surface. Because neutrons that are affected within the shallow subsurface diffuse back into the air, the neutron intensity above the surface is inversely correlated with soil moisture. This provides a non-invasive means for measurement of soil moisture over a spatial scale. A study described by Zreda *et al.* (2008) located southeast of Tucson, Arizona showed very strong agreement between the non-invasive cosmic-ray method for determining soil moisture and other methods such as TDR measurements and gravimetric analysis. Stations just like the one tested in the Tucson study are currently being installed throughout portions of the United States in an effort called COSMOS (Cosmic Ray Soil Moisture Observing System) (Desilets *et al.*, 2010).

The use of this COSMOS method shows great promise towards providing accurate soil moisture estimates on the field scale and at depths greater than that achievable by remote sensing methods. As the technology develops and application spreads to more areas, the use of measurement of ambient neutron fluxes above the soil surface to get at soil moisture could provide one solution to filling the field scale gap in soil moisture measurement.

SECTION 3. DTS THEORY and PREVIOUS STUDIES

It is evident that there exists a gap in scale at which soil moisture cannot be easily and accurately predicted. The small watershed scale ranging from 0.1 to 80 km² is implausible to measure with high resolution using point measurement techniques, and is not adequately assessed using remote sensing. Efforts have been made to fill this known gap in soil moisture measurement, and so far the technique of cosmic-ray neutron counting seems to show the most potential. The focus of this study is in filling the gap in our ability to measure soil moisture at these small watershed scales, utilizing the method of passive distributed temperature sensing (passive DTS).

3.1 THEORY

Distributed temperature sensing effectively transforms a standard fiber optic cable into a thermometer, capable of providing an average temperature measurement every meter for cables up to 5 kilometers in length and every 1.5 meters for cables up to 10 kilometers in length (Tyler *et al.*, 2009). Temporal resolution of the newest DTS devices can be as fine as 1 Hz (cycle per second), and is not limited in the other direction. To make a measurement, laser pulses are fired down the length of the fiber optic cable. The laser light gets scattered or backscattered along the cable's length due to imperfections within the glass fiber and interactions with the fiber's molecular structure. Most of the light that is backscattered to the source is elastic, and so returns at the same wavelength as the incident light. This elastic scattering is termed Rayleigh scattering (Tyler *et al.*,

2008). A small fraction of the laser energy experiences inelastic scattering (Raman and Brillouin). This inelastic scattering produces light at higher frequencies (anti-Stokes signal) and lower frequencies (Stokes signal) than the incident laser light initially transmitted. Figure 3.1.1 is a diagram illustrating the various scattering that takes place within fiber optic cables.

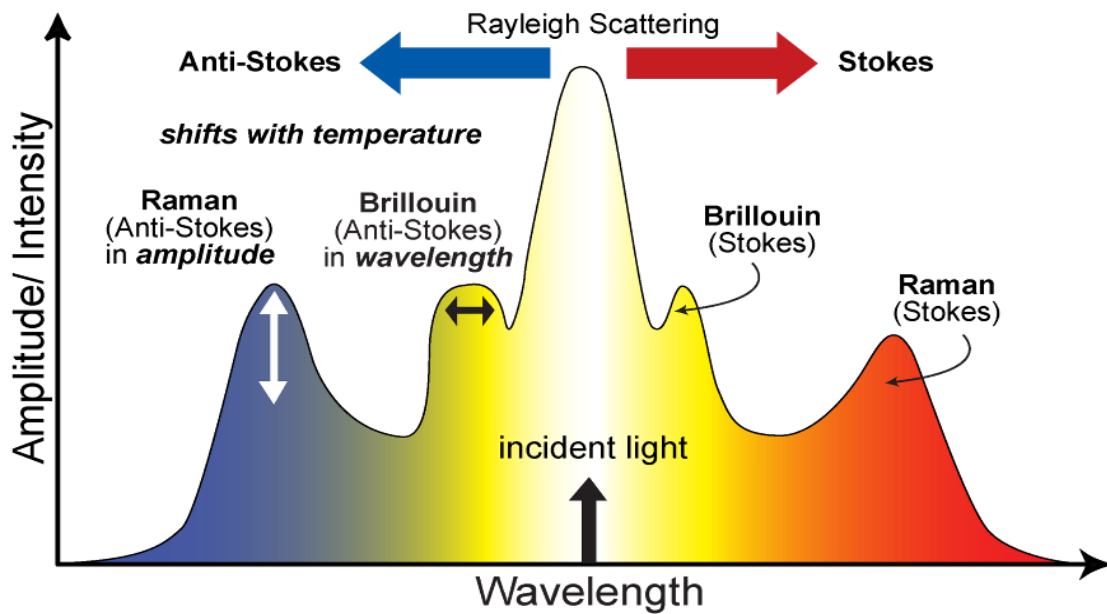


Figure 3.1.1. Diagram depicting Rayleigh, Brillouin, and Raman scattering and the relative wavelengths and amplitudes of each. Modified from Selker *et al.*, 2006.

As is evident in the above diagram, temperature affects the wavelength in Brillouin scattering but affects the amplitude in Raman scattering. The amplitude of the anti-Stokes signal is a function of both laser intensity and temperature at the point of reflection. In contrast, the amplitude of the Stokes signal is a function of the laser intensity alone.

Consequently, the ratio of anti-Stokes to Stokes yields a measure of the cable temperature.

It is now known how firing a laser pulse down a fiber optic cable provides temperature readings. However, it is not yet known how the location of each temperature reading is determined. In other words, from where along the cable does a certain temperature reading originate? This is determined via a time of flight approach. Because the scattered light returns to the detector at the speed of light, knowledge of the time between the emitted pulse and the returned signal provides the location of that reflected signal.

$$X = (0.5t) \frac{c}{n}, \quad \text{Equation 3.1.1}$$

where X is distance down the cable, t is the time between the emitted pulse and the returned signal, c is the speed of light in a vacuum, and n is the refractive index of the cable. In a typical fiber found in standard fiber optic cables, laser light travels approximately two meters in 10 nanoseconds. Therefore, during the first 10 nanoseconds after a pulse is emitted, all of the reflected signals that arrive back to the detector come from a maximum of one meter out on the cable (one meter out and then 1 meter reflected back to the DTS unit for two meters of total distance travelled). Signals returning between 10 and 20 nanoseconds after a pulse is fired will therefore provide an average temperature value over the second meter of cable, and so on. This enables temperature measurements to be made with one meter resolution on both a spatial and temporal scale.

3.2 PREVIOUS STUDIES

Fiber optic distributed temperature sensing (DTS) systems can provide high resolution temperature measurements over both a spatial and temporal scale at high temporal frequencies. This fact lends DTS to a variety of interesting and important environmental sensing applications. In the previous few years, numerous studies have been conducted that demonstrate several of the many potential applications of DTS technology in hydrologic settings (Hoes *et al.*, 2009; Robinson *et al.*, 2009; Roth *et al.*, 2010; Selker *et al.*, 2006; Tyler *et al.*, 2008; Tyler *et al.*, 2009; Westhoff *et al.*, 2007). All of these applications make use of temperature measurements at high temporal and spatial resolution by either using the temperature data as the final product, or by using temperature data as a surrogate to estimate a different variable of interest.

Of particular interest to this thesis are those studies that used distributed temperature sensing to investigate soil moisture. Studies have been conducted using both forms of distributed temperature sensing, active and passive. Sayde *et al.*, (2009) was able to effectively demonstrate that active DTS technology can be used to provide accurate and repeatable estimates of soil moisture in a laboratory setting. Active DTS involves providing a heat pulse into the surrounding soil and observing temperature change with time as recorded by fiber optic cables. The theory behind active measurements is very similar to the heat pulse method described previously in Section 2.1. Past studies involving active distributed temperature sensing determined that the method was only able to distinguish between wet, dry, and saturated soils with little

sensitivity to small changes in water content (Sayde *et al.*, 2009). By interpreting the data using a different approach than these previous studies used however, Sayde *et al.* (2009) was able to obtain volumetric moisture content measurements accurate to within about 10 percent of the actual moisture content. This was achieved with moisture contents ranging from 0.05 to 0.41 m³/m³. This accuracy is much higher than previously attained using active DTS technology, and also covers a much larger range of soil moisture values.

Whereas Sayde *et al.* (2009) demonstrated the potential for accurate soil moisture measurements with active distributed temperature sensing in a laboratory setting, this study will make use of passive DTS technology in a field setting. Unlike active DTS, passive DTS does not require an external source of power or an additional heating element. Instead, passive distributed temperature sensing uses fiber optic cables within the soil to measure the thermal response to the diel cycle. This fact makes it cheaper as well as logistically simpler to install a passive DTS system.

A recent study by Steele-Dunne *et al.* (2009) demonstrated the feasibility of estimating soil moisture on spatial scale using a passive DTS system. That study, located in Monster, the Netherlands, used two fiber optic cables buried in a vertical profile at mean depths of 7.85 and 9.98 centimeters. In order to attain soil moisture estimates from collected temperature measurements, the temperature data was used to estimate thermal diffusivity of the soil, via an implicit difference scheme solving the conduction equation (Steele-Dunne *et al.*, 2009). Two thermal diffusivity and conductivity models were then used and compared to determine soil moisture values based upon the solved diffusivity

values. Results of the study showed that passive DTS can indeed be used to detect changes in soil moisture. Changes in soil moisture created changes in soil thermal properties which were detectable from the temperature data collected by the fiber optic cables. However, in terms of accurately quantifying the soil moisture content along the length of the cables, there were still improvements to be made.

Previous work by Hausner (2010) represented an initial effort to reveal soil moisture using a passive DTS approach in Smith Valley, near Yerington, Nevada. The effort was located in an agricultural field adjacent to the plots used for this study. Hausner's (2010) experimental design consisted of one fiber optic cable buried at a depth of 15 centimeters. A portion of that single cable was left on the ground surface to provide the surface reference temperature. By analyzing the daily phase shifts and amplitudes in the temperature signal recorded at the ground surface and also by the buried cable, bulk soil thermal properties were estimated. These thermal properties were then used in an effort to estimate soil moisture. Results presented by Hausner (2010) revealed that an accurate estimate of soil moisture based on predicted thermal properties was unattainable. Potential reasons for the inability to estimate soil moisture accurately were discussed, as well as several recommendations for experimental improvement.

SECTION 4. PROBLEM STATEMENT and OBJECTIVES

The following section will provide the problem statement of this study. In addition, specific objectives towards achieving a successful study will be discussed.

4.1 PROBLEM STATEMENT and PROJECT GOALS

There is currently an abundance of methods used to measure soil moisture on point scales, with current emphasis being placed on the development of less disruptive, in situ sensors. Likewise, focus on the measurement of soil moisture at large, basin scales has also been evident, with emphasis being placed on remote sensing advancements. It is becoming more apparent that the remaining intermediate spatial scale is experiencing a lack in our ability to routinely monitor shallow subsurface water movement as well as the quantification of soil moisture. There currently exists no simple, proven method to measure these parameters on the field or subwatershed scale (1 to 80 square kilometers). Measurement of soil moisture on these scales is particularly important for closing water balances, understanding biogeochemical processes, and the further development of complete hydrologic models (Robinson *et al.*, 2009).

This study effectively has three overall project goals:

- 1.** Effectively use a passive DTS system to analyze the effect that both surface vegetation type and irrigation have on subsurface soil temperatures in an agricultural setting.

2. Using temperature data collected via passive DTS technology, estimate thermal properties on the field scale.

3. Using estimated thermal properties, accurately predict soil moisture on the field scale.

The inherent ability of DTS to provide temperature measurements at sub-meter spatial resolution and at sub-minute temporal resolution over several kilometers lends itself very well towards these applications.

4.2 SPECIFIC OBJECTIVES

The first part of this study is the analysis of subsurface temperatures under various crop types and under different irrigation schedules. Specific objectives required to achieve this analysis are as follows:

- 1) Successful installation of a fiber optic system with three cables positioned in a vertical profile in the shallow subsurface, then
- 2) Assess temperature signals for various crop types under the same irrigation schedule, and
- 3) Assess temperature signals for the same crop type under differing irrigation schedules.

The last two objectives of this research include using passive distributed temperature sensing to fill the field scale gap in both thermal property estimation and also in soil moisture measurement. In order to achieve these overall goals, several specific objectives need to be accomplished along the way. These specific objectives include

- 1) Obtain thermal diffusivity estimates originating from collected temperature data along the length of the cables,
- 2) Develop a relationship particular to the site of interest between thermal conductivity/thermal diffusivity and soil moisture content, and
- 3) Estimate soil moisture along the length of the cables based on the relationship to estimated soil thermal properties.

Further discussion on the methods utilized to actually achieve these objectives will be found in the Methods section of this thesis.

SECTION 5. FIELD SITE DESCRIPTION

This study takes place in Smith Valley, Nevada, at an experimental agricultural ranch within the Mason valley. Located along the lower reaches of the Walker River, the site is part of an ongoing effort towards developing alternative agricultural crops and land restoration while maximizing water use efficiency. This effort is part of the Walker Basin Project, a program developed in response to the declining water levels and subsequent increase in total dissolved solids in Walker Lake, one of only three desert terminus lakes in the United States that supports a fishery (Miller *et al.*, 2010). The overall objective of the project is to provide the hydrologic, agricultural, and economic data needed to best inform water acquisition decisions as well as future management practices within the basin.

The alternative agricultural site in Smith Valley that is being used for this study is the 5C Cottonwood Ranch. The 5C Ranch is comprised of two separate fields. The first, more southerly field, contains different vegetation types that have potential for land restoration activities. The second field slightly north of the first contains 135 plots (each plot being approximately 9.1 by 7.3 meters) of 14 different annual and perennial crops (Miller *et al.*, 2010). Of the 14 different crops being grown, 9 are crops with potential as biomass producers for biofuel technology, and the other 5 are alternative grains with potential for both animal feed and human consumption. It is in this second field that this study takes place. An aerial view of this site is provided in Figure 5.1.1.

Very important to this study are the soil characteristics of the field in which the fiber optic cables are buried. Within Project C of the Walker Report, titled “Plant, Soil, and Water Interactions” (Miller *et al.*, 2010), much of the recent work towards these soil characteristics has been recorded. A key characteristic to be taken from the project report for its role in determining the heat capacity of the soil is the particle size distribution. The 5C Cottonwood Ranch is located on a sandy textured Malpais Complex which is described as consisting of 79.7% sand, 16.9% silt, and 3.4% clay (Miller *et al.*, 2010). This fits into the distribution of a typical loamy sand.



Figure 5.1.1. Aerial view showing the location of the 5C Cottonwood Ranch. The red box outlines the field used. To the east is the Walker River and Nevada State Highway 339 is to the west (Googlemaps, 2012).

SECTION 6. METHODS

This section of the thesis will feature discussion on all of the steps that were taken towards achieving the overall goals of this study. Section 6 will be broken down into three subsections. The first subsection will discuss all of the fieldwork that was employed, the second subsection will discuss the lab work, and the final section will include the computer modeling that was used.

6.1 FIELDWORK

6.1.1 Plow Design

The original plow design used for this research was developed by a group of Dutch professors and students from the Delft University of Technology. They developed and constructed a tractor pulled plow, specifically intended to lay three fiber optic cables in a vertical profile in the shallow subsurface. This was completed in Delft and provided the basis for the previously mentioned work of Susan Steele-Dunne (Steele-Dunne *et al.*, 2009). Two of the students involved with the initial plow construction, Jop Jansen and Philip Stive, came to the University of Nevada, Reno and were able to recreate the plow. Several small adjustments were made to the original design to compensate for the dry, rocky soil characteristic of typical Nevada soils, and the final plow design is displayed in Figure 6.1.1.



Figure 6.1.1. The plow setup as used to install three cables into the shallow subsurface at the 5C Cottonwood Ranch. The ripper tooth (closest to tractor), cable deploying blade (middle), cement roller (farthest from tractor), and crossbeams to hold spools of cable (top) are shown.

The plow attaches to the back of a tractor, and consists of a sturdy steel frame with three cross bars at the top on which three spools of fiber optic cable can spin freely. The three cables are fed through three plastic guiding wheels and then down into a steel blade. The blade has three circular tubes inside, running from the top (where the cables enter) and then curving to the back side (where the cables leave). These tubes in the blade ensure that the cables are always the same distance apart in the ground. In front of the cable deploying blade is either a cutting disk or a ripper tooth, depending on the soils

encountered. The original design utilized the cutting disk to cut a slot in the soil with minimal disturbance. However, due to the abundant rocks at the 5C Ranch, a ripper tooth was used instead. The ripper tooth was used to push aside rocks and lift them to the surface. In reality, the ripper tooth moved only small rocks and then served as an indicator of larger rocks which were then removed by hand. This prevented the plow from riding up over rocks and affecting the depth of the installed cables. Both the ripper tooth and the cable deploying blade behind it are angled at 45 degrees and aligned together as they enter the soil. This ensures that the cables do not fall on top of one another and remain at the desired depths. In addition, the 45 degree angle also helps to ensure that there is soil entirely surrounding each cable, providing the best possible contact. Behind the blade is a cement filled roller used to push down any mounded soil. In such a position, the three cables were laid into the ground at approximate depths of 5, 10, and 15 centimeters.

6.1.2 Cable Installation and DTS System Setup

The particular fiber optic cable used in this installation was a loose tube 50/125 μm Kaiphone Mini Armored Fiber Optic Cable (Kaiphone, 2012). Immediately surrounding the fiber is a hydrophobic gel-filled capillary that protects the fiber from water exposure, as well as providing some physical protection. Water contacting the fiber itself can cause hydrogen contamination of the fiber, ultimately leading to light loss in the fiber (Tyler *et al.*, 2009). Surrounding the gel-filled capillary is metal tubing that is coiled down the length of the fiber. This metal tubing provides added strength and

protection for the fiber. Kevlar fibers surround this metal tubing to provide tensile strength, and metal braiding then surrounds both the metal tubing and Kevlar fibers. The metal braiding further protects against physical damage to the cable. A primarily PVC jacket then covers all of the inner components and serves as the first physical contact to the outside environment. Figure 6.1.2a depicts a typical Kaiphone cable.

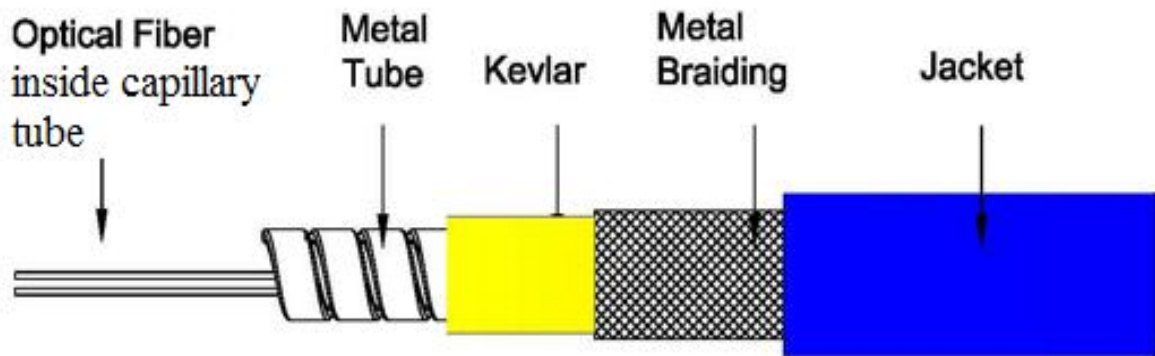


Figure 6.1.2a. Diagram depicting typical Kaiphone fiber-optic cable as used in this study (Kaiphone, 2012).

Approximately 220 meters of cable at each depth was deployed into the shallow subsurface. From a soil science perspective, the shallowest cable was located in the A horizon (0 to 8 cm) of a typical Malpais soil, while the middle and deepest cables were both located in the Bw1 horizon (8 to 30 cm). The two fibers in the bottom cable were connected to a DTS Oryx computer into Channels 1 and 2. This bottom cable then ran the length of the 220 meters through plots of different vegetation types. At this point the fibers in the bottom cable were spliced to the fibers in the middle cable, which then ran the 220 meters back to the original position at the Oryx. This middle cable was then spliced to the top cable, running the same 220 meters back to the other end. At this point,

the two fibers in the top cable were spliced to one another, creating a double-ended configuration, and effectively doubling the entire signal length. All splices were placed securely into splice boxes to protect the splice from tension as well as the outside environment. These splice boxes containing the fiber ends were then stored inside of buried irrigation boxes outside of the agricultural plots. The following aerial photograph shows the path of the cables as they travel through the various agricultural plots.

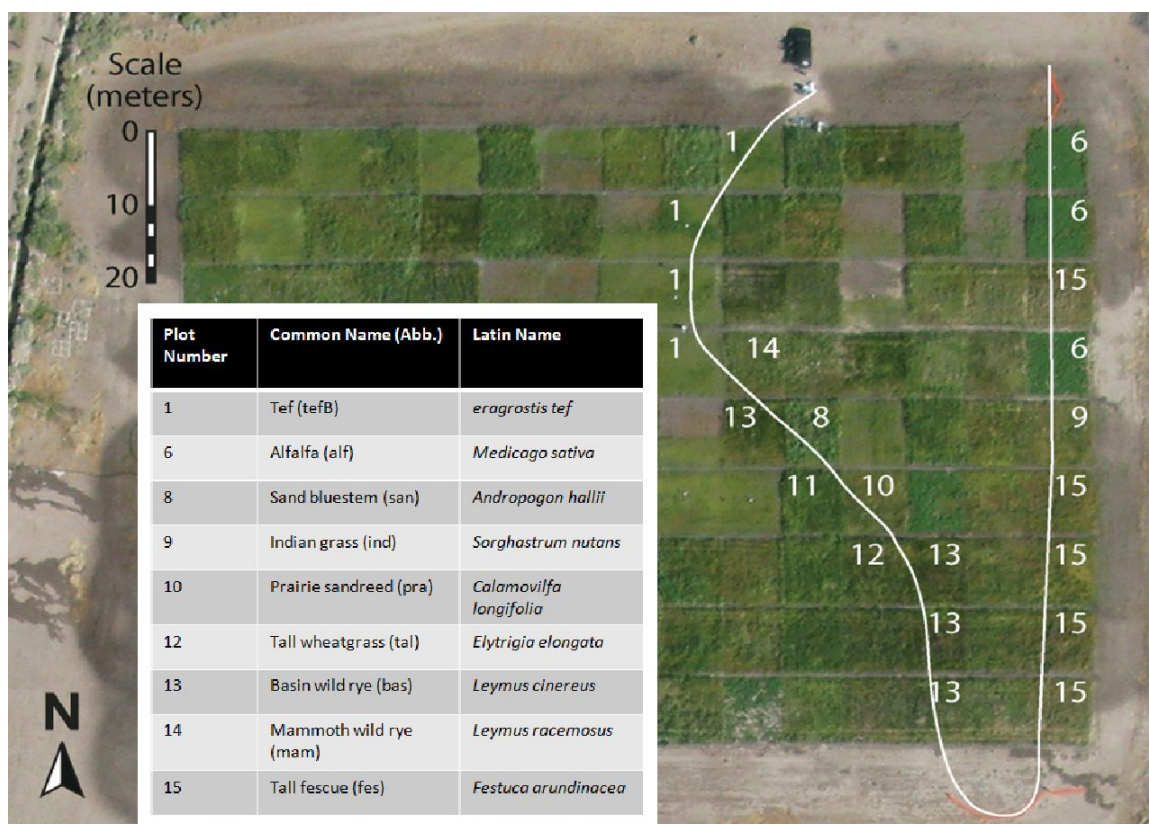


Figure 6.1.2b. Aerial photograph with cable path marked out. The northwest end of the cable path is where the DTS unit is located. Photo courtesy of Greg Arehart.

A portion of each cable was placed into both an ice water bath and also an ambient temperature bath. In conjunction with independent temperature measurements in

these baths, this provided a means of temperature calibration for the temperatures recorded along the cable.

In an effort to reduce system noise and with the thought that soils under vegetation would not experience rapid temperature change, the Oryx was set up to take double-ended measurements, with data being collected every 5 minutes. The Oryx unit samples every meter of the cable. A double-ended measurement occurs when both ends of the fiber are connected to the DTS unit, and provides much higher quality data for long-term installations (Tyler *et al.*, 2009). On site single-ended field calibration was completed upon initial setup of the September run. Slope of the temperature signal was adjusted through space to ensure that corresponding sections from forward and reverse data matched (recall that forward and reverse signals should match and be symmetric around the turnaround). Also, a temperature offset was completed to match DTS derived temperatures from within the ice bath to independent temperature measurements within the ice bath. Several runs were collected at the field site, the last and longest of which provided the data for this study. From September 2nd through September 27th of 2010, temperature data was collected every 5 minutes. A total of 25 days of data was collected during this installment.

6.1.3 Weather Stations

Concurrent with the previously mentioned 25-day DTS installment from September 2nd through September 27th, several weather stations were collecting basic meteorological data. An eddy covariance tower was positioned in a plot of Indian grass

on the northern edge of the field, one plot away from the path of the cable. This eddy station collected measurements every 15 minutes, throughout the entire duration of DTS data collection. Variables measured included net solar radiation, wind speed and direction, air temperature, relative humidity, barometric atmospheric pressure, CO₂ concentration, soil heat flux, soil temperature, and a point scale measure of soil moisture.

In addition to the eddy covariance tower, two wireless meteorological stations were also co-located in plots containing the fiber optic cables. One met station was located in a Tef (Brown variety) plot under a 50 percent irrigation schedule, and the other in a plot of Prairie sandreed under a 100 percent irrigation schedule. These stations each measured wind speed and direction, shortwave radiation, relative humidity, air temperature, barometric atmospheric pressure, precipitation, and two different point measurements of soil moisture.

6.1.4 Core Samples

In addition to soil moisture and other meteorological data collected by the eddy covariance tower and the two wireless met stations, destructive core sampling was also completed. Soil cores were collected on August 10th, 2010 and also on September 10th, 2010. Although only the cores collected on September 10th could be used for comparison to end results of soil moisture estimates based off the DTS temperature data (the August cores do not overlap with the study dates), all cores collected were used to analyze basic soil properties at the site. In each plot that soil cores were taken, three cores were collected. Soil samples collected with a large corer of 15 centimeters length and 645

cubic centimeters volume were used primarily for bulk density measurement in the lab. A smaller corer with a length of 7.5 centimeters and a volume of 130 cubic centimeters was used to collect two samples of 7.5 centimeter increments to a depth of 15 centimeters. In this way soil moisture was determined back in the lab in two components: the top 7.5 centimeters of soil, and soil from 7.5 to 15 centimeters of depth. For all cores collected, both bulk density and volumetric moisture content were measured.

6.2 LABORATORY WORK

6.2.1 Bulk Density and Gravimetric Moisture Content

All of the soil cores that were collected from the 5C Cottonwood Ranch were taken back to the soil lab for bulk density determination and soil moisture measurement. Both of these measurements are very straightforward, but also very important. Each of the soil cores were collected in a corer of known volume, measured beforehand. To determine the bulk density of a soil sample, the soil was removed from its corer and placed into a previously weighed aluminum tin. The sample was then weighed to the nearest hundredth gram. This provided the mass of the wet sample. The tin and sample were then taken and placed into a Cole Parmer 120 volt laboratory oven, where they baked at 105 °C for 24 hours. This amount of baking effectively dries the sample entirely, without burning off any organic matter. Once dry, the sample and tin were again weighed, providing the mass of the dry soil. To calculate bulk density, the mass of the

dry soil is divided by the volume of the soil core in which it was collected (which equals the volume of the soil). This provides a mass per cubic volume measurement of bulk density.

The difference between the mass of the wet sample and the mass of the oven-dried sample provides the mass of water originally in the soil sample. This is then divided by the mass of the dried sample to provide the gravimetric moisture content. To obtain a volumetric moisture content, the gravimetric moisture content is simply multiplied by the bulk density of the soil.

6.2.2 Organic Matter Content

Organic matter influences many of the physical, chemical, and biological properties of a soil. In particular, organic matter plays a role in determining the particle density of a soil, and therefore affects porosity and is related to bulk density. Particle density is a combination of the mineral and organic constituents of soil and was found by utilizing the following equation:

$$\rho_s = \rho_m X_m + \rho_{om} X_{om} , \quad \text{Equation 6.2.2}$$

where ρ is density, X is volume fraction, and subscripts s , m , and om , denote particle, mineral and organic matter respectively (Jury and Horton, 2004). Determining the volume fraction of organic matter is important, if one is to accurately determine particle density. The American Society for Testing and Materials standard reference D 2974 was followed to determine the organic matter content (ASTM, 1987). This provides the

standard test method for moisture, ash, and organic matter of peat and other organic soils. Soil samples that had just been oven dried to determine soil moisture (as described in 7.2.1) were used to determine organic matter content. Four small porcelain dishes were weighed, and then a small amount of dried sample placed into each dish. All porcelain dishes were then re-weighed. The porcelain dishes containing dried soil sample were then placed into a Lindberg/Blue muffle furnace. The temperature in the furnace was then gradually increased until reaching 440 °C. Here the samples remained for approximately 22 hours, long enough for the specimens to become completely ashed, where no change in mass occurred with further heating (ASTM, 1987).

At this point, the porcelain dishes were removed with tongs and reweighed. The mass of the ash (burned soil) was then determined by subtracting the mass of the porcelain dish from that of the dish and burned sample. The mass of the organic matter was determined by then subtracting the mass of the ash from the mass of the original dried soil placed into the porcelain dish. The organic matter content is presented as a mass percentage of the original dried soil. This then provided four individual organic matter contents, from which an average value was determined and used in subsequent calculations.

6.2.3 Quartz Fraction

The amount of quartz present in a soil sample has a very large effect on the thermal properties of that soil, specifically the thermal conductivity and thermal diffusivity. This is because the thermal conductivity of quartz is much larger than all of

the other soil constituents present in most soils. The thermal conductivity of quartz is $8.80 \text{ W m}^{-1} \text{ K}^{-1}$, compared to 2.92, 0.25, and $0.57 \text{ W m}^{-1} \text{ K}^{-1}$ for clay minerals, organic matter, and water respectively (Campbell, 1985). In the process of going from soil temperatures to soil moisture, the relationship between thermal conductivity and soil moisture is a crucial component. There are several pre-existing models for different soil types that provide an estimate of thermal conductivity or thermal diffusivity as it relates to soil moisture. However, even for the same soil type, different models will yield very different soil moisture estimates. For most of these models however, the volume fraction of quartz is a key factor in determining the shape of the relationship between thermal conductivity and soil moisture. For this reason, this section will discuss the methods used to determine the volume fraction of quartz in the soil at the 5C Ranch.

Several samples of soil collected via coring at the study site were used for the quartz content determination. Upon initial inspection it was clear that the sample was not a quartz sand, and appeared to be comprised mostly of various lithics, feldspar, and mica. A small soil sample was chosen at random, and scrubbed thoroughly with soap and water. This cleaning was to ensure that as much clay was removed from the individual particles as possible. The sample was then rinsed thoroughly to remove any potential soap residue. After rinsing and letting air dry, the sample was then packaged and shipped to Spectrum Petrographics Inc., based in Vancouver, Washington.

Spectrum Petrographic created an epoxy grain mount with cover slip from the sample that was shipped, and performed a dual K-feldspar and plagioclase stain. These stains serve to effectively color the feldspar and plagioclase, particles that could

potentially be confused with quartz when looking under a microscope. It leaves only the quartz in the sample as uncolored, providing an easy way to distinguish quartz from the rest of the sand sample. Once the grain mount was returned, the soil thin section was analyzed under a petrographic microscope. In order to quantify the volume fraction of quartz from a 2-dimensional image, area was used as a proxy for volume. A camera was attached to the microscope, and photos taken of each of the field of views that was looked at. In an effort to make distinguishing the quartz as easy as possible, the images were separated into their blue, green, and red components. The blue component of each image provided the clearest visual distinction between the quartz and the rest of the stained sample. Using the camera software, each of the quartz crystals was manually outlined and area automatically calculated. The total area of quartz was then divided by the total area of the field of view. This value then provided an area fraction of quartz, which was used as a proxy for volume fraction of quartz. This volume fraction of quartz can then be used as an important variable for many pre-derived empirical relations between thermal conductivity and soil moisture. The following three figures provide images of the soil thin section, the soil thin section divided into its blue component, and the blue component with quartz outlined.

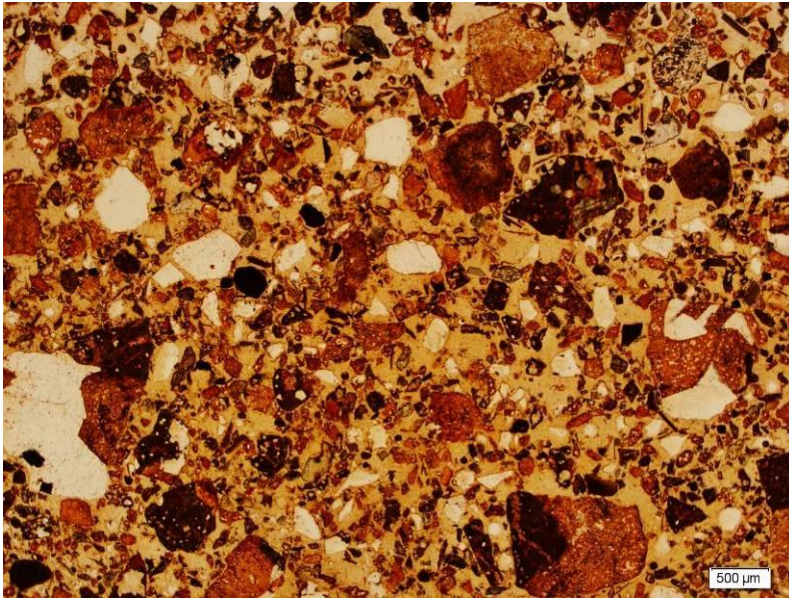


Figure 6.2.3a. Photograph of part of the soil thin section. All white particles are quartz.

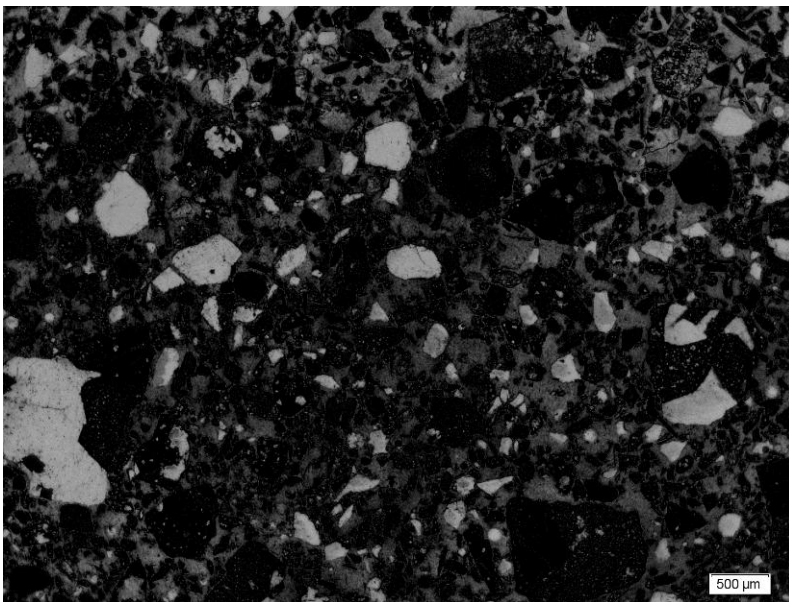


Figure 6.2.3b. Same photograph, but showing only its blue component. The visual distinction of quartz is more obvious than in the original thin section photograph.

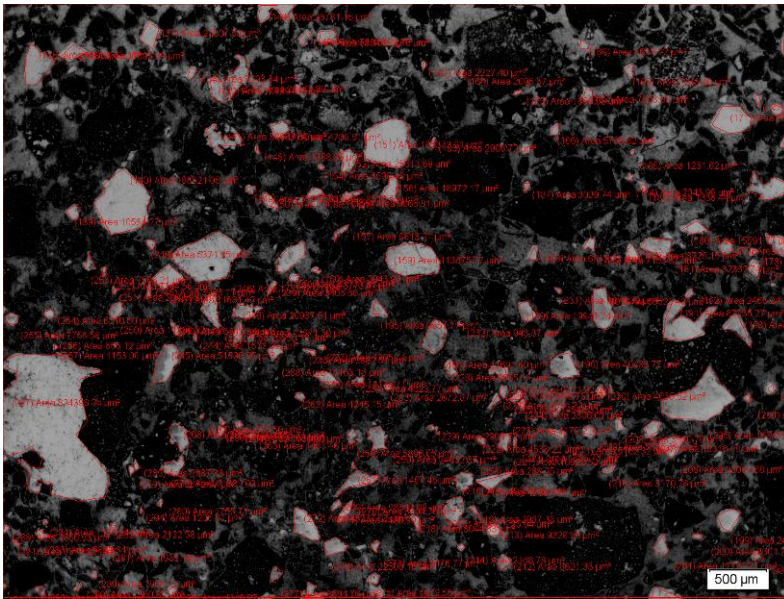


Figure 6.2.3c. Showing the result after each quartz crystal was manually outlined and the area automatically calculated.

6.2.4 Thermal Conductivity – Soil Moisture Relationship

The volume fraction of quartz determination outlined in the previous section is crucial if one is to develop a relation between thermal conductivity and soil moisture based on pre-existing empirical equations. Such a relationship was completed using the Campbell model of thermal conductivity (Campbell, 1985). The equation for the Campbell model is as follows:

$$\lambda = A + B\theta - (A - D)\exp[-(C\theta)^E], \quad \text{Equation 6.2.4a}$$

where λ is thermal conductivity, θ is volumetric water content, and A , B , C , D , and E are coefficients that were derived from curve fitting (Campbell, 1985). Campbell (1985) in

conjunction with deVries (1963) then provides physical meaning to the above listed coefficients.

For mineral soils with a particle density of 2.65 g/cm^3 , the coefficient B is given as

$$B = 1.06 \rho_b \theta, \quad \text{Equation 6.2.4b}$$

where ρ_b is the bulk density of the soil. Similarly for mineral soils, the coefficient D is given as

$$D = 0.03 + 0.1 \rho_b^2. \quad \text{Equation 6.2.4c}$$

The coefficient C determines at which water content thermal conductivity begins to rapidly increase, which is highly correlated with a soil's clay content. Campbell (1985) provides the following relationship:

$$C = 1 + 2.6m_c^{-1/2}, \quad \text{Equation 6.2.4d}$$

where m_c is the clay fraction. The coefficient A is not as simple and is determined by the solid components of a soil.

$$A = \frac{(0.57 + 1.73\phi_q + 0.93\phi_m)}{(1 - 0.74\phi_q - 0.49\phi_m)} - 2.8\phi_s(1 - \phi_s), \quad \text{Equation 6.2.4e}$$

where ϕ_q is the volume fraction of quartz, ϕ_m is the volume fraction of other minerals, and ϕ_s is the volume fraction of solids which is equal to the sum of ϕ_q and ϕ_m . The constant E is purely a curve fitting parameter, and is assigned a value of 4. It is important to note

that the thermal conductivities calculated using equation 6.2.4a may have a small temperature dependence. This is because the conductivities calculated include both the sensible and latent heat components. Therefore, at high volumetric moisture contents and high temperatures, a small portion of the conductivity could be attributed to latent heat transport. At cooler temperatures and lower soil moisture contents, latent heat transport is only a negligible factor. With knowledge of the soil characteristics at the field site, the above described Campbell model was used to develop a curve relating thermal conductivity, thermal diffusivity, and soil moisture.

Knowledge of quartz content and other soil characteristics are necessary if one is to use a model (such as the Campbell model) to develop the thermal conductivity and soil moisture relationship. However, in the ideal situation, thermal conductivity would be measured *in situ* under various soil moisture contents. Steele-Dunne *et al.* (2009) states that the relationship between thermal conductivity and soil moisture should be developed through *in situ* measurements over the full dynamic range of soil moisture, and that this relationship is the key link between soil temperature and soil moisture. Although truly *in situ* measurements proved difficult, measurements of thermal conductivity on the actual soil of interest were conducted in a laboratory setting. These results would be used to ensure whether or not the use of the Campbell model was an accurate selection. The following discusses the methods used to develop the relationship between soil moisture and thermal conductivity in the lab.

The sensor used was a Decagon Devices KD-2 Pro Thermal Properties Analyzer. The KD-2 Pro is a handheld device consisting of a controller and three different needle

sensors that can be inserted into the medium being studied. The three sensors for use with the KD-2 Pro are the KS-1 single needle sensor for measurement of thermal conductivity and thermal resistivity mainly within liquid samples, the TR-1 single needle sensor for measurements of thermal conductivity and thermal resistivity in soil, concrete, rock, and other solid materials, and lastly the SH-1 dual needle sensor for measurement of volumetric heat capacity, thermal conductivity, thermal diffusivity, and thermal resistivity in soils and other granular materials (Decagon, 2008). The SH-1 dual needle sensor was chosen for use for two reasons. First, it is the only one of the three sensors to also measure thermal diffusivity and volumetric heat capacity. Additional information is always a benefit, and this also allowed for comparison of measured diffusivity and heat capacity results with the values calculated using empirical equations. Second, the dual needle sensor is the smallest of the sensors at 30 millimeters in length and with 6 millimeter spacing. A minimum radius of 2 centimeters of soil is needed to surround the sensor in order to ensure that boundary effects do not come into play when the heat pulse is initiated. Therefore, the smaller SH-1 sensor provided the safer choice to ensure that measurement errors were minimized.

The Decagon KD-2 probe for thermal conductivity utilizes the transient line source measurement method to determine the thermal conductivity of a material (Decagon, 2008). In such a method, the needle probe is assumed to be of infinite length and heats the material with a constant heat input from a uniform heat source. Typically, these sensors consist of one needle containing both a heater and a temperature sensor. A current is applied to the heater, and the temperature change monitored over time.

However, in the SH-1 dual needle sensor chosen for this study, the heater and the temperature sensor are placed in separate needles. This spacing between heater and temperature sensor allows for thermal diffusivity and volumetric heat capacity to also be calculated.

Recall from Section 2.2 for point scale measurements of soil moisture the following theory behind heat pulse probes. For a heat pulse of duration t_0 , the solution for the temperature change ΔT at distance r from the infinite line heat source is given by

$$\Delta T(r, t) = \frac{q'}{4\pi C \kappa} \left[Ei\left(\frac{-r^2}{4\kappa(t-t_0)}\right) - Ei\left(\frac{-r^2}{4\kappa t}\right) \right], \quad \text{for } t > t_0, \quad \text{Equation 6.2.4f}$$

where q' is the energy input per unit length per unit time (W m^{-1}), C is volumetric heat capacity, κ is thermal diffusivity, and Ei is the exponential integral function (de Vries, 1952; Mori *et al.*, 2003; Mori *et al.*, 2005; Young *et al.*, 2008). The above equation is basically the same equation used within the KD-2 Pro when the heat is being applied (see Equation 7.2.4h), except that the KD-2 Pro uses fitting parameters.

As measurements are underway with the KD-2 Pro sensor, the temperature is recorded over time. The raw temperature measurements are then automatically processed according to the following equation.

$$T^* = \frac{4\pi(T - T_0)}{q}, \quad \text{Equation 6.2.4g}$$

where T^* is the transformed temperature, T is the raw temperature measurement, T_0 is the ambient temperature at time 0, and q is the heat input per unit length (Decagon, 2008).

The transformed temperatures and corresponding time are then fit to the following equation using a least squares procedure built into the KD-2 Pro.

$$T^* = b_0 t + b_1 \left\{ Ei\left(\frac{b_2}{t}\right) - Ei\left[\frac{b_2}{(t-t_h)}\right] \right\}, \quad \text{Equation 6.2.4h}$$

where Ei is the exponential integral, t is time, t_h is time while the heat is on, and b_0 , b_1 , and b_2 are the fitting constants (Decagon, 2008). Equation 6.2.4h is used only when heat is actively being applied to the sensor. When the heat is off and cooling is taking place, the following equation is used.

$$T^* = b_0 t + b_1 Ei\left(\frac{b_2}{t}\right). \quad \text{Equation 6.2.4i}$$

The values of b_0 , b_1 , and b_2 are found by minimizing the sum of the squares of error between the previous equations and the measurements that are taken. Thermal conductivity is then calculated as

$$\lambda = \frac{1}{b_1}, \quad \text{Equation 6.2.4j}$$

and thermal diffusivity as

$$D = \frac{r^2}{4b_2} \quad (\text{Decagon, 2008}). \quad \text{Equation 6.2.4k}$$

In the laboratory, a pressure plate extractor was used in conjunction with the KD-2 Pro Thermal Properties Analyzer in order to develop the relationship between thermal conductivity and soil moisture using soil from the study site. Two soil cores were placed onto a 3 bar ceramic pressure plate. Standing water was then applied to the plate and periodically checked in case more water was required. Once fully saturated, the above described dual needle sensor of the KD-2 Pro was inserted into one of the soil cores. Here the sensor remained for approximately 20 minutes to ensure temperature equilibrium was reached. At this point, the power was turned on, heating occurred, and thermal measurements made and recorded by the KD-2 Pro. This process was then repeated again in the same soil core, and twice in the second soil core. Multiple measurements in the same core serve to ensure accurate measurements in the sample. Once all thermal measurements were taken and recorded, a very small sample of soil was taken from each core and volumetric moisture content determined via the gravimetric method. This then provided a thermal conductivity value (as well as thermal diffusivity and volumetric heat capacity) and a corresponding soil moisture value. The samples were then placed into the pressure plate extractor and air pressure applied. By applying air pressure in small increments and letting equilibrium be reached after each such increment, the soil cores can effectively be measured under drying conditions. By applying air pressure, determining thermal measurements and moisture content, then applying air pressure again, a complete curve from saturation to dry conditions was created relating thermal properties to soil moisture. These results were then compared to the curves produced using the Campbell model.

6.3 MODELING

This section culminates all methods, and will be used to present all of the computer modeling that was performed for this study. However, it is important to first clarify the use of the term ‘modeling’ as it is being used throughout this study. Modeling is most often thought of as a simulation of reality in which predictions are made for the future based upon appropriate governing equations (Sun, 1994). This is achieved through forward simulation of the variables of interest. In the case of this study however, the term ‘modeling’ is actually referring to the inverse of this situation. Here, it is actually a calibration being used to estimate parameters via numerical inversion. The parameter being estimated is thermal diffusivity, and this is being completed through inversion of the conduction equation by matching observed temperature data. Use of the term ‘Modeling’ in this study will therefore be used to refer to this numerical inversion.

As described in Section 6.2.4, a curve relating thermal diffusivity and soil moisture has been developed. However, this relationship is only useful towards estimating soil moisture if thermal diffusivity values are attainable along the cable’s length. Recall that thermal diffusivity, D , and thermal conductivity, λ , are easily relatable by volumetric heat capacity, C , all of which are functions of soil moisture. This is illustrated by the conduction equation for heat transfer.

$$\frac{\partial T}{\partial t} = D(\theta) \frac{\partial^2 T}{\partial z^2} = \frac{\lambda(\theta)}{C(\theta)} \frac{\partial^2 T}{\partial z^2}, \quad \text{Equation 6.3}$$

where T is temperature, t is time, and z is depth (Behaegel *et al.*, 2007). Therefore, if thermal diffusivity can be successfully modeled, then these values should provide reasonable estimates of volumetric moisture content. First, the thermal conductivity values produced from the Campbell model will be converted to thermal diffusivity by dividing by the volumetric heat capacity of the soil over the entire moisture range. At this point, there is a relationship between thermal diffusivity and soil moisture, and thermal diffusivity along the cable is ready to be modeled.

6.3.1 Excel Finite-Difference Mesh

An explicit finite-difference mesh was created in Excel as a first attempt at estimating thermal diffusivity values based on the temperature signals collected using distributed temperature sensing. This mesh assumes only 1-dimensional unsteady conduction, with no internal heat generation and otherwise constant properties. Given these parameters and deriving from the energy conservation principle (see equation 2.1.5), the finite-difference mesh is created explicitly,

$$T_m^{i+1} = Fo(T_{m-1}^i + T_{m+1}^i) + (1 - 2Fo)T_m^i, \quad \text{Equation 6.3.1a}$$

with the mesh Fourier number provided as

$$Fo = \frac{D\Delta T}{\Delta x^2}, \quad \text{Equation 6.3.1b}$$

where D is thermal diffusivity, T is temperature, and x is the chosen spatial step (Mills A.F., 1999). Equation 6.3.1a is a relationship providing the temperature at node m at the $(i + 1)th$ time step, in terms of temperatures at the previous time step (Mills A.F., 1999).

The created mesh effectively models thermal diffusivity over a 10 centimeter domain (from 5 centimeters depth to 15 centimeters depth in the soil). Using temperature series collected from the upper cable (5 cm depth) as the top boundary condition and temperatures collected from the bottom cable (15 cm depth) as the lower boundary condition, temperatures at the depth of the middle cable (10 cm depth) were simulated. Linearly interpolated temperature values at time 0 between the upper and lower cable served as the initial boundary conditions. This then created all of the boundaries necessary for the explicit finite-difference mesh. The major drawback with the use of such explicit methods is that the allowable size of the time step is limited by stability requirements. Because 1 centimeter was assumed to be an adequate spatial step, the limit on the time step becomes

$$\Delta t \leq \frac{\Delta x^2}{2D}, \quad \text{Equation 6.3.1c}$$

where Δt is the time step, x is the chosen spatial step, and D is thermal diffusivity (Mills A.F.,1999). Since a spatial step of 1 centimeter was used for this mesh, a time step of 30 seconds was appropriate and allowed for stability requirements to be met. By marching forward in time, the model populates the entire model domain with simulated temperatures based entirely on the observed temperatures in the top and bottom cables.

To estimate thermal diffusivity, the root mean squared error, or RMSE, between observed and predicted temperatures at the depth of the middle cable was minimized using the solver function, allowing only the thermal diffusivity variable from Equation 6.3.1b to change. Various temporal resolutions were considered, including 2 hours, 12 hours, and 24 hours. To get a diffusivity estimate over the first 2 hours for example, the RMSE was minimized over the entire two hour span by allowing the diffusivity variable to change. The process was then repeated for the next two hours. Because of the manual input required to initialize each time step, and because this finite-difference method in Excel was used simply as a first look at thermal diffusivity values, analysis was conducted only within one plot of tall fescue. Therefore, only an individual meter of observed temperature values was considered.

This model assumes that each respective plot is homogeneous in regards to soil structure, vegetation type and thus root structure, and also water applied. Also, in using such a method, one thermal diffusivity value and therefore one soil moisture value is provided for the entire 10 centimeter domain. Because the finite-difference mesh was created in Excel, it required a lot of manual input of initial conditions for each time step, and only one meter of cable could be investigated at a time. Diffusivity values were modeled using this method over a 5 day drying period in a plot of tall fescue.

A series of routines developed in MATLAB was created by Susan Steele-Dunne that greatly simplifies the above described finite-difference scheme used in Excel. Steele-Dunne's model was utilized and will be discussed in the following section.

6.3.2 MATLAB Conduction Model

The MATLAB conduction model that was utilized in this study was developed separately by Susan Steele-Dunne for her own use on a similar study in Delft, Netherlands. Through personal and email correspondence, it was determined that Steele-Dunne's model was effectively doing the same thing that the previously mentioned Excel finite-difference mesh was doing, just in a much more fluid and automated way. Very comparable results were achieved using the two methods over the same time frame and same location. It was thus decided that the use of the MATLAB conduction model could be applied in this study as well.

The conduction model developed in MATLAB uses an inversion approach and assumes that conduction is the only heat transfer process. The model domain is from 0 to 10 centimeters depth, which corresponds to 5 to 15 centimeters depth in the real world. The spatial resolution used is 0.5 centimeters. The time step used for this model is 60 seconds, so the 5 minute data resolution originally collected from the DTS Oryx system was linearly interpolated to 1 minute data resolution. The chosen window length was 24 hours. Using smaller window lengths resulted in very noisy data, with no clear trends. The 24 hour window was then shifted in 6 hour increments. Therefore, one diffusivity value based off of 24 hours of temperature data was collected for every 6 hours.

Four input variables are required in order for the conduction model to simulate soil temperatures and output thermal diffusivity values. Three of the four input variables are the time series of temperatures from the 5 centimeter depth, 10 centimeter depth, and

15 centimeter depth, and the last variable is the date and time series corresponding to each temperature observation. For the very first window, an initial guess for thermal diffusivity of $0.50 \text{ mm}^2/\text{sec}$ was used. Just as with the finite-difference mesh, the conduction model used the temperatures from the 5 centimeter depth as the top boundary condition, and the temperatures from the 15 centimeter depth as the lower boundary condition. A linear interpolation between the temperatures at the three cable depths provided the initial temperatures at time zero. For each subsequent window, the resulting simulated temperatures from the last time step of the previous window were used to initialize the temperature values.

Again making use of the Fourier number from Equation 6.3.1b, simulated temperatures were populated throughout the model domain using the same principle as Equation 6.3.1a described previously in discussion of the finite-difference mesh. The root mean squared error between the simulated temperatures at the depth of the middle cable and the observed temperatures from the middle cable was then minimized by allowing for variance in thermal diffusivity. The result was that a thermal diffusivity value was estimated every 6 hours for each meter along the cable. Because temperatures from the entire domain of 5 to 15 centimeters were used to estimate each thermal diffusivity value, the result is a single diffusivity value for the entire soil column. Therefore, although diffusivity estimates change over time, at any one time the diffusivity is assumed to be uniform throughout the vertical soil column.

The model was applied to each individual plot, as opposed to running the model for the entire length of the cable at once. Because of irrigation pipes and the transition

space from one vegetation type to the next, diffusivities were not estimated for the outside meter on either side of each plot. The thermal diffusivity values calculated within each plot could then be compared to the developed relation between thermal conductivity and soil moisture in order to determine the corresponding soil moisture within each plot.

6.3.3 Soil Moisture Estimation

Thus far, a curve relating thermal diffusivity to volumetric moisture content via use of the Campbell model has been developed. This same relationship has again been developed making use of actual measurements on soil cores brought back to the laboratory. Theoretically, these curves should match up fairly well. Furthermore, using the conduction model in MATLAB, thermal diffusivity has been modeled along the length of the cable within in the field. Within each plot, there are now estimated thermal diffusivity values integrated over each meter, and provided on 6 hour temporal resolution. With this considered, the section will now discuss how soil moisture was estimated.

The progression from estimated thermal diffusivity values along the cable to estimated soil moisture values is straightforward. From Section 2 of this thesis, the basic shape of the relationship between these two variables is provided.

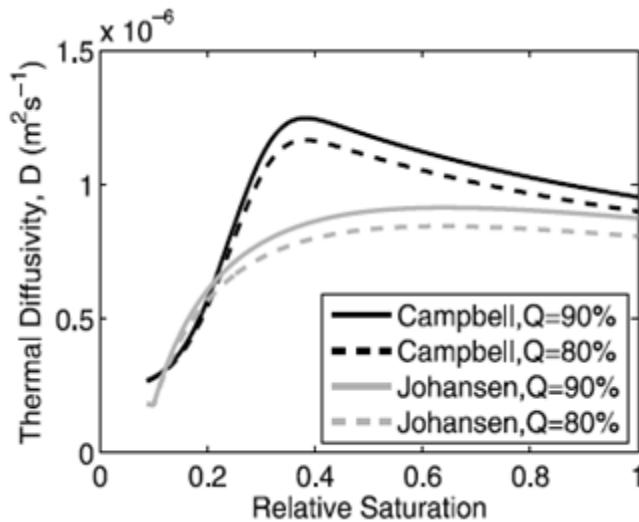


Figure 6.3.3. Example of basic relation between thermal diffusivity and soil moisture. Only the shape of the Campbell model is important here, since the Johansen model was not used in this study (Steele-Dunne *et al.*, 2009).

It is clear that there is a non-uniqueness that exists (i.e. for many values of diffusivity, there can be more than one corresponding soil moisture value). Therefore, an equation of best fit was created for both sides of the developed Campbell curve, relating the variables mathematically. In the field, some of the plots were consistently on the wetter side of this curve, and some were consistently on the drier side. Therefore, only the equation for the right side of this curve was applied to those plots that received irrigation, while the equation for the left side of the curve was only applied to those plots that did not receive irrigation and were therefore drier throughout the study period. This provided estimates of volumetric moisture content over the length of the cable. The resulting soil moisture estimates over time will be presented for a few particular locations, followed by the compiled results of soil moisture over the field scale.

SECTION 7. RESULTS

The following section will provide the collected results throughout this study, organized into four separate subsections. The first subsection provides results from the field work, the second subsection provides laboratory results, the third subsection will provide results from temperature analysis across the field, and the final subsection provides the modeling results, including results for both thermal diffusivity and soil moisture

7.1 FIELD WORK RESULTS

Because most of the field work resulted in samples being returned to a laboratory setting, these results will be discussed in the next subsection. Quantifiable results that fit solely under the classification of field work to be provided here include weather station results, as well as the raw data collected from the Sensornet Oryx device.

Meteorological variables that were measured by the eddy covariance tower included net solar radiation, wind speed and direction, air temperature, relative humidity, barometric atmospheric pressure, CO₂ concentration, soil heat flux, soil temperature, and a point scale measure of soil moisture. The following plot displays the air temperature measured as well as the net radiation over the 25-day study period.

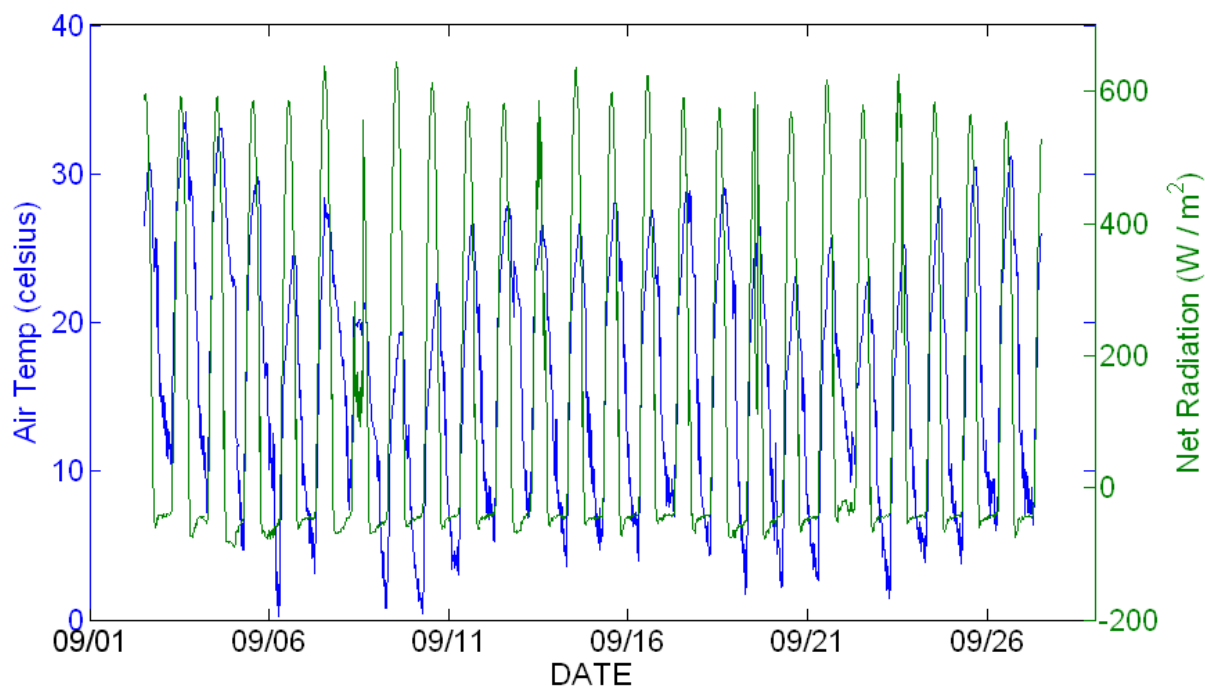


Figure 7.1.1. Air temperature and net radiation as measured by the eddy covariance tower.

In addition to the eddy covariance tower, two wireless meteorological stations were also placed in the field, co-located with the path of the DTS cables. These wireless stations measured wind speed and direction, shortwave radiation, relative humidity, air temperature, barometric atmospheric pressure, precipitation, and two different point measurements of soil moisture. One met station was located in a Tef (Brown variety) plot under a 50 percent irrigation schedule, and the other in a plot of Prairie sandreed under a 100 percent irrigation schedule. During the month of study, the 50 percent irrigation plots did not receive any irrigation because September is towards the end of the season and so the allocated water for these plots was already exhausted. Adjacent plots

to the Tef plot did receive irrigation however, hence soil moisture was affected in the Tef plot even though no direct irrigation was applied. Figure 7.1.2 shows soil moisture as measured by the Decagon EC-5 soil moisture sensors connected to each wireless meteorological station.

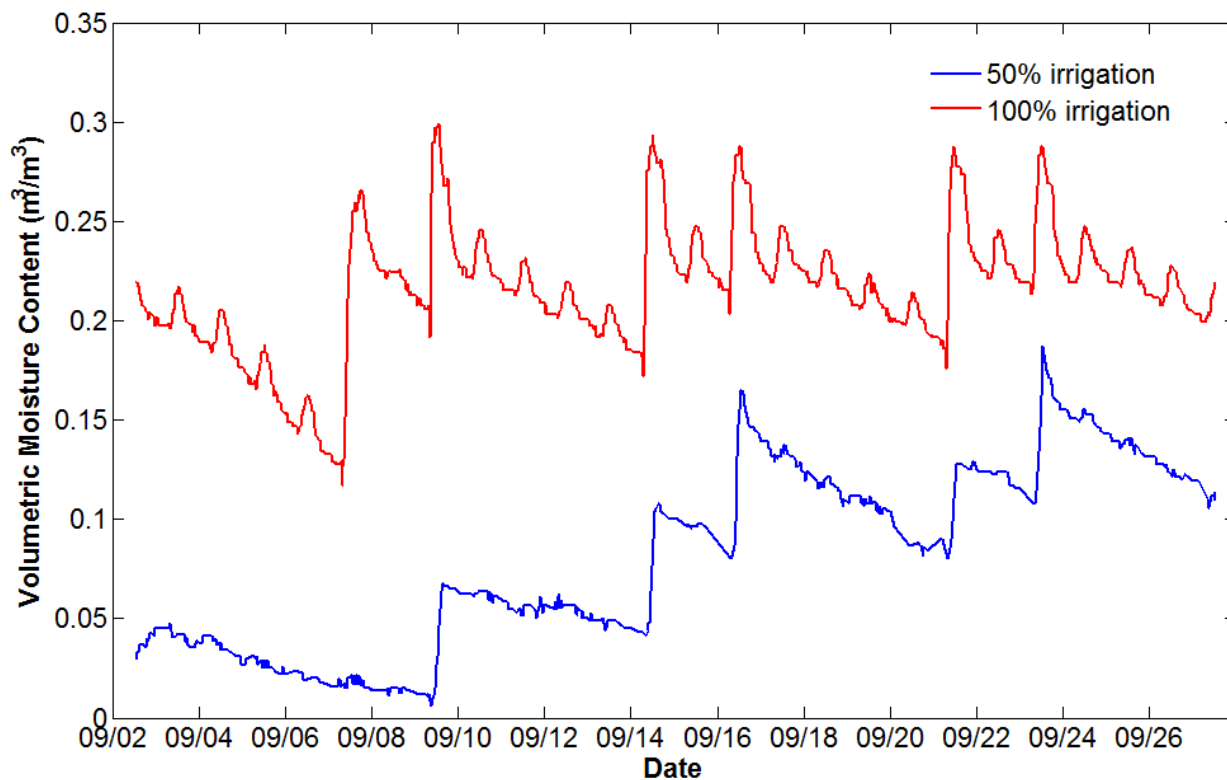


Figure 7.1.2. Soil moisture measurements as measured by wireless meteorological stations in two different plots. Measurements from 50 percent irrigation were from a Tef plot and actually received no direct irrigation. The 100 percent irrigation measurements were taken in a prairie sandreed plot.

When considering the soil moisture values in Figure 7.1.2, especially those measured in the plot under a 100% irrigation scheme, a noticeable diurnal increase in soil moisture is observed throughout the study. However, this is caused by a temperature

dependence of the dielectric properties of the soil and on the response of the sensor (Assouline *et al.*, 2010). The soil moisture sensor used by the wireless meteorological stations is the Decagon ECH₂O-EC5 sensor. These sensors measure soil moisture content indirectly by making use of the soil's dielectric properties as discussed previously in Section 3 of this thesis. The sensors were placed vertically into the soil, beginning at the soil surface. Therefore, large diurnal temperature fluctuations have an effect on the sensor response. The dielectric permittivity of water, ϵ_w , is dependent on temperature in accordance with the following linear empirical relationship:

$$\epsilon_w = 88 - 0.35T, \quad \text{Equation 7.1.1.}$$

for water temperature T varying between 5 and 40 °C (Assouline *et al.*, 2010; Weast, 1986). Assouline *et al.* (2010) references Bogona *et al.* (2007) in stating that the Decagon ECH₂O-EC5 sensors showed an increase in measured soil moisture content with increasing temperature. This error in measured soil water content because of temperature effects on the sensor varied between -1.1 percent at 5 °C to 1.8 percent at 40 °C (Bogona *et al.*, 2007), explaining why the soil moisture contents in Figure 8.1.2 appear to increase by a couple percent during the warmest part of each day.

The DTS Oryx computer was set up to take double-ended measurements, with data being collected every 5 minutes. The benefit behind use of a double-ended configuration as opposed to a single-ended configuration is that calibration required is generally only a temperature offset. When light transmission occurs in only one direction (single-ended configuration) differential attenuation between Stokes and anti-Stokes

returning signals must be accounted for as well (Tyler *et al.*, 2009). Double-ended measurements provide a consistent amount of precision along the length of the cable, although closer to the instrument, measurements are noisier than if single-ended measurements were taken. For this application, a double-ended configuration offered the most accurate and consistent results along the length of the cable for the entire study period.

It is important to look at the raw data directly collected from the Oryx system. In this case, Figure 7.1.3 depicts temperature during the first day of the installation, at noon time. This is after the DTS was calibrated to ensure that independent measurements of temperature in the ice baths matched observed temperatures from the Oryx also in the ice baths. Note that the signal is a mirror image with the symmetry line occurring around a distance of 900 meters where the turnaround in the top cable is located.

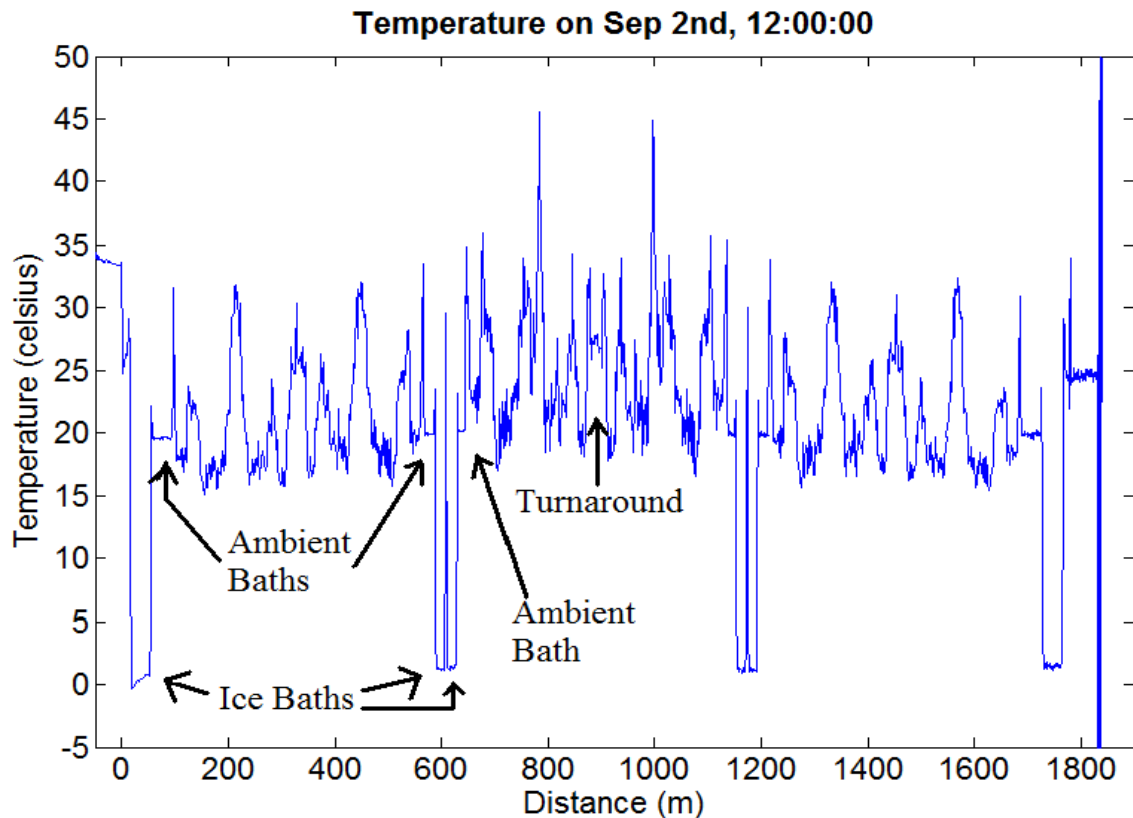


Figure 7.1.3. Temperature signal collected from the Oryx. Note the evident locations of the water baths: ice baths at 20-60m, 590-610m, and 610-630m; and ambient baths at 60-100m, 570-590m, and 630-640m. The turnaround in the cable occurs at 890 meters.

Figure 7.1.3 depicts the temperature output at one point in time over the entire length of the cable. Because the bottom, middle, and top cables are all spliced together, the result is one continuous temperature measurement. Section 7.3 will provide much more detailed temperature results, with temperature signals being broken down into the 5 centimeter, 10 centimeter, and 15 centimeter depths.

7.2 LABORATORY RESULTS

7.2.1 Soil Core Results

The first results presented are the basic bulk density and moisture content determinations that were calculated from soil cores brought back to the lab. Soil cores were collected on August 10th, 2010 and also on September 10th, 2010. Although only the cores collected on September 10th can be used for comparison to end results of soil moisture estimates based off the DTS temperature data (the August cores do not overlap with the study dates), all cores collected can be used to analyze basic soil properties at the site. In each plot from which soil cores were taken, three cores were collected. The first core was taken with a corer of volume 645.12 cubic centimeters. This large core was used for bulk density determination. The second and third cores taken in each plot were with a smaller corer of volume 130 cubic centimeters. The first of the small cores sampled from the ground surface to 7.5 centimeters depth, and the second of the small cores sampled from 7.5 to 15 centimeters depth. The following tables provide the results to the August 10th, 2010 and the September 10th, 2010 soil core collections.

August 10th, 2010 Soil Cores

Sample	Empty Tin (g)	Tin w/wet sample (g)	Tin w/dried sample (g)	Bulk Density (g/cm³)	Volumetric Moisture Content (cm³/cm³)	Time	Plot
1Bulk	17.84	1272.20	1131.62	1.72	0.22	14:44	Alf
1A	8.28	241.32	212.74		0.24		
1B	8.27	268.80	239.08		0.22		
2Bulk	17.92	1158.88	1077.93	1.64	0.13	15:08	Ind
2A	8.31	202.02	179.11		0.22		
2B	8.23	185.21	178.67		0.06		
3Bulk	17.88	1255.42	1168.19	1.78	0.14	15:20	Fes
3A	8.35	225.00	207.17		0.16		
3B	8.31	186.42	174.36		0.13		
4Bulk	17.89	1205.44	1120.36	1.70	0.13	15:42	Bas
4A	8.30	220.95	206.35		0.13		
4B	8.34	210.44	197.19		0.12		
5Bulk	17.87	1208.06	1112.04	1.69	0.15	16:09	Tal
5A	8.27	228.54	200.53		0.25		
5B	8.33	219.80	205.37		0.12		
6Bulk	17.82	1297.14	1139.79	1.73	0.24	16:24	San
6A	8.21	247.04	215.23		0.27		
6B	8.23	252.67	221.21		0.26		
7Bulk	17.82	1332.55	1178.71	1.79	0.24	16:46	Tef
7A	8.26	228.63	202.36		0.24		
7B	8.28	230.40	205.77		0.22		
8Bulk	17.93	1332.55	1092.29	1.66	0.11	17:10	Ind

Table 7.2.1a. Bulk density and volumetric moisture content results from soil core collection that occurred on August 10th, 2010. Note that “Bulk” samples include the entire top 15 centimeters of soil. “A” samples are from 0 to 7.5 centimeters, and “B” samples are from 7.5 to 15 centimeters.

September 10th, 2010 Soil Cores

Sample	Empty Tin (g)	Tin w/wet sample (g)	Tin w/dried sample (g)	Bulk Density (g/cm ³)	Volumetric Moisture Content (cm ³ /cm ³)	Time	Plot
1Bulk	17.90	1304.25	1178.24	1.80	0.20	13:17	Alf
1A	13.40	493.26	446.21		0.20		
1B	13.62	556.39	501.59		0.20		
2Bulk	17.84	932.52	903.08	1.37	0.05	13:35	Fes
2A	13.49	525.51	513.19		0.03		
2B	13.43	583.29	559.20		0.06		
3Bulk	17.86	1199.48	1199.48	1.62	0.21	13:53	Fes
3A	13.57	629.60	629.60		0.23		
3B	13.31	243.14	243.14		0.18		
4Bulk	17.87	1322.30	1322.30	1.79	0.23	14:06	Bas
4A	13.32	676.69	676.69		0.25		
4B	13.35	622.40	622.40		0.19		
5Bulk	17.95	1247.84	1247.84	1.71	0.20	14:21	Tef
5A	13.53	677.96	677.96		0.22		
5B	13.57	581.85	581.85		0.20		

Table 7.2.1b. Bulk density and volumetric moisture content results from soil core collection that occurred on September 10th, 2010. Note that “Bulk” samples include the entire top 15 centimeters of soil. “A” samples are from 0 to 7.5 centimeters, and “B” samples are from 7.5 to 15 centimeters.

From all soil cores collected throughout the course of this study, the average bulk density was $1.75 \text{ g/cm}^3 \pm 0.061$. Note that Sample 2Bulk contains a bulk density of only 1.3722 g/cm^3 . This however, must be derived from a sampling error on *in situ* anomaly. The bulk density from Sample 2 was therefore excluded when calculating the average bulk density. The average value of 1.75 g/cm^3 is perfectly in line with the above presented

bulk densities measured from soil cores collected on August 10th and September 10th of 2010.

Since both core samples and the EC-5 sensors were used to measure soil moisture, it is a good idea to compare results from both methods. Figure 7.2.1 presents volumetric moisture contents as determined via the gravimetric approach on 5 core samples as well as the concurrent EC-5 moisture readings.

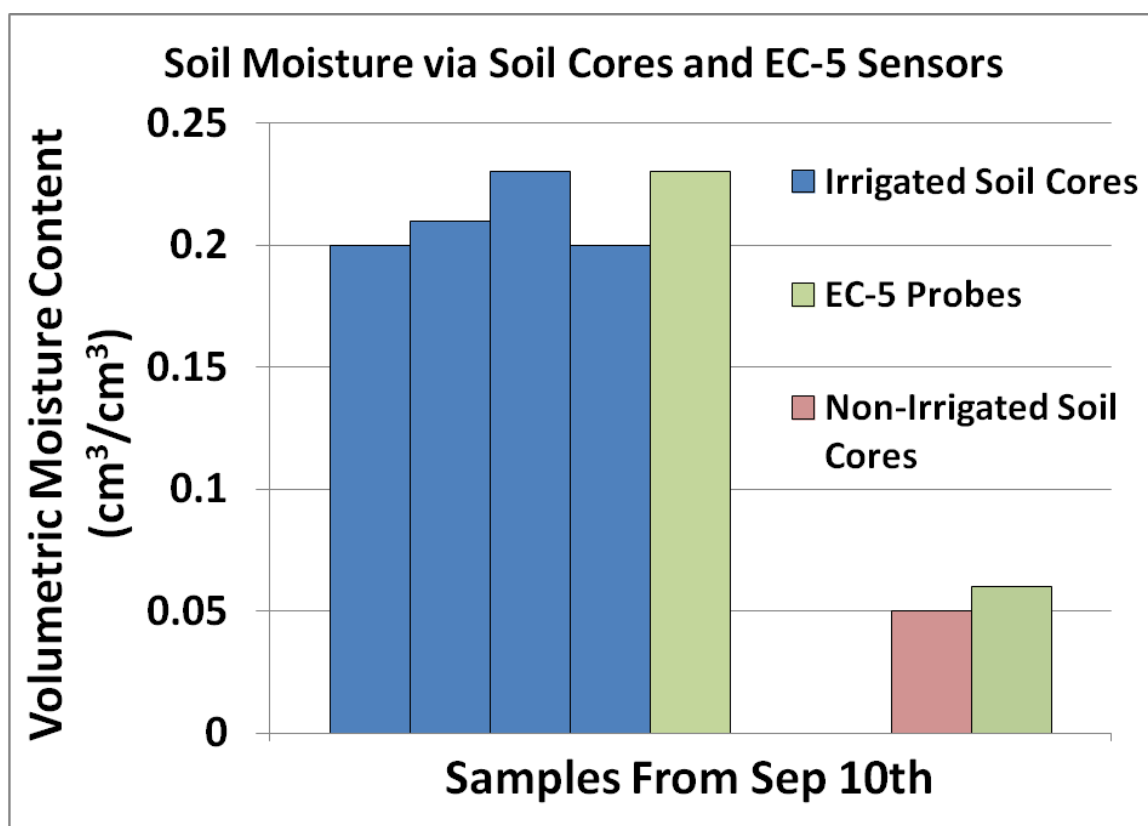


Figure 7.2.1. Moisture contents determined from 4 soil cores taken from irrigated plots (blue bars) presented next to the moisture reading from the EC-5 sensor also located in an irrigated plot. Also, results from a soil core collected in a non-irrigated plot (red bar) presented next to the moisture measurement from the EC-5 sensor located in a non-irrigated plot. All measurements come from September 10th, from 1:17 PM to 2:21 PM.

Figure 7.2.1 shows agreement between the various methods of soil moisture measurement. The fact that the EC-5 sensors show elevated moisture contents as temperature increases could explain the slightly higher moisture values when compared to those values derived from soil cores.

Because irrigation is the primary source of moisture in the shallow subsurface for these agricultural fields during summer months, it is important to know when these soil cores were collected in relation to the irrigation events. Table 7.2.1c provides the dates and amounts of water applied during the months of August and September of 2010.

Irrigation Schedule

Date (2010)	Amount of Water Applied in Acre Feet (centimeters)	
August 3 rd	0.46 ac-ft (5.6 cm)	
August 5 th	0.11 ac-ft (1.3 cm)	Plots on 50% irrigation schedule with grass crops – irrigation done for season
August 10 th	0.06 ac-ft (1.0 cm)	
August 12 th	0.40 ac-ft (6.3 cm)	
August 17 th	0.40 ac-ft (6.3 cm)	
August 19 th	0.41 ac-ft (6.5 cm)	
August 24 th	0.31 ac-ft (4.9 cm)	Plots on 50% irrigation schedule with alternative crops – irrigation done for the season
August 26 th	0.19 ac-ft (3.6 cm)	
August 31 st	0.29 ac-ft (5.5 cm)	
September 7 th	0.32 ac-ft (5.9 cm)	
September 9 th	0.34 ac-ft (6.3 cm)	
September 14 th	0.36 ac-ft (6.8 cm)	
September 16 th	0.38 ac-ft (7.2 cm)	
September 21 st	0.34 ac-ft (6.3 cm)	
September 23 rd	0.35 ac-ft (6.5 cm)	
September 28 th	0.11 ac-ft (2.1 cm)	Plots on 75% irrigation schedule with grass crops – irrigation done for season
September 30 th	0.30 ac-ft (8.1 cm)	

Table 7.2.1c. Date and amount of water applied for each scheduled irrigation event. During August, irrigation of all plots that fell under the 50% irrigation schedule was stopped for the remainder of the season.

Soil cores were collected on August 10th and September 10th of 2010. The cores collected on August 10th (Table 7.2.1) were used for bulk density determination and not for soil moisture because DTS measurements were not being taken during that time. That being said, it is worth noting that irrigation was actively occurring on the 10th of August, the same day that the cores were collected. Only 0.06 acre feet of water was applied to the field on that day.

The cores collected on September 10th were collected one day after irrigation occurred, when 0.34 acre feet of water was applied. At this point on September 10th, all of the plots from which soil cores were taken were still being irrigated except for the tall fescue plot from which sample 3 was taken. The results from sample 3 in Table 7.2.2 show that soil moisture is much lower than in the other plots. It is also worth noting that the bulk density from sample 3 is also much lower than in the other plots, 1.37 g/cm³ compared to the other bulk density values ranging from 1.60 to 1.80 g/cm³. This would also result in a lower soil moisture content than in reality, since gravimetric moisture content is multiplied by bulk density to obtain a volumetric moisture content.

7.2.2 Organic Matter Content Results

In the process of characterizing soil from the field site, many soil properties needed to be determined. Particle density is a combination of the mineral and organic constituents of soil and was found by utilizing the following equation:

$$\rho_s = \rho_m X_m + \rho_{om} X_{om} , \quad \text{Equation 7.2.2a}$$

where ρ is density, X is volume fraction, and subscripts s , m , and om , denote particle, mineral and organic matter respectively (Jury and Horton, 2004). It is evident that determining the organic matter content is important if one is to determine particle density. The following table provides the results to the procedure outlined in section 6.2.2 on measuring the organic matter content.

Organic Matter Content Determination

Sample Number	1	2	3	4
Mass of Porcelain Dish (g)	17.07	18.70	18.00	17.09
Mass of dish + dry soil (g)	35.16	41.15	36.95	37.16
Mass of dish + ash (g)	34.99	40.89	36.74	36.94
Mass of dry soil (g)	18.09	22.45	18.95	20.07
Mass of ash (g)	17.92	22.19	18.74	19.85
Mass of organic matter (g)	0.17	0.26	0.21	0.22
Organic Matter content fraction	.009	.012	.011	.011
Average organic matter content fraction = .011 ± 0.001				

Table 7.2.2. Results from organic matter content determined via loss-on-ignition procedure as outlined in ASTM D 2974. The soil at 5C Ranch is a highly mineral soil with very little organic matter content.

Once organic matter content is known, equation 7.2.2 can be used to determine particle density specific to the soil at the field site. Particle density of a soil is often assumed to be 2.65 g/cm^3 . However, to be as accurate as possible, it is important to include the fraction of organic matter that is included in the soil. Using the assumption provided by Jury and Horton (2004) that mineral density, ρ_m , is 2.65 g/cm^3 and that organic matter density, ρ_{om} , is 1.30 g/cm^3 , the previous equation becomes

$$\rho_s = (2.65)(0.989) + (1.30)(.011), \quad \text{Equation 7.2.2b}$$

$$\rho_s = 2.635 \text{ g/cm}^3. \quad \text{Equation 7.2.2c}$$

At this point, the porosity of the soil can also be calculated using the previously determined bulk and particle densities. The equation relating these three soil properties is as follows:

$$n = 100 * [1 - (\rho_b / \rho_s)], \quad \text{Equation 7.2.2d}$$

where n is soil porosity, ρ_b is bulk density, and ρ_s is particle density (Hillel, 2004).

Plugging in the previously determined bulk density of 1.75 g/cm^3 and particle density of 2.635 g/cm^3 , the porosity then equals:

$$n = 100 * [1 - (1.75 / 2.635)], \quad \text{Equation 7.2.2e}$$

$$n = 33.59 \%. \quad \text{Equation 7.2.2f}$$

The measurement of organic matter content led to the determination of particle density, which in turn allowed for the calculation of soil porosity. Another very

important soil property can also be determined at this point. Volumetric heat capacity of a soil depends on the volume fractions of the different soil constituents.

$$C_{soil} = X_a C_a + X_w C_w + \sum_{j=1}^N X_{sj} C_{sj}, \quad \text{Equation 7.2.2g}$$

where X refers to volume fraction, C to volumetric heat capacity, and the subscripts a , w , and sj to air, water, and solid constituent j (out of a total of N different solid materials in the soil) (Jury and Horton, 2004). Based upon the fact that the primary minerals found in soil differ very little in heat capacity values, de Vries (1963) recommends using an average value of $1.92 \text{ MJ m}^{-3}\text{K}^{-1}$ for the volumetric heat capacity of soil minerals (Jury and Horton, 2004). Likewise, an average value of $2.51 \text{ MJ m}^{-3}\text{K}^{-1}$ was suggested for the volumetric heat capacity of organic matter. Because the heat capacity of air is small, it may be neglected. The above equation therefore becomes

$$C_{soil} = 4.18\theta + 1.92(1 - n - X_{om}) + 2.51(X_{om}), \quad \text{Equation 7.2.2h}$$

where θ is volumetric moisture content, n is soil porosity, X_{om} is the volume fraction of organic matter, and $(1 - n - X_{om})$ represents the volume fraction of the soil minerals (Jury and Horton, 2004). It is now known that the soil porosity is 0.3359 and the volume fraction of organic matter content is 0.011. Using these determined values, equation 8.2.2h becomes

$$C_{soil} = 4.18\theta + 1.92(1 - 0.3359 - 0.011) + 2.51(0.011), \quad \text{Equation 7.2.2i}$$

$$C_{soil} = 4.18\theta + 1.2816, \quad \text{Equation 7.2.2j}$$

in units of $\text{MJ m}^{-3}\text{K}^{-1}$. This equation provides volumetric heat capacity for a given soil moisture content.

In calculating thermal properties such as the volumetric heat capacity above, the air phase of soil is often neglected. There are several justifications for doing so during this study. The thermal conductivity of air is very low compared to the other soil constituents (only $0.026 \text{ W m}^{-1} \text{ K}^{-1}$) as is the specific heat capacity (Jury and Horton, 2004). Also, because this study is using a simplified heat transfer equation assuming conduction is the primary mode of transfer, potential effects of water vapor flux and diffusive vapor flow are ignored. Studies surrounding the measurement and occurrence of vapor flux have shown that the amount of water and energy transported via vapor flux can be a significant portion of mass and energy balances in dry, bare soil environments (Cahill and Parlange, 1998; Parlange *et al.*, 1998). The study domain for this research however, occurs under various surface crop types experiencing varying degrees of irrigation. Therefore, as is often seen in the calculation of soil thermal properties, the air phase is ignored.

7.2.3 Quartz Content Results

Under a petrographic microscope, a thin section stained for K-feldspar and plagioclase was analyzed. Using the built in camera software, a photo of part of the thin section was taken, divided into just its blue component, and then quartz particles outlined and total area of quartz determined. This was completed for 8 photos, each being randomly positioned over the thin section. The total area of quartz was then divided by

the total area of the entire field of view. The percentage of area that was composed of quartz was then used as a proxy for volume fraction of quartz. The following photograph taken with the camera built into the petrographic microscope is an example of one of the photos, divided into its blue component, and then each quartz crystal outlined and area calculated.

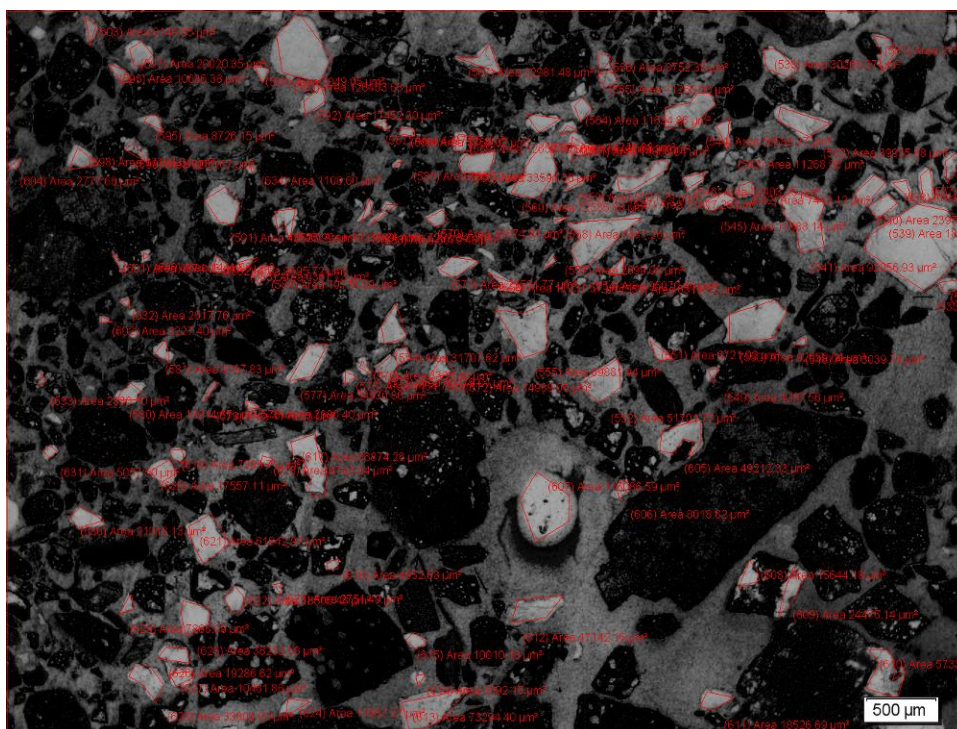


Figure 7.2.3. Blue component of soil thin section with quartz crystals outlined in red.

The same procedure used to create the above photograph was performed 7 more times. This resulted in an area fraction of quartz for 8 different photos, the average of which was then used. Results are provided in the following table.

Volume Fraction of Quartz Determination

Sample Number	Total Area of Quartz (μm^2)	% Area of Quartz (Total area of field of view = 36431196.05 μm^2)
1	3809448.37	10.46
2	3391195.98	9.31
3	2401053.33	6.59
4	4128463.76	11.33
5	2585429.24	7.10
6	3664091.19	10.06
7	4432621.12	12.17
8	3747448.17	10.29
Average % area of quartz = 9.66 ± 1.94		

Table 7.2.3. Results from volume fraction of quartz determination. Area fraction of quartz is used as a proxy for volume fraction of quartz.

Even given the fact that in this analysis, area is being used as a proxy for volume, there is one remaining issue in need of consideration. The percent area of quartz for each sample was calculated relative to the area of the total field of view of the particular photo. However, included within this field of view is all of the empty pore space within the soil. Because the volume fraction of quartz is only in regards to total solid matter, the percent of quartz should actually be greater than that calculated in the above table. To derive a more accurate percent of quartz within the sample, a very simple calculation can be performed. Recall that porosity of the soil is 0.3359. Subtracting this porosity value from unity then leaves 0.6641 volume fraction as solid material. Using this 0.6641 as the

new total area, and dividing the 9.66% by 0.6641, the new value for average percent area of quartz becomes

$$0.0966 / 0.6641 = 0.14546 = 14.55\%. \quad \text{Equation 7.2.3}$$

Therefore, again utilizing area as a proxy for volume, the percent volume fraction of quartz was considered to be about 15% percent.

7.2.4 Thermal Conductivity – Soil Moisture Relationship Results

Developing the relationship between thermal conductivity and soil moisture is easily one of the most important steps in the effort to progress from soil temperature measurements to soil moisture estimates. Although technically an empirical model, the Campbell model of thermal conductivity that was created using soil properties determined in the lab and will be presented here. The equation for the Campbell model is presented as

$$\lambda = A + B\theta - (A - D)\exp[-(C\theta)^E], \quad \text{Equation 7.2.4}$$

where λ is thermal conductivity, θ is volumetric water content, and A , B , C , D , and E are coefficients that were derived from curve fitting (Campbell,1985). Refer to section 6.2.4 of the Methods section for an in depth description of this Campbell model. It is sufficient to know that this model requires knowledge of the following soil properties: bulk density, porosity, volume fraction of quartz, volume fraction of other minerals, clay fraction, and of course, an input of volumetric soil moisture. Clay fraction was not measured in the laboratory, but was previously determined and reported in Project C of the Walker

Report, titled “Plant, Soil, and Water Interactions” (Miller *et al.*, 2010). Within this report is the particle size distribution measured at the 5C Ranch consisting of 79.7% sand, 16.9% silt, and 3.4% clay.

Inserting all of these determined soil characteristics into the equations for each coefficient of the Campbell model as discussed in section 6.2.4, the resulting thermal conductivity curve is derived.

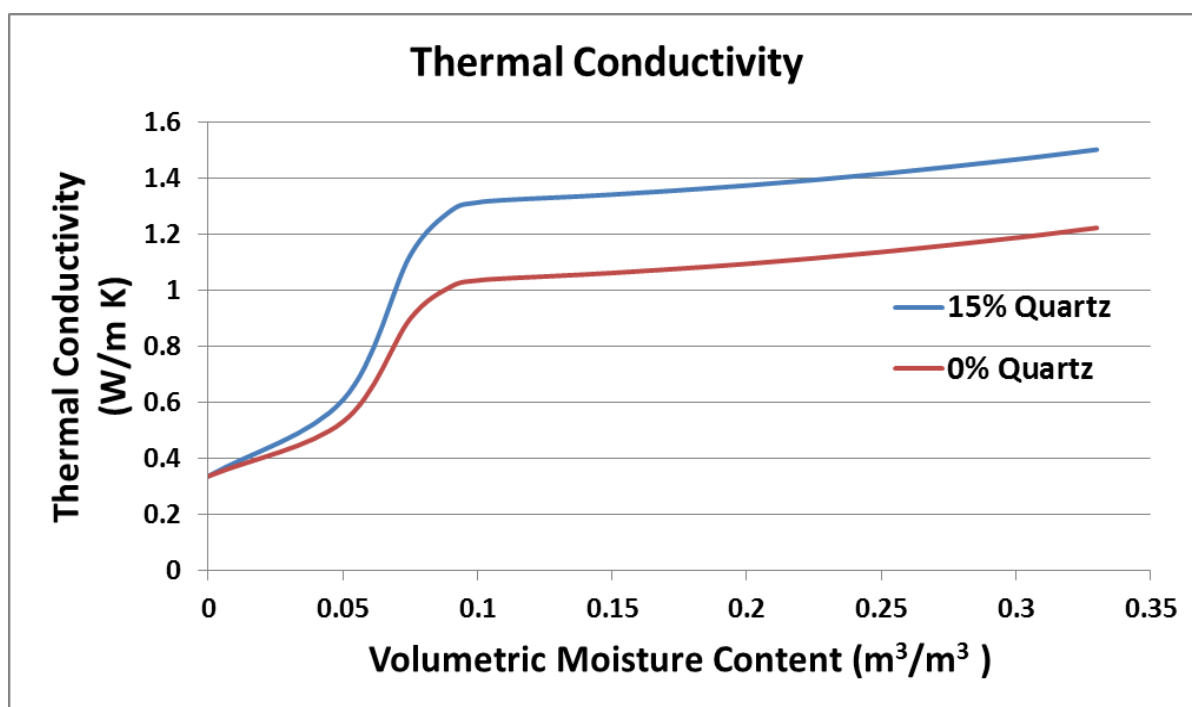


Figure 7.2.4a. Curve relating thermal conductivity and volumetric moisture content according to Campbell model. For comparison purposes, curves are presented using the actual quartz fraction (14.55%) and also assuming the soil contains no quartz.

The above figure shows the impact that quartz content has on the thermal conductivity of bulk soil. In addition, the curve follows the typical thermal conductivity and soil moisture relationship. Thermal conductivity is very low under dry conditions because air is filling of the pores. As moisture content increases, thermal conductivity

rapidly increases because well conducting water not only displaces the poorly conducting air, but also serves to connect the solid grains. As more water is added, thermal conductivity continues to increase but at a much slower rate, because at this point most connections between solid particles are already complete.

Recall that thermal diffusivity is the ratio of thermal conductivity to heat capacity. In addition, when modeling thermal properties based off of soil temperatures, it is thermal diffusivity that is directly modeled and not thermal conductivity. It is much easier to convert the above curve to a relationship between thermal diffusivity and soil moisture than it is to convert all modeled thermal properties to thermal conductivity. Also recall that volumetric heat capacity as it depends on soil moisture content was previously determined to be

$$C_{soil} = 4.18\theta + 1.2816. \quad \text{Equation 7.2.4}$$

By dividing the thermal conductivity results created using the Campbell model by the above defined volumetric heat capacity over the entire range of saturation, the Campbell model can be used to create a relationship between thermal diffusivity and volumetric moisture content.

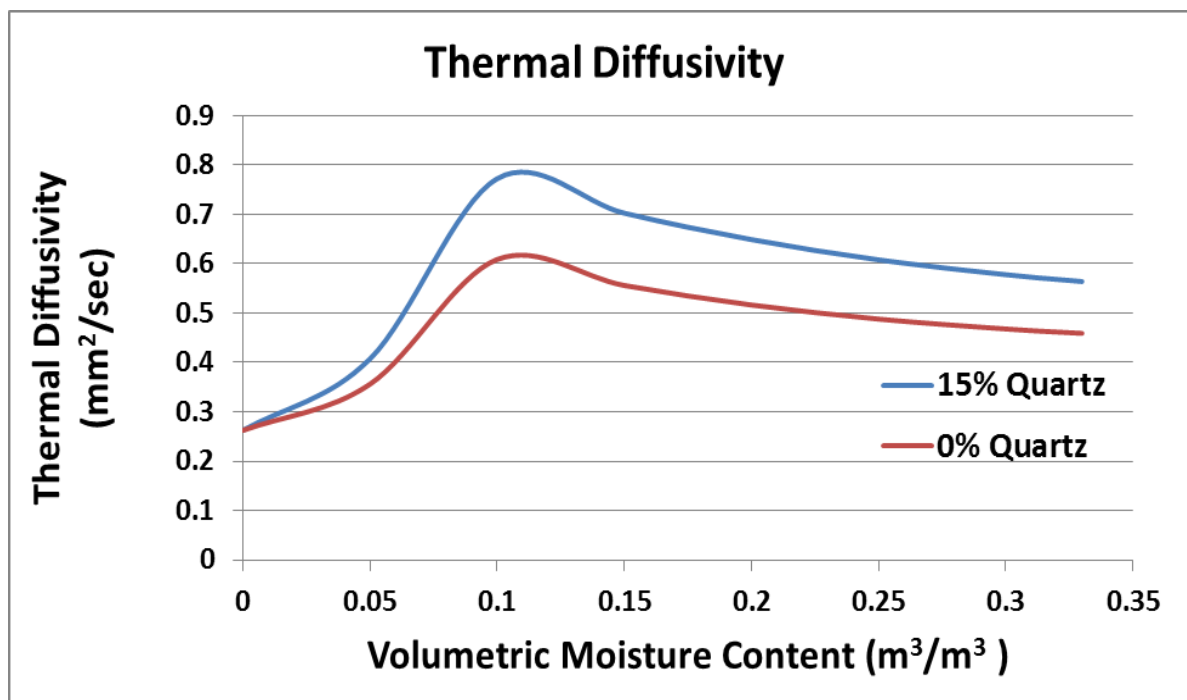


Figure 7.2.4b. Curve relating thermal diffusivity and volumetric heat capacity according to Campbell model. For comparison purposes, curves are presented using the actual quartz fraction (14.55%) and also assuming the soil contains no quartz.

Apparent in the above figure is the non-uniqueness that exists between thermal diffusivity and soil moisture. For a given thermal diffusivity value, there is potential for two corresponding moisture contents. Hence, when trying to estimate soil moisture based on thermal diffusivity, it is important to have prior knowledge of where on the moisture curve the soil is located; i.e. whether the soil is wet or dry.

Efforts were also carried out in an attempt to create the above relationships using measurements on the soil of interest to ensure that the Campbell model did in fact fit the soil at the field site. Whereas the Campbell model was developed empirically to fit as many soil types as possible, it is still important to develop a similar relationship with the

specific soil of interest. Ideally, measurements of thermal properties would be completed *in situ* under various soil moisture contents. This proved very difficult to achieve for this study however, so measurements were conducted on soil cores brought back to the lab instead, with varying soil moisture conditions achieved via use of a pressure plate extractor. The following table presents the results, followed by several figures showing the curves relating the measured thermal properties to volumetric moisture content, and how these relate to the curves developed using the Campbell model.

Measured Thermal Properties and Moisture Contents

Sample Number	Volumetric Moisture Content (m^3/m^3)	Thermal Conductivity (W/m K)	Thermal Diffusivity (mm^2/sec)
1	0.27	1.46	0.65
2	0.23	1.38	0.67
3	0.19	1.38	0.65
4	0.15	1.38	0.70
5	0.13	1.36	0.73
6	0.13	1.23	0.72
7	0.11	1.16	0.57
8	0.06	0.97	0.43

Table 7.2.4. Averaged results from lab experiment measuring thermal properties using a Decagon KD-2 Pro Thermal Properties Analyzer under drying conditions.

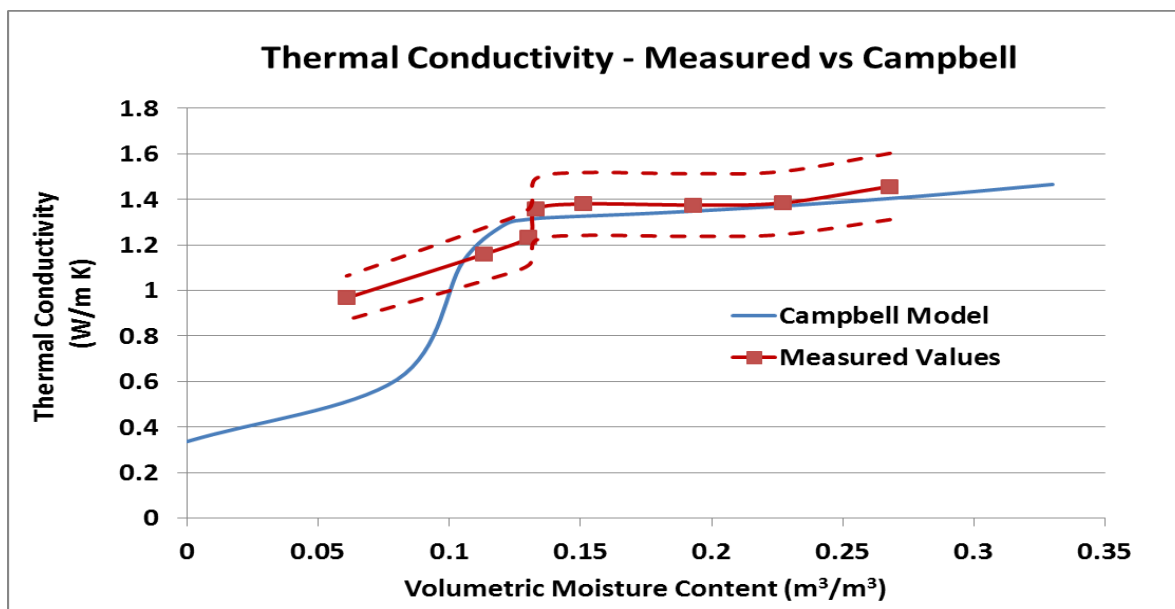


Figure 7.2.4c. Comparison between the thermal conductivity results obtained via measurement of soil cores and those created according to the Campbell model. The dashed red lines show the $\pm 10\%$ accuracy range provided by the KD-2 Pro sensor.

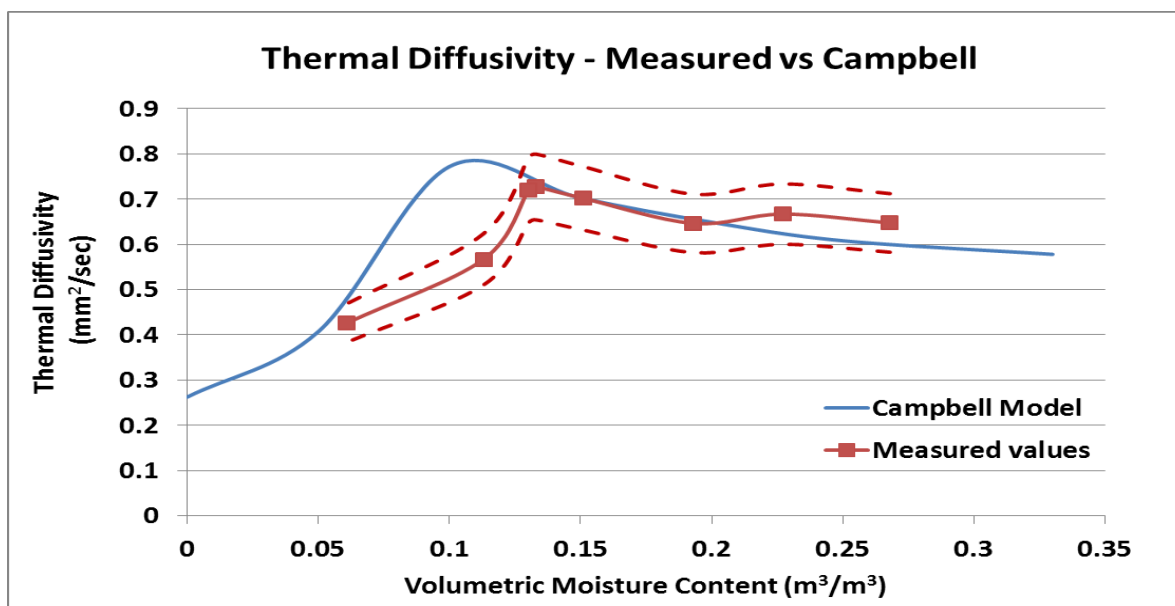


Figure 7.2.4d. Comparison between the thermal diffusivity results obtained via measurement of soil cores and those created according to the Campbell model. The dashed red lines show the $\pm 10\%$ accuracy range provided by the KD-2 Pro sensor.

The SH-1 dual-needle sensor of the KD-2 Pro Thermal Properties Analyzer provides thermal conductivity measurement accuracy of $\pm 10\%$ in the range of 0.2 to $2 \text{ W m}^{-1} \text{ K}^{-1}$ and thermal diffusivity measurement accuracy of $\pm 10\%$ at conductivities larger than $0.1 \text{ W m}^{-1} \text{ K}^{-1}$ (Decagon, 2008). The dashed red lines on the two preceding figures provide the measured values plus or minus this 10% accuracy.

Considering the previous figures, it is apparent that the measured values and the modeled values agree fairly well, especially in regards to the magnitude of the thermal properties. The primary discrepancy lies in the water content at which the peaks in the curves occur. The Campbell model for thermal diffusivity features a peak value that occurs at a volumetric moisture content of $0.11 \text{ m}^3/\text{m}^3$. The curve derived in the lab, however, features a thermal diffusivity peak that occurs at a volumetric moisture content of $0.14 \text{ m}^3/\text{m}^3$. The primary cause for a shift in the location of peaks is the amount of clay in the sample. Generally speaking, varying the amount of quartz content in the Campbell model shifts the curve up or down, while varying clay content shifts the curve to the left and right. This slight difference in curves will be further discussed in section 7.4.3 when soil moisture results are presented.

7.3 TEMPERATURE ANALYSIS

A key component of this study is the analysis of temperatures observed at three depths in the shallow subsurface under varying crop types. The patchwork layout of the field in which different crop types are located about every 9 meters provides an ideal

setup for investigation of temperatures under these different crops. The high resolution temperature measurements obtainable with distributed temperature sensing technology allows for very easy investigation of temperatures over large ranges as well as smaller ranges of interest. To illustrate the basic diurnal cycle of temperatures in the shallow subsurface, the following figure presents temperature series from three depths at the same location in a tall fescue plot, over a span of 8 days. The expected lag time in daily temperature maximums as well as decreased amplitude as depth increases is clearly evident.

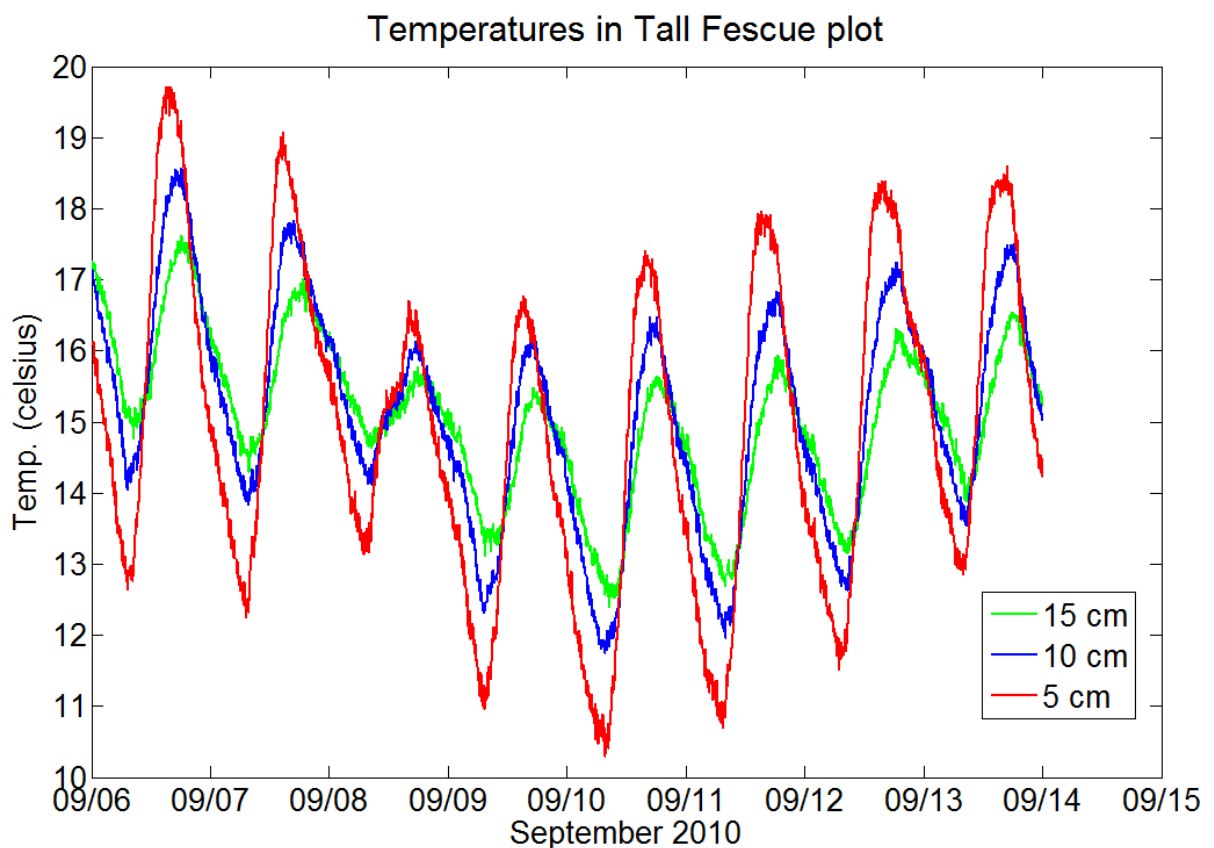


Figure 7.3.1. Example of diurnal temperature series from 5, 10, and 15 centimeters depth. Note the decreased amplitude and lag time between daily maximums as depth increases.

Many of the figures that follow present temperature data on a per plot basis. Using every meter of data would produce noisy data making it difficult to distinguish between plot and crop type boundaries. In an effort to provide easily understandable and presentable data, two points within each plot were selected. These points are used as representative locations for the entire plot from which they are located. Within each plot, the locations selected for use in analysis were equally spaced and away from plot edges where boundary conditions could come into play. For example, the cables ran through many of the plots for a total of 9 meters. Instead of including all 9 meters in the following figures, meters 3 and 6 were selected and used to represent that particular plot. Before the temperature results can be shown however, the crop type that corresponds with each plot number needs to be specified. Table 7.3 provides this information.

Plot Number Descriptions

Plot Number	Description	Plot Number	Description
1	Ice Water Bath	14	Basin Wild Rye (Bas)
2	Ambient Water Bath	15	Basin Wild Rye (Bas) – NO irrigation
3	Tef Brown variety (TefB)	16	Insulated Foam Tube
4	Tef Brown variety (TefB)	17	Tall Fescue (Fes) – NO irrigation
5	Tef Brown variety (TefB) – NO irrigation	18	Tall Fescue (Fes)
6	Tef Brown variety (TefB) – NO irrigation	19	Tall Fescue (Fes)
7	Mammoth Wild Rye (Mam)	20	Tall Fescue (Fes)
8	Basin Wild Rye (Bas)	21	Indian Grass (Ind)
9	Sand Bluestem (San)	22	Alfalfa (Alf) – NO irrigation
10	Bluestem (Blu)	23	Tall Fescue (Fes) – NO irrigation
11	Prairie Sandreed (Pra)	24	Alfalfa (Alf)
12	Tall Wheatgrass (Tal)	25	Alfalfa (Alf)
13	Basin Wild Rye (Bas)		

Table 7.3.1. Description of what each plot number on upcoming figures represents. Note that plot numbers 1, 2, and 16 do not represent crops. Plots 1 and 2 are water baths for DTS calibration purposes, and plot 16 is a foam tube outside of the crops in which all three cables were buried together. Also, plots 5, 6, 15, 17, 22, and 23 were under the 50% irrigation schedule and so received no direct irrigation during this study period, as the irrigation for 50% plots was already turned off for the season.

The mean daily temperature across the field should be fairly consistent, no matter the depth of measurement or the surface crop type. From Figure 7.3.1, it is easy to see

that although the daily maxima and minima are clearly different for the different depths, the daily average temperature of each cable is approximately the same. Temperature extremes at shallower depths stray farther from the daily mean, but the mean is nevertheless similar for all three depths. Considering this fact, the most telling variable to consider when comparing temperature measurements across various crop types is the maximum daily temperature of the top cable. The maximum or minimum daily temperature at any of the depths would provide the same analysis, but the shallowest depth provides the least amount of temperature damping and therefore the most noticeable results. The following figure presents the maximum daily temperature of the top cable across all plots over the 25-day study period.

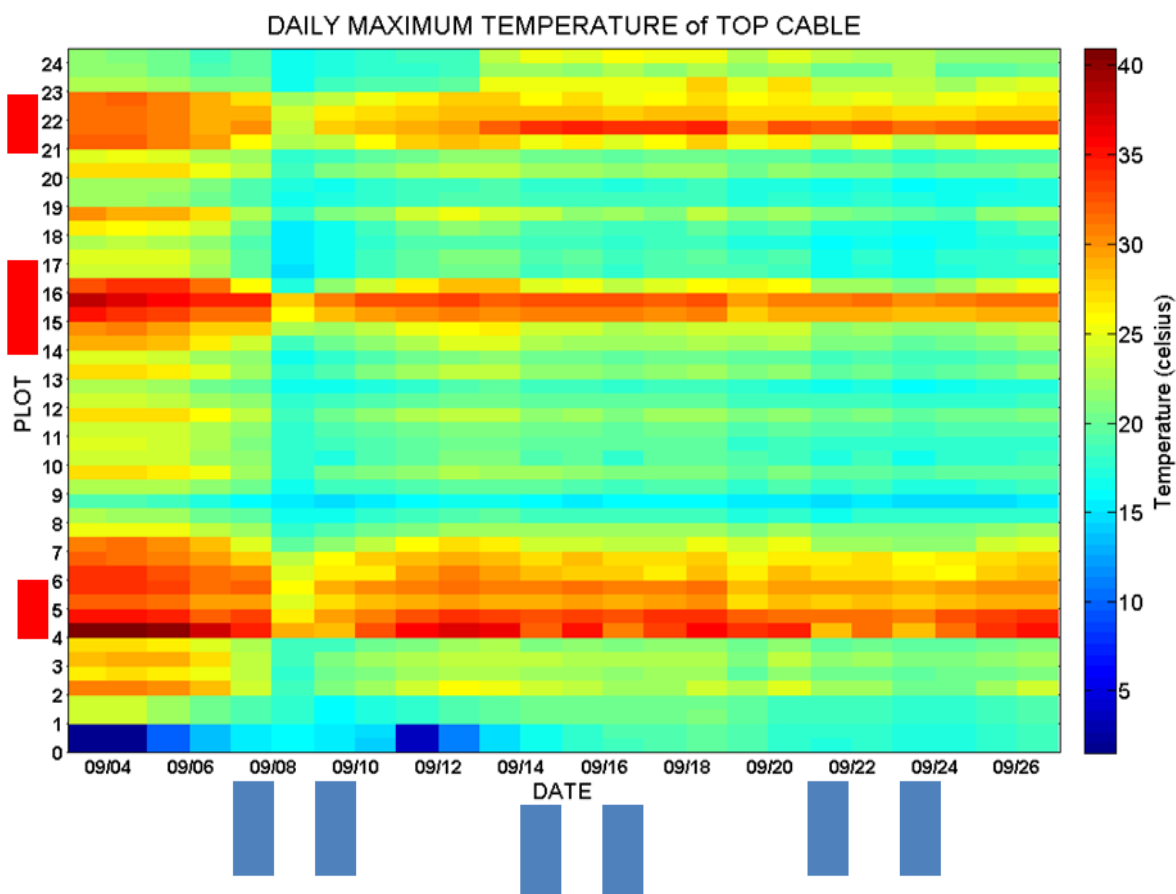


Figure 7.3.2. Daily maximum temperature observed at a depth of 5 centimeters. There are two measurement points within each plot. Table 8.3 provides the description of each plot number. Blue rectangles on x axis represent irrigation events and red rectangles on y axis delineate those plots that received no irrigation throughout the study.

From the figure 7.3.2, it is apparent that the shallow subsurface within certain plots stays noticeably warmer throughout the study period than other plots. There are also certain dates during the 25-day study period where all measurements within each plot were cooler than the average temperature for the respective plot. This will be further analyzed in the Discussion section of this thesis.

An obvious secondary analysis when comparing temperatures across varying crop types within a field is simply the average daily maximum temperature of each crop. Figure 7.3.2 presents temperature data through time for each plot, with plot number determined by path of the cables. In other words, in the field, the cable first goes through plot 1, then 2, then 3, all the way through plot 25. However, the same crop types are not always adjacent to one another in the field, and so figure 7.3.2 does not provide an ideal means to simply compare average daily maximum temperature across each crop type. By taking the average daily maximum temperature from 5 centimeters depth for each plot, then averaging the same crop types together, the following figure was created.

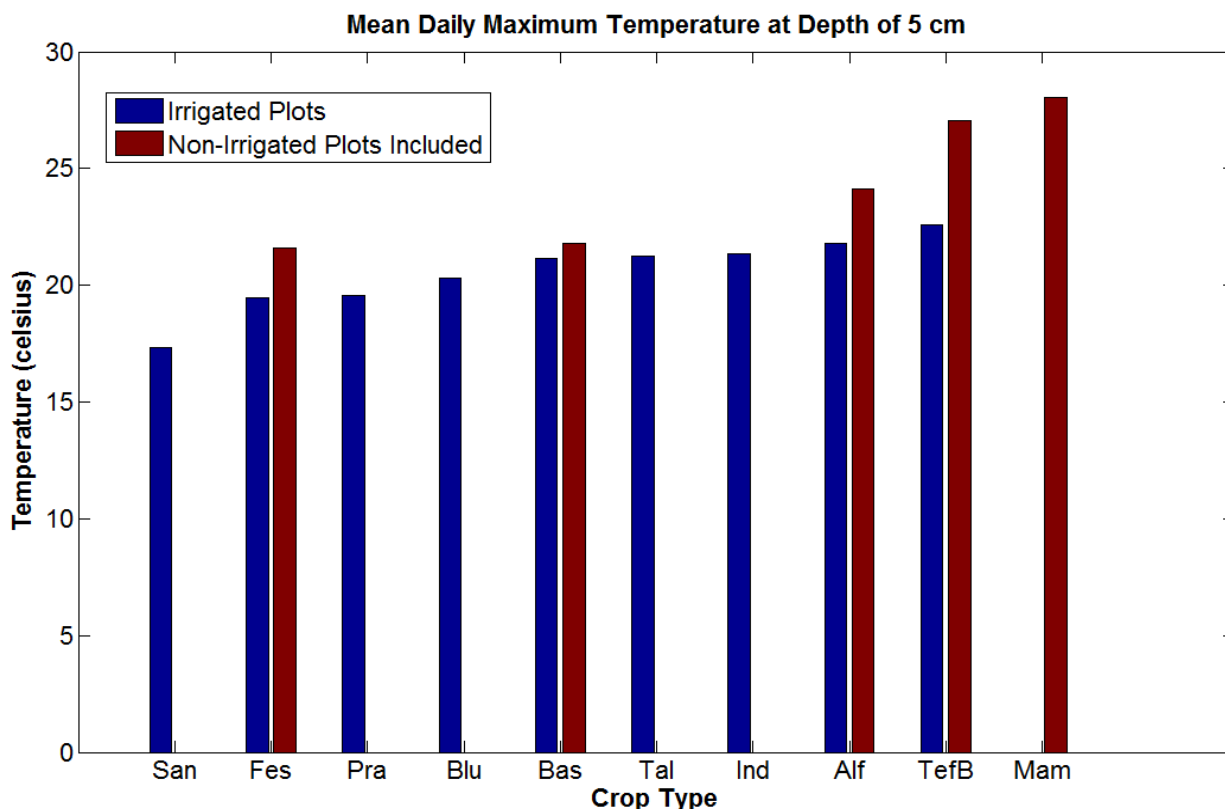


Figure 7.3.3. The mean daily maximum temperature from a depth of 5 centimeters for each crop type. The red non-irrigated bars provide the average temperature of that crop type when plots that received no irrigation are included in the calculated average.

Figure 7.3.3 shows that there is approximately a 4 to 5 degree difference between the highest mean daily maximum temperature and the lowest mean daily maximum temperature, when considering only the irrigated crops. It is also evident that plots that did not receive irrigation exhibit a noticeable increase in shallow subsurface temperatures. Recall from Table 7.2.1c that irrigation typically only occurred on Tuesdays and Thursdays. Therefore, only two days of irrigation per week was sufficient to greatly reduce the average mean daily maximum temperature observed at a depth of 5 centimeters. Note that the cables were only installed through one plot containing Mammoth Wild Rye (Mam) and that plot received no irrigation during the 25-day study period.

The previous figures were primarily the results of investigations into the effect that surface crop type has on soil temperatures in the shallow subsurface. Some investigation into the effect that irrigation has on these same subsurface temperatures is also warranted. Unfortunately during the particular month of study, none of the individual plots experienced a change in irrigation pattern. Plots either received irrigation according to the schedule outlined in table 7.2.1c for September of 2010, or they received no irrigation. Therefore, while a change in overall irrigation schedule cannot be investigated, the potential effect of an irrigation event on soil temperatures should still be apparent. Upon irrigation, water is added to the soil matrix resulting in a damping of the diurnal temperature signal. The maximum soil temperature reached under wet conditions should be lower than under dry conditions. Likewise, the minimum temperature reached under wet conditions should also be higher than under dry

conditions. The greater this effect, the more heat transfer that is occurring due to advection and not conduction. Therefore, a simple soil temperature analysis that should reveal the effect irrigation has on subsurface temperatures is a plot of the difference between the daily maxima and the daily minima across the 25-day study period. The minimum daily temperature observed at a depth of 5 centimeters was subtracted from the maximum daily temperature observed at a depth of 5 centimeters, and the results shown per plot over the length of this study. The same analysis was conducted for a depth of 10 centimeters, and again for a depth of 15 centimeters (Figures 7.3.4, 7.3.5, and 7.3.6).

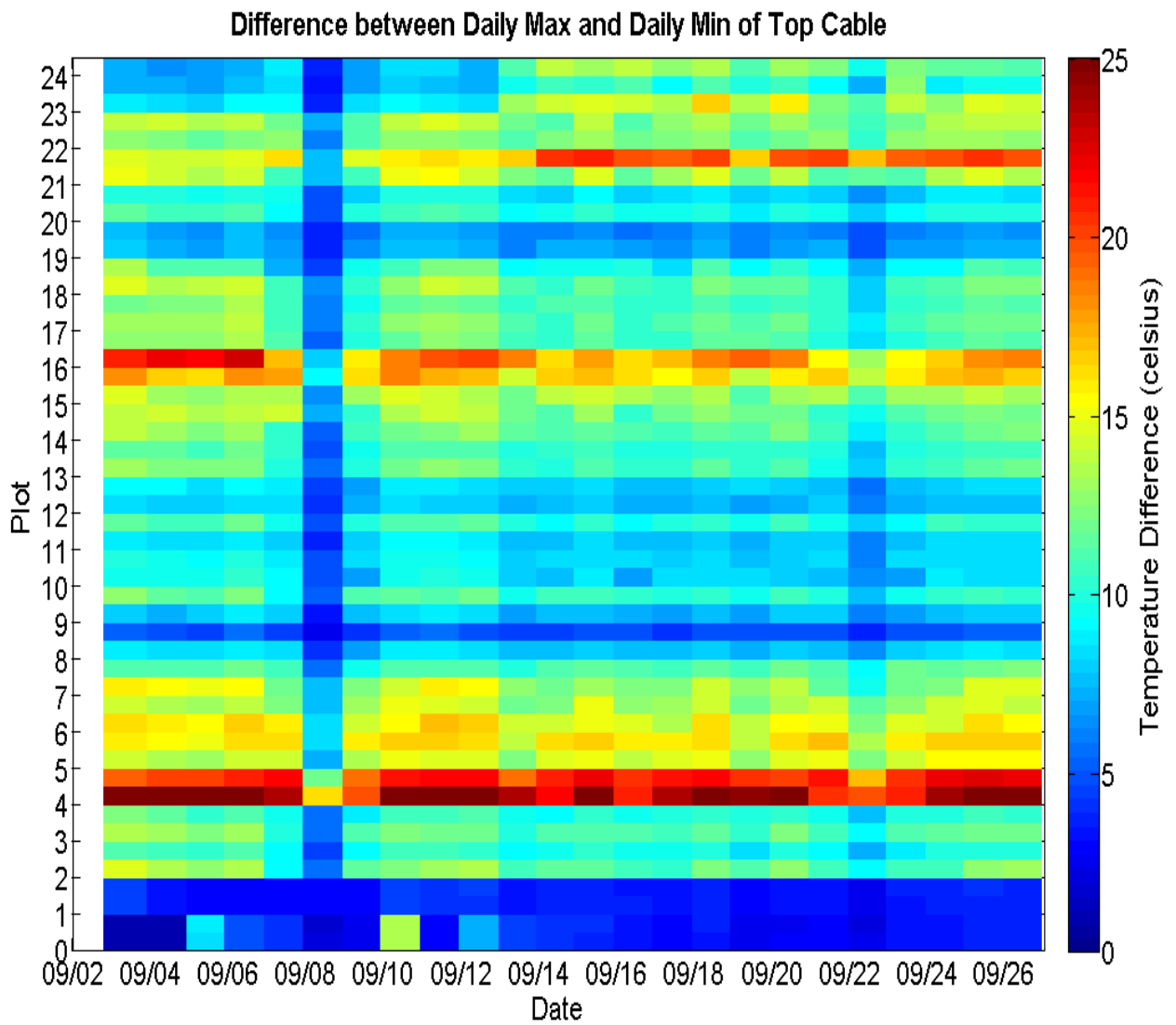


Figure 7.3.4. Temperature difference between the daily maximum and daily minimum temperatures at a depth of 5 centimeters.

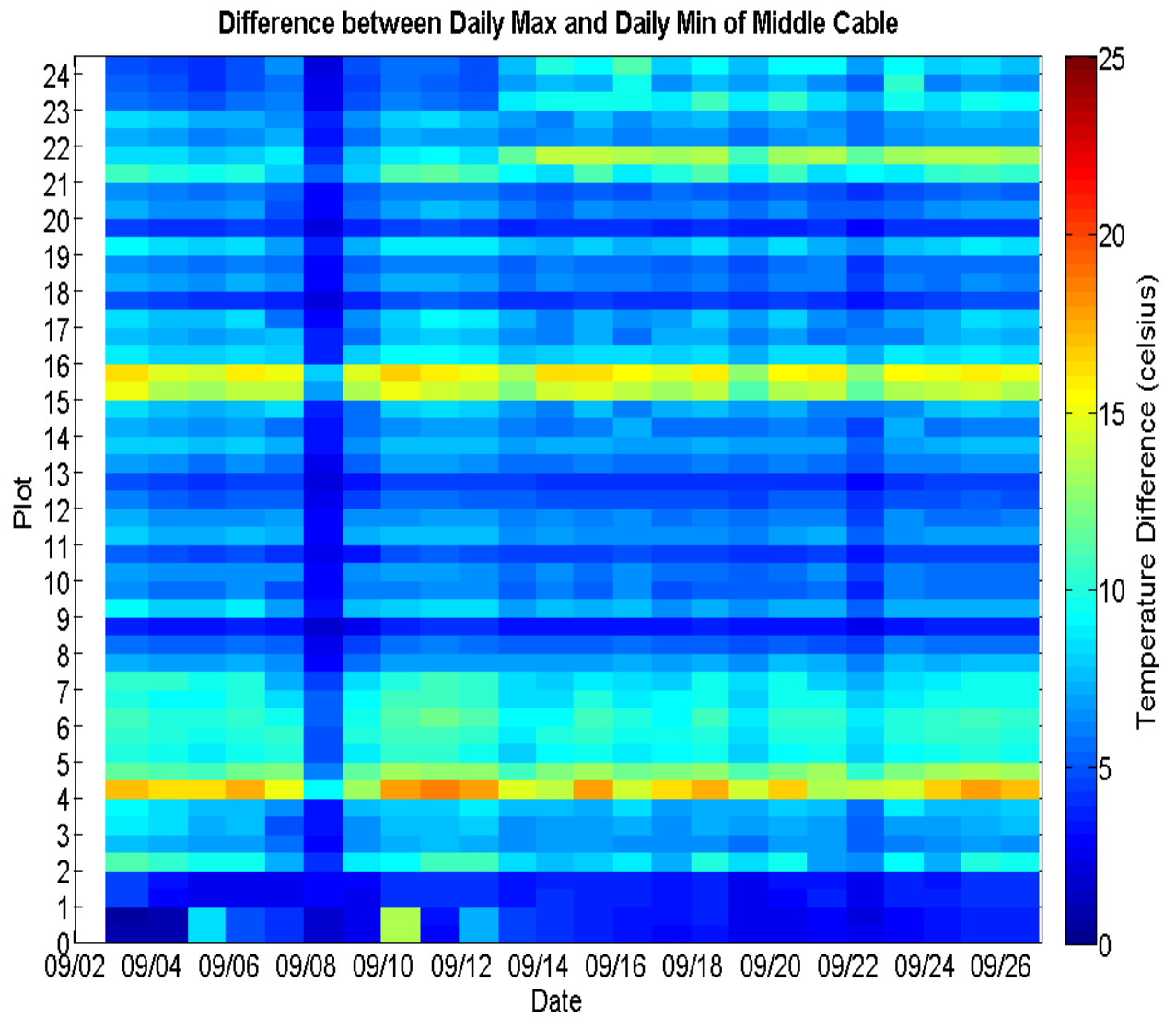


Figure 7.3.5. Temperature difference between the daily maximum and daily minimum temperatures at a depth of 10 centimeters.

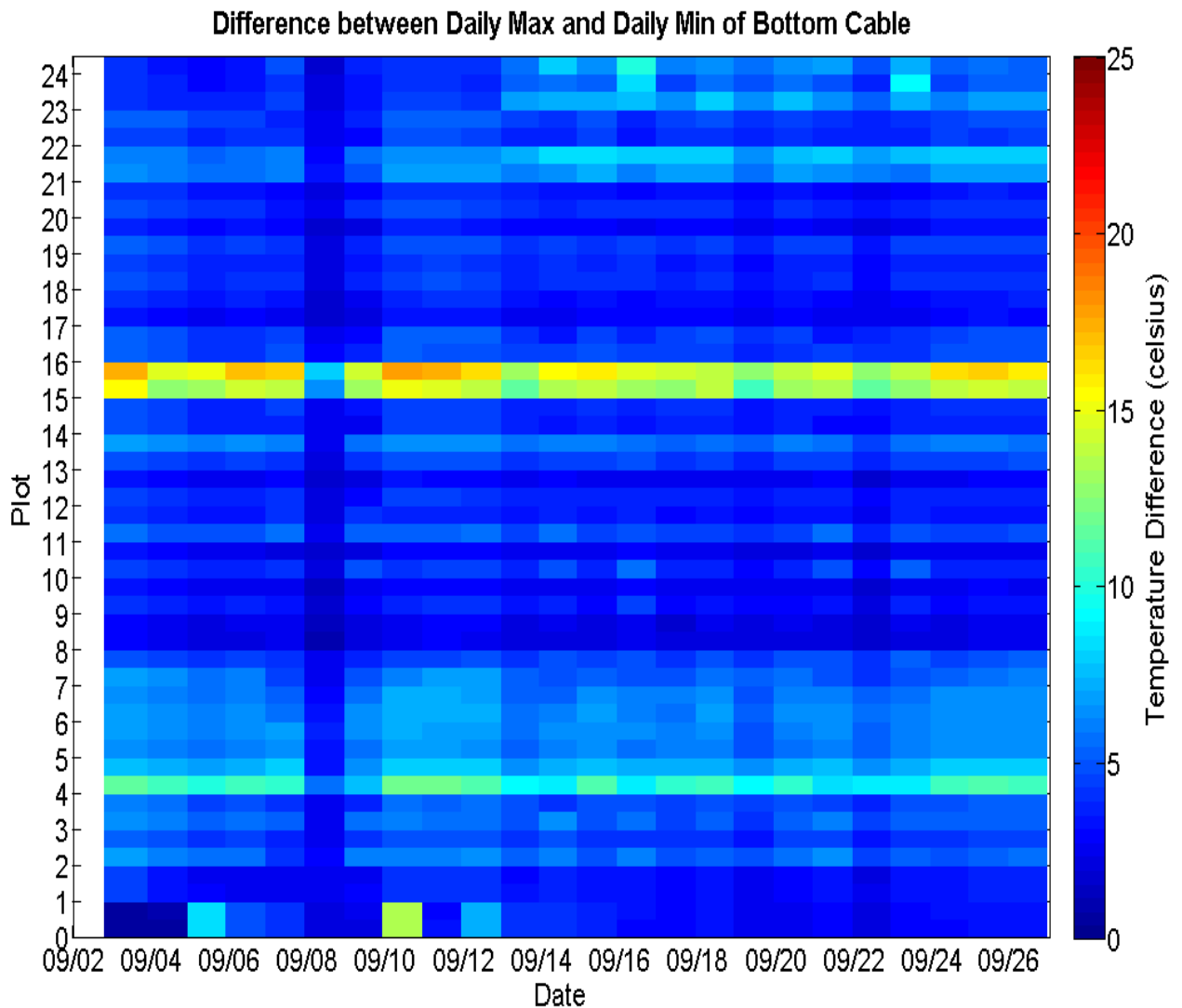


Figure 7.3.6. Temperature difference between the daily maximum and daily minimum temperatures at a depth of 15 centimeters.

From the three previous figures it is apparent that at greater depths the difference between the daily maximum and daily minimum decreases. This is as expected and is because the temperature damping that occurs as depths increase. It is also apparent that the highest temperature difference occurs within the same plots for all three depths considered. It is worth reiterating here that plot 16 is where the three cables were all

buried together and placed within a black, foam tube. Because they were all buried together, the top, middle, and bottom cables are actually at the same depth, and therefore the difference between maximum and minimum daily temperatures should not change within plot 16 even when looking at different cables. A quick reference to the irrigation data is provided below, where the timing of irrigation is presented just for the month of September, which is the month in which these temperature analyses take place.

Irrigation Schedule

Date (2010)	Amount of Water Applied (acre feet)	Amount of Water Applied (centimeters)
September 7 th	0.32	5.9
September 9 th	0.34	6.3
September 14 th	0.36	6.8
September 16 th	0.38	7.2
September 21 st	0.34	6.3
September 23 rd	0.35	6.5
September 28 th	0.11	2.1
September 30 th	0.30	8.1

Table 7.3.2. Date and amount of water applied for each scheduled irrigation event for the month of September, 2010.

A cross reference between the irrigation schedule and the preceding figures does not reveal any obvious trend of decreased difference between daily maximum and daily minimum temperatures during days when irrigation occurred, as was expected. This fact lends validity towards the simplified assumption used in the conduction model that at the

depths considered, conduction is the primary mode of heat transfer. This will be further analyzed in the upcoming Discussion section.

7.4 MODELING RESULTS

7.4.1 Excel Finite-Difference Mesh compared to MATLAB Conduction Model

The modeling results presented in this section will include brief results comparing the thermal diffusivity estimates obtained from the Excel finite-difference mesh and the MATLAB conduction model at one particular location. Because the Excel finite-difference mesh was used primarily as a means for initial investigation into thermal diffusivity, in depth results were not completed once similar results were obtained using the much easier to work with MATLAB model. Following the comparison between models, the overall results from the MATLAB conduction model over the entire cable length and study period are presented. Subsequent to the presentation of the spatial distribution of thermal conductivity on the field scale, the modeling results of soil moisture will then be presented.

A finite-difference approach was initially followed in Excel in an effort to estimate thermal diffusivity given observed temperature data at three depths. The mesh utilized a spatial step of 1 centimeter and a temporal step of 30 seconds. Thirty seconds was necessary for stability requirements within the method. Assuming conduction is the

only form of heat transfer taking place, an equivalent of the conduction equation is used to explicitly populate the model domain with simulated temperatures. By minimizing the error between simulated temperatures at 10 centimeter depth and the observed temperatures at 10 centimeters depth, the best diffusivity value is estimated for that particular window of time. In using the finite-difference mesh, resolutions of 2, 12, and 24 hours were investigated over the same 5 day period. For example, when considering 12 hour resolution, one thermal diffusivity value was estimated for the first 12 hours, then a new thermal diffusivity value was estimated for the subsequent 12 hours, and so on. These values are all derived from temperature data collected at the same point within a tall fescue plot.

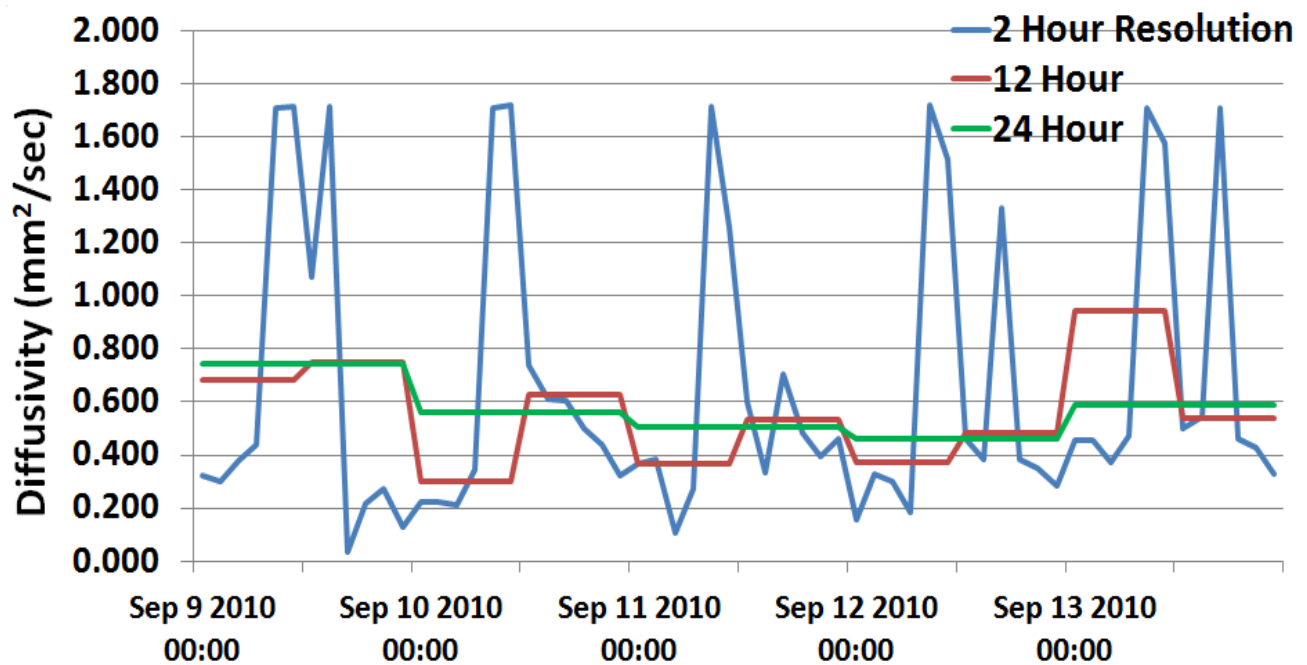


Figure 7.4.1a. Thermal diffusivity results from finite difference mesh assuming only 1-dimensional unsteady conduction. Estimates presented for three different temporal resolutions.

It is apparent from the above figure that as the resolution becomes coarser, the diffusivity estimates become less noisy. The high peaks that are seen with 2 hour resolution occur roughly at 11 AM every day. At this time in the diurnal temperature series, the temperatures at all three depths are roughly the same. Therefore, the change in temperature over the 10 centimeter model domain approaches zero. Mathematically speaking, if ΔT (change in temperature) approaches zero, then with all other things equal, the thermal diffusivity must become very large to compensate. Because this effect is not masked with small temporal resolutions and leads to aberrant thermal diffusivity estimate, this lends validity towards utilizing longer temporal resolutions.

Through correspondence with Susan Steele-Dunne, it was determined that a conduction model written in MATLAB that she had separately developed modeled thermal diffusivity under the same assumptions used in the finite-difference mesh. The scripts written in MATLAB provided a much more automated and efficient means to estimate thermal diffusivity over space and time. Before utilizing the MATLAB code however, it was first necessary to see how results obtained via the MATLAB conduction model and the finite-difference mesh compared. The following figure provides this comparison between the two models. Ideally, the results should be identical since they are predicting thermal diffusivity over the same time frame and at the same location in the field. Estimates are presented over the same three temporal resolutions as in figure 7.4.1.

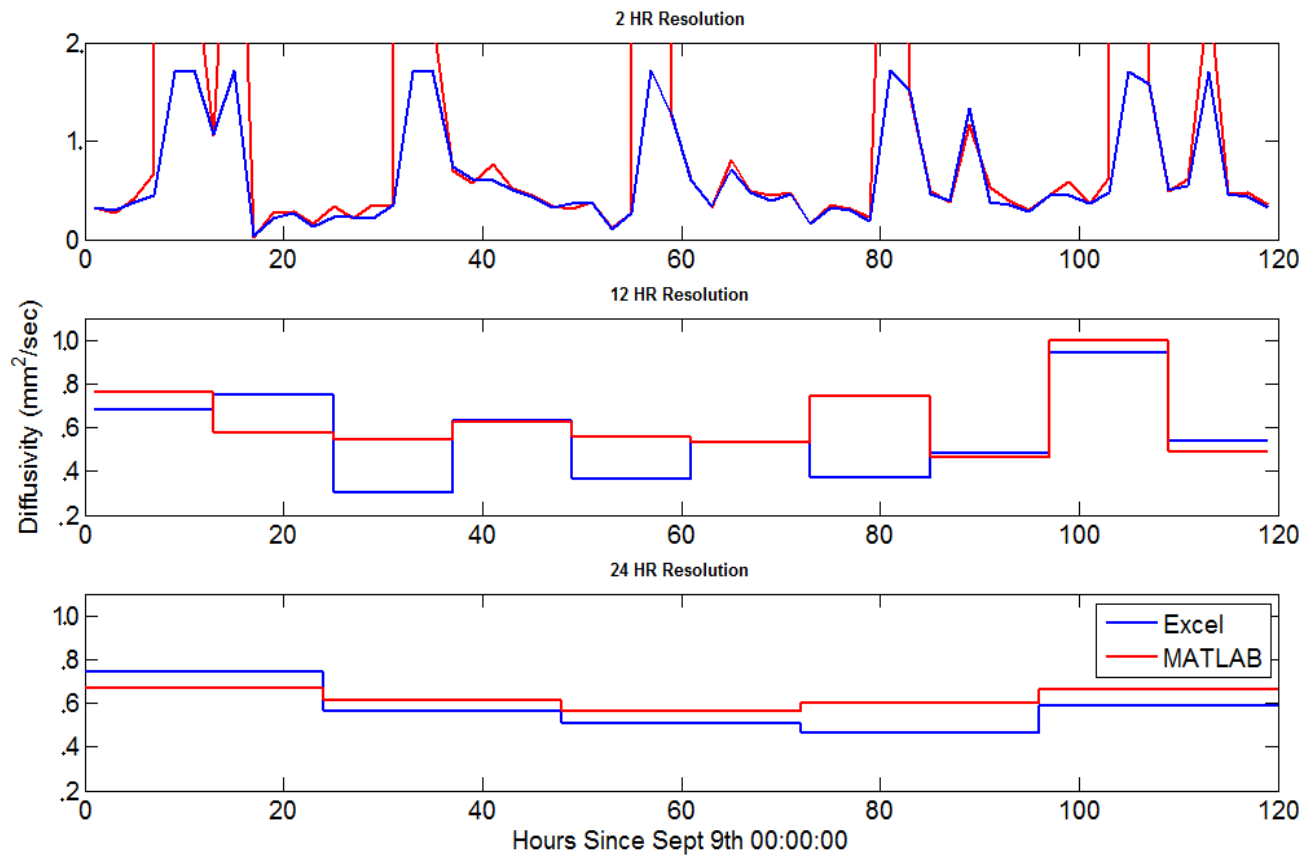


Figure 7.4.1b. Comparison between thermal diffusivity estimates obtained using a finite-difference mesh in Excel and a conduction model in MATLAB. Blue lines represent the Excel data, and red represents the MATLAB data.

It is clear that there is a good match between thermal diffusivity estimates obtained via both modeling methods. With 2 hour resolution, the diffusivity results match very well at all times other than during those previously described peaks that occur when the temperatures at all three depths are nearly equal. Observance of the 12 hour resolution data then shows this same pattern. The 12 hour increments that do not include the aberrant peaks match almost perfectly, while those increments that do include the peaks result in the MATLAB diffusivity estimates being higher than those derived from

the Excel model. Because there is more data included that can “dampen” the effect of the aberrant peaks, the estimates using 24 hour resolution match even better over the time frame. Since very similar results were obtained using both diffusivity estimating models, the more efficient MATLAB conduction model was used for modeling diffusivity over the entire length of the cable for the entire 25 days.

8.4.2 Estimated Thermal Diffusivity

A conduction model created in MATLAB was used to model soil temperatures and to produce thermal diffusivity estimates. Unlike in the previous figures, where a diffusivity was estimated for one window length, and then again for the next window length with no overlap, this conduction model utilizes a window shift. A window length of 24 hours was chosen, and this window length was then shifted in 6 hour increments. Therefore, one diffusivity value based on 24 hours of temperature data was collected for every 6 hours. This setup allowed for the benefit of less noisy data from the 24 hour window length, but also compensated for lower temporal resolution by providing a thermal diffusivity estimate every 6 hours.

Because thermal diffusivity estimates are based off of simulated temperature profiles derived from inversion in the conduction model, it is important that simulated temperatures match observed temperatures at the three soil depths. Figure 7.4.2a and 7.4.2b present predicted temperatures versus observed temperatures in an irrigated and non-irrigated plot, respectively.

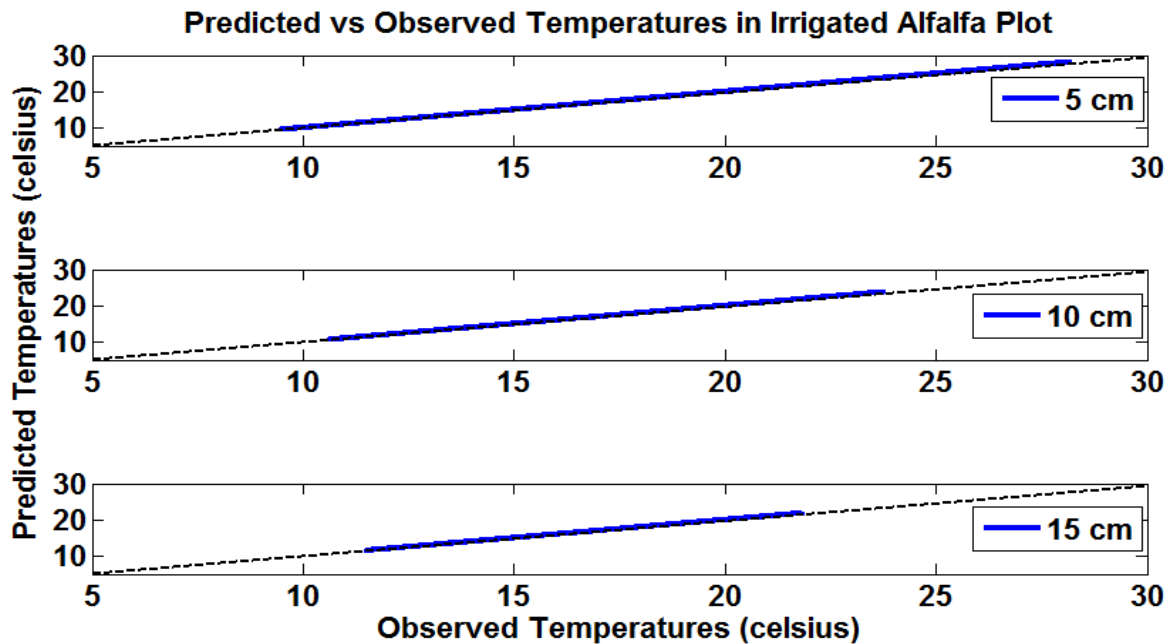


Figure 7.4.2a. Predicted versus observed temperatures at three depths within an irrigated alfalfa plot. A perfect 1 to 1 relationship will fall along the dashed line.

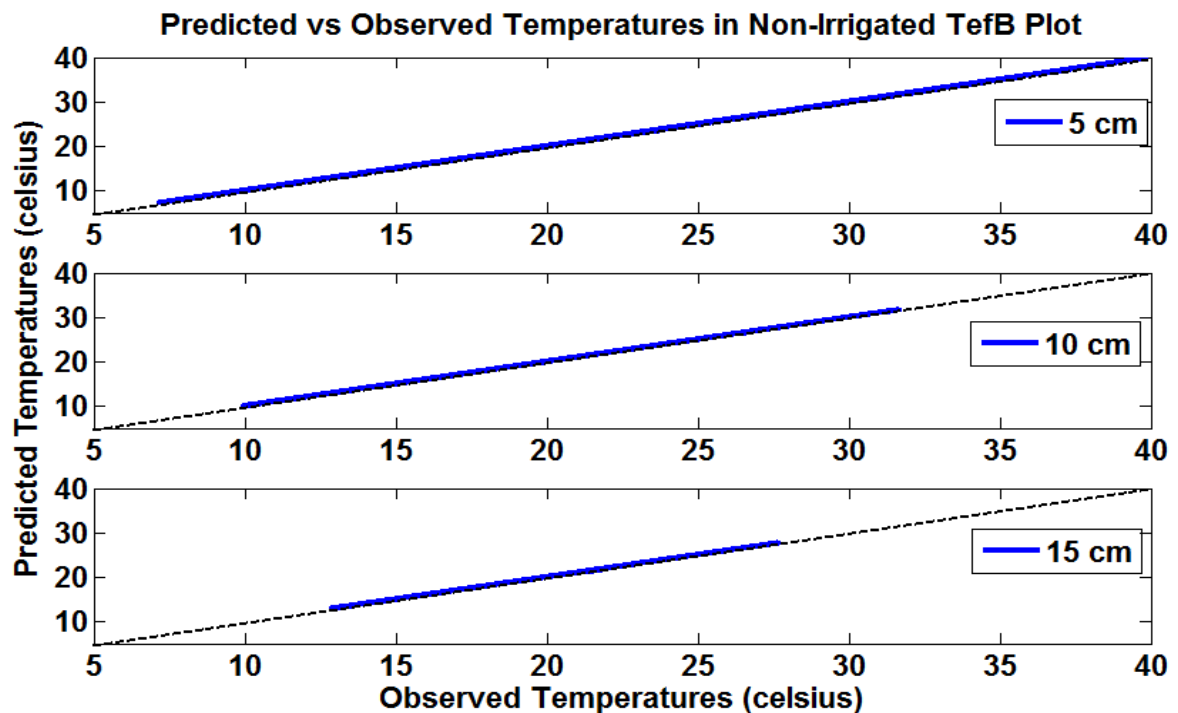


Figure 7.4.2b. Predicted versus observed temperatures at three depths within a non-irrigated tefB plot. A perfect 1 to 1 relationship will fall along the dashed line.

The simulated temperature profiles produced from the conduction model match observed temperatures very well.

The following figures show the resulting diffusivity estimates over time at one particular location. Three figures will be presented, each coming from within a plot of differing crop types and from different parts of the field. Note that the scale of the y-axis differs for each plot.

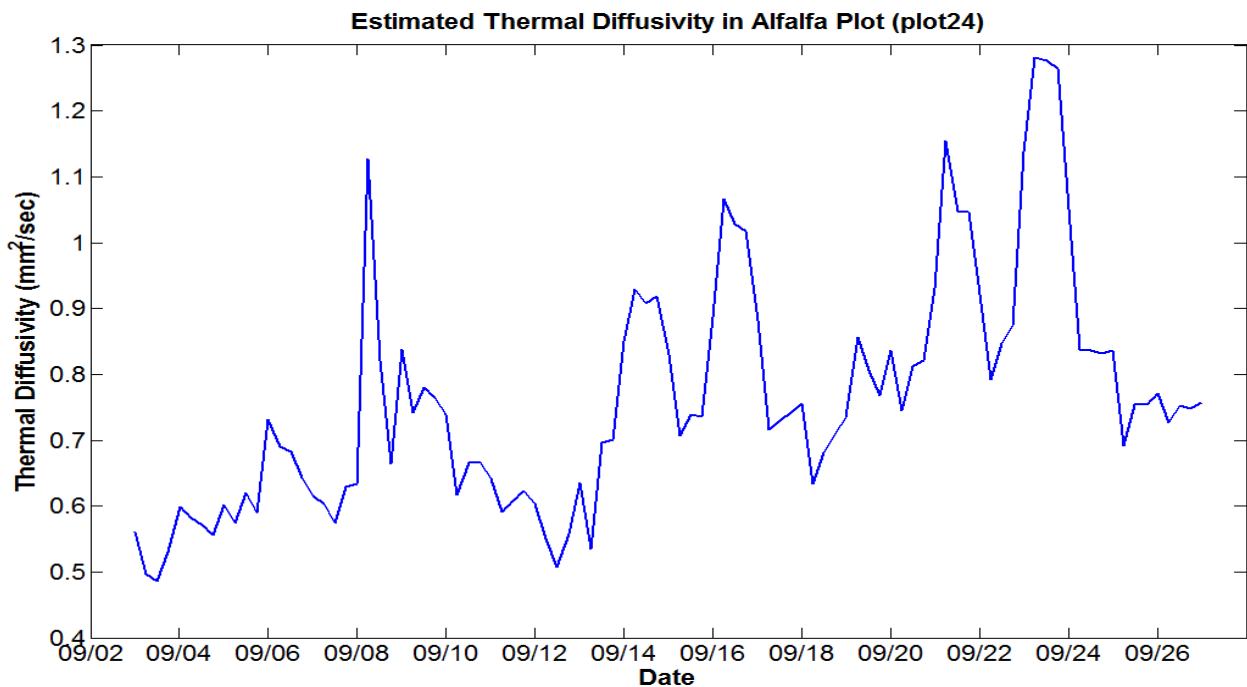


Figure 7.4.2c. Estimated thermal diffusivity in plot 24, an Alfalfa plot, over the 25-day study period.

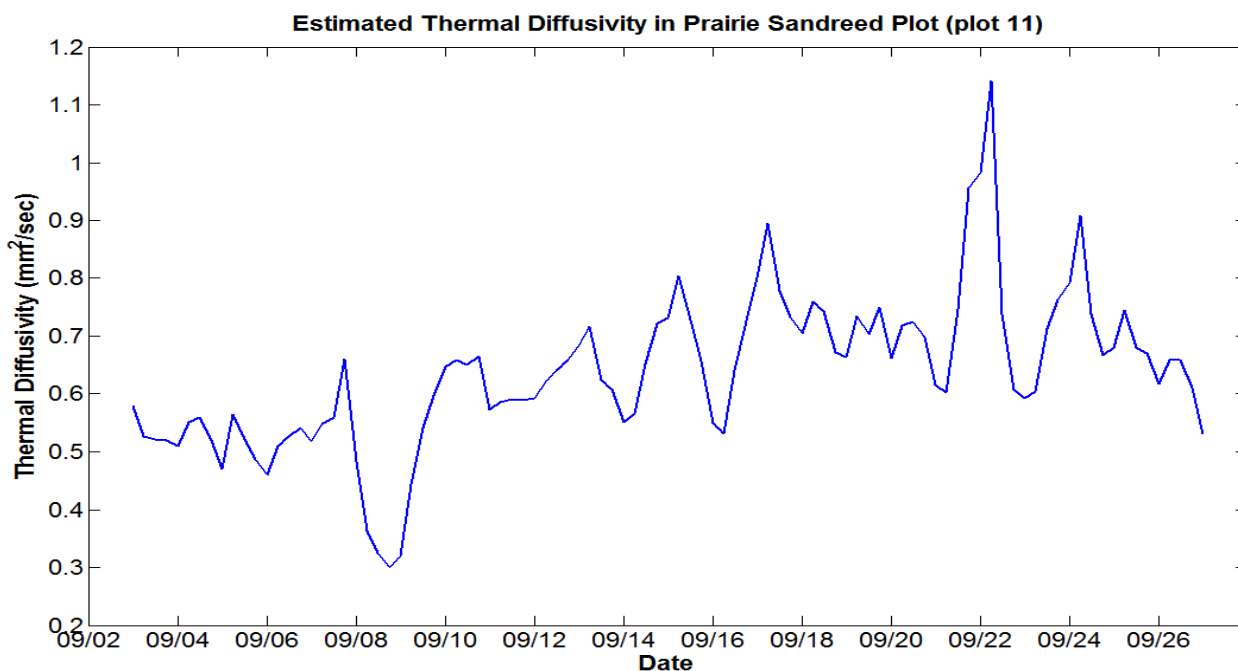


Figure 7.4.2d. Estimated thermal diffusivity in plot 11, a Prairie Sandreed plot. This is the plot in which soil moisture was recorded under 100% irrigation by a wireless met station.

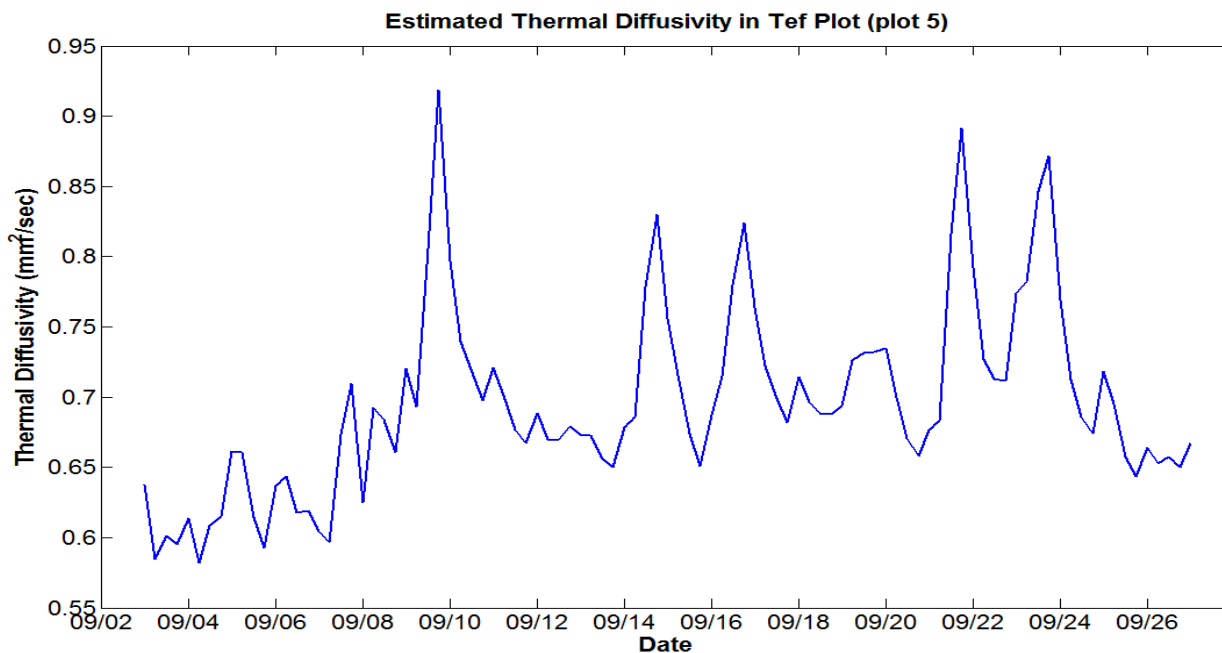


Figure 7.4.2e. Estimated thermal diffusivity in plot 5, a TefB plot. This is the plot in which soil moisture was recorded under 50% irrigation by a wireless met station (i.e. no active irrigation).

The previous three figures present modeled thermal diffusivity results in three different crop types and in three different locations along the cable. These three locations were chosen to provide examples of what thermal diffusivity looks like throughout the field. These provide a detailed look into a specific location. Of particular interest are plots 7.4.2d and 7.4.2e, because these are the same plots from which the wireless meteorological stations recorded soil moisture values throughout the study. However, since the spatial distribution of thermal diffusivity is really the point of interest for this study, a better way to examine the data spatially is necessary.

Unlike with the temperature analyses, there was no point in modeling thermal diffusivity in the water baths, or in the foam tube located outside of the plots in which all three cables were buried together. In addition, two plots were not modeled because of splices that were necessary to repair broken cables. These splices made precisely aligning the top, middle, and bottom cables very difficult. One plot was a tall fescue plot, and the other was an alfalfa plot. The modeled thermal diffusivity results over a spatial scale are presented with total distance as the y-axis. This total distance corresponds to actual meter length. However, because these cables did not run through each plot for the same length, a secondary y-axis is provided. This secondary y-axis provides a means to determine the plot boundaries, with the location of the plot number representing the end of that particular plot. The same plot numbers that were used for temperature analysis are used here for comparative purposes. Refer to table 7.3.1 for plot number descriptions. The plot numbers that were not modeled are plots 1, 2, 16, 20, and

22. The following figure presents the modeled thermal diffusivity results over the field scale.

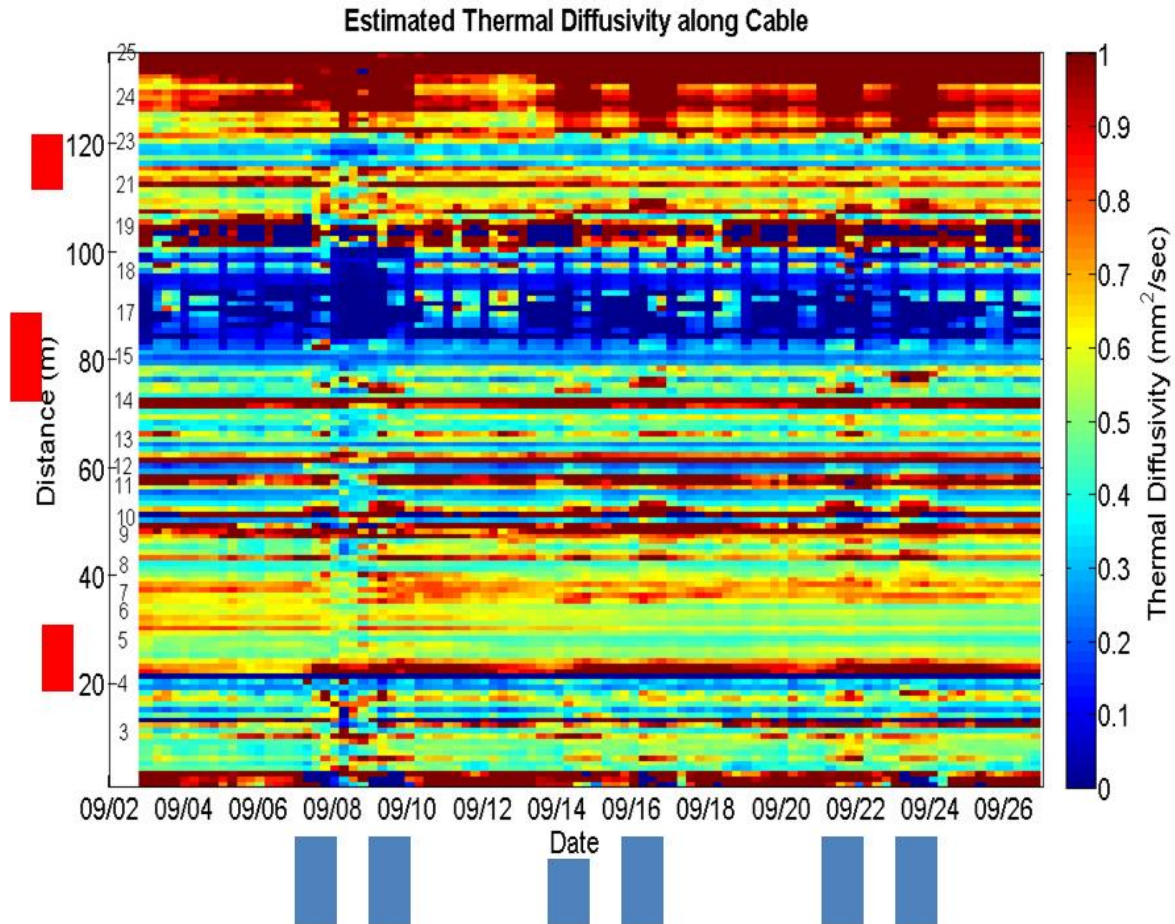


Figure 7.4.2f. Resulting spatial distribution of thermal diffusivity estimates over 25-day study period as produced from MATLAB conduction model. The secondary y-axis (on left) delineates the location of those plot boundaries. The middle of each number marks the end of that particular plot. For example, plot 4 runs from the middle of the “3” to the middle of the “4” on the secondary y-axis.

Figure 7.4.2f presents thermal diffusivity over a spatial scale, based upon observed temperature traces collected at three depths using distributed temperature

sensing. A thermal diffusivity value was estimated for every selected meter over a 25 day period. It is apparent that thermal diffusivity varies greatly over even just a couple of meters. Contrastingly, thermal diffusivity does not appear to vary greatly over time when considering the same location. These results will be further analyzed in the discussion section.

7.4.3 Estimated Soil Moisture

In order to obtain estimates of soil moisture along the cable, the modeled thermal diffusivity values from the previous section must be applied to some equation relating thermal diffusivity to soil moisture. Below is the same figure that was presented in section 7.2.4.

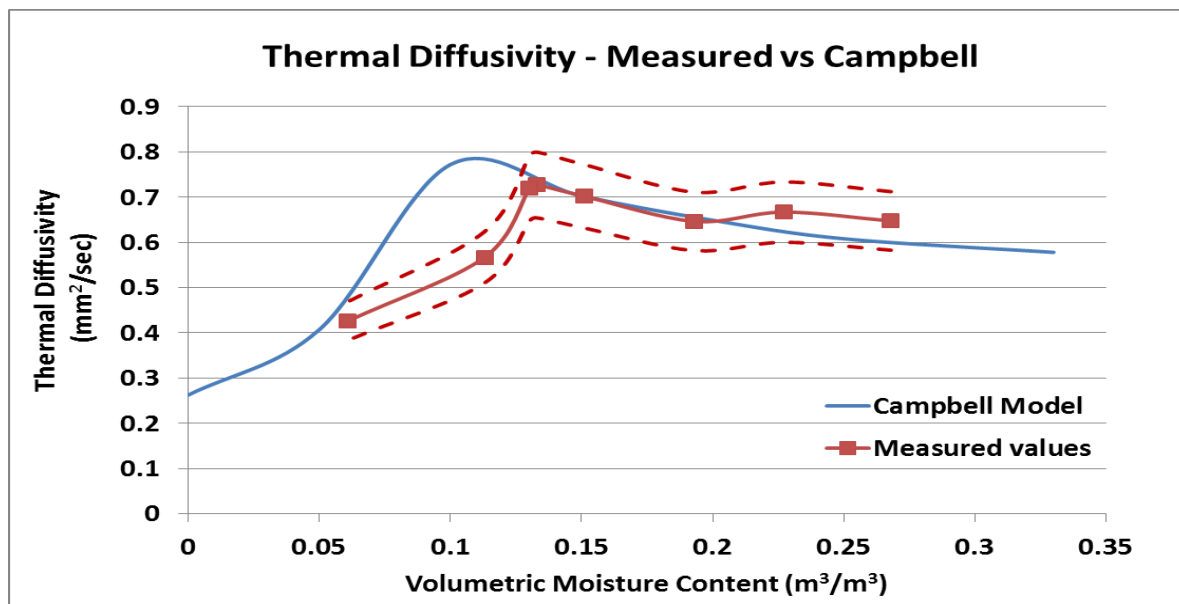


Figure 7.4.3a. Relationship between thermal diffusivity and soil moisture as produced by both the Campbell model and from direct thermal measurements on soil cores.

Ideally, the above two curves would perfectly match. As it is, the derived relationships are very comparable. As mentioned in section 7.2.4, horizontal shifting of the peak in the above relationship is primarily caused by variation in clay content. The above discrepancy is due to a difference in clay content of only 3 to 5 percent. A possible explanation describing the discrepancy in clay content is that the clay content taken from Project C of the Walker Report (Miller *et al.*, 2010) is either an anomaly, doesn't apply to the field of interest, or the measurement method isn't accurate enough to precisely measure clay content to within only a few percent. The method used to determine the clay content was the hydrometer method for determination of particle size distribution (Lu *et al.*, 2000). As Lu *et al.* (2000) states, the hydrometer method utilizes Stokes Law which assumes soil and clay particles are spherical in shape. However, clay particles are much more plate-like than they are spherical. Therefore, the discrepancy is most likely not due to an error, but rather is due to the precision of the measurement method. The second explanation is that because only two soil cores were used to create the above measured curve, the cores do not accurately represent the clay content in the field as a whole. Because both curves are very similar, and to account for the probable slight difference in clay content, the Campbell model was simply shifted over slightly by a moisture content of $0.03 \text{ m}^3/\text{m}^3$. The resulting Campbell relationship as it compares to the measured relationship from the lab is presented below.

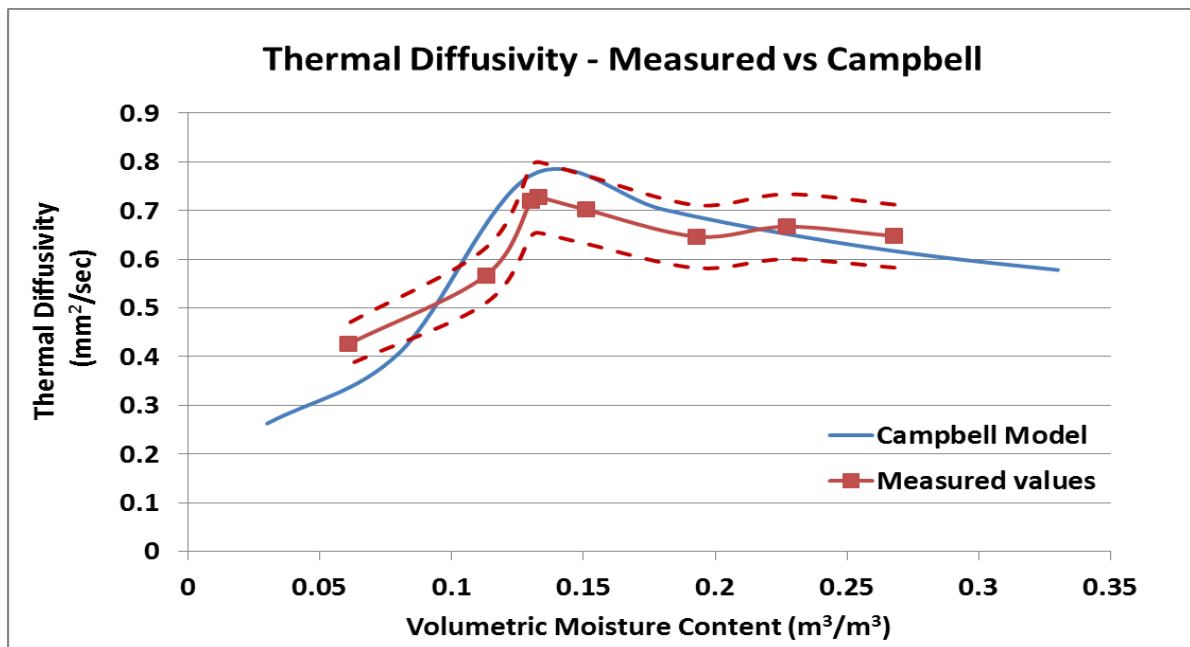


Figure 7.4.3b. Campbell curve shifted to the right by a moisture content of $0.03 \text{ m}^3/\text{m}^3$. Considering the error bars surrounding the measured values, the relationships now match very well.

From the above Campbell relationship, two equations can be fit to the curve to facilitate processing. One equation will fit the data on the dry side of the curve, and the other equation to fit the data on the wet side of the curve. Figure 7.4.3c provides these trend lines and corresponding equations.

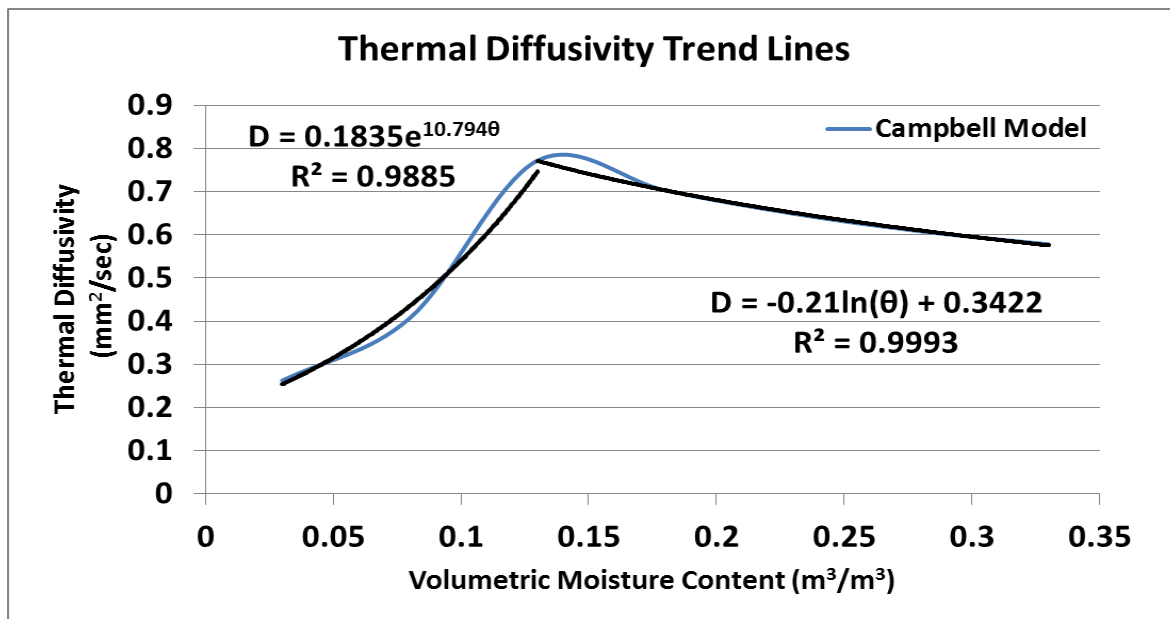


Figure 7.4.3c. Equations fitting trend lines to the Campbell model. On the dry side of the curve (left side) the fit is exponential, and it is a logarithmic fit for the data on the wet side of the curve (right side).

The trend lines fit the measured data fairly well. However, as they stand now, the equations provide a thermal diffusivity for a given soil moisture. Note that the x axis is soil moisture, and the y axis is thermal diffusivity. Simple algebra is needed to solve the trend line equations for volumetric moisture content. The exponential equation for the soil under dry conditions is

$$D = 0.1835e^{10.794\theta} \quad \text{Equation 7.4.3a}$$

Solving for volumetric moisture content θ , this becomes

$$\theta = [\ln (D/0.1835)] / 10.794. \quad \text{Equation 7.4.3b}$$

The logarithmic trend line fitting the data for the soil under wet conditions is

$$D = -0.21 \ln(\theta) + 0.3422. \quad \text{Equation 7.4.3c}$$

Again, solving for moisture content θ , this equation now becomes

$$\theta = e^{[(D - 0.3422) / -0.21]}. \quad \text{Equation 7.4.3d}$$

Equations 7.4.3b and 7.4.3d are the equations that can now be used to estimate volumetric moisture content given a value of thermal diffusivity and an estimate of whether the soil is on the dry or wet side of the diffusivity curve.

It must be noted that using the trend line equations will only produce valid soil moisture results if the estimated thermal diffusivity values actually occur in the range of the curve. The primary times when the diffusivity values are above the curve occur during irrigation events, and so the assumption of conduction as the primary mode of heat transport is not valid. This will be further analyzed in the discussion section. However, what is necessary to recognize is that when estimated thermal diffusivity values are above $0.80 \text{ mm}^2/\text{sec}$ (the maximum value in the provided thermal diffusivity – soil moisture relationship), no soil moisture value is given. Therefore, these times simply appear as gaps in soil moisture estimates. When an estimated thermal diffusivity value falling below the curve is encountered on the left (dry) side of the curve, the corresponding moisture content is assigned as $0.035 \text{ m}^3/\text{m}^3$, which is a typical residual moisture content for a loamy sand (Rawls *et al.*, 1982). When encountered on the right (wet) side of the curve, an estimated thermal diffusivity value falling below the curve is assigned a saturated moisture content of $0.33 \text{ m}^3/\text{m}^3$.

Results of soil moisture estimates are presented just as they were for the estimated thermal diffusivity results. Figures 7.4.2c through 7.4.2e present modeled thermal diffusivity results at 3 individual locations. Estimated soil moisture contents are presented for those same 3 locations along the cable. Gaps in soil moisture estimates occur during times of incorrectly high estimates of thermal diffusivity.

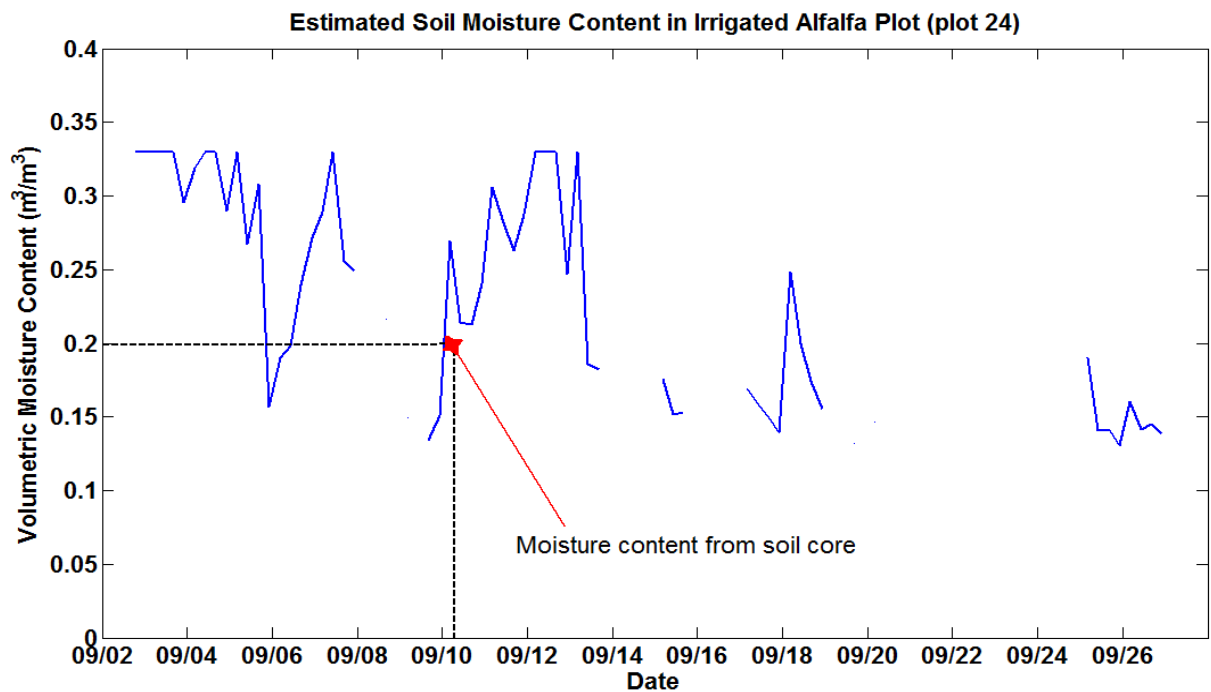


Figure 7.4.3d. Estimated soil moisture content in plot 24, an irrigated alfalfa plot. The red star denotes a moisture content measured via gravimetric method on September 10th.

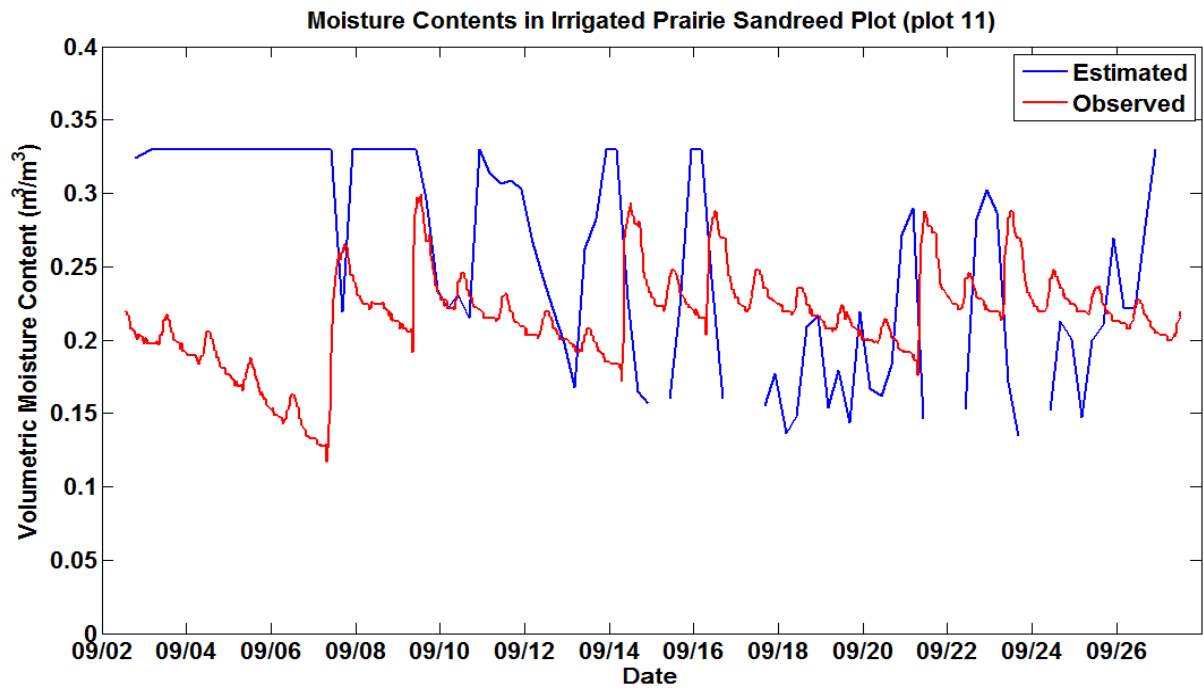


Figure 7.4.3e. Estimated soil moisture in plot 11, an irrigated prairie sandreed plot. The observed measurements come from an EC-5 soil moisture sensor located within the same plot.

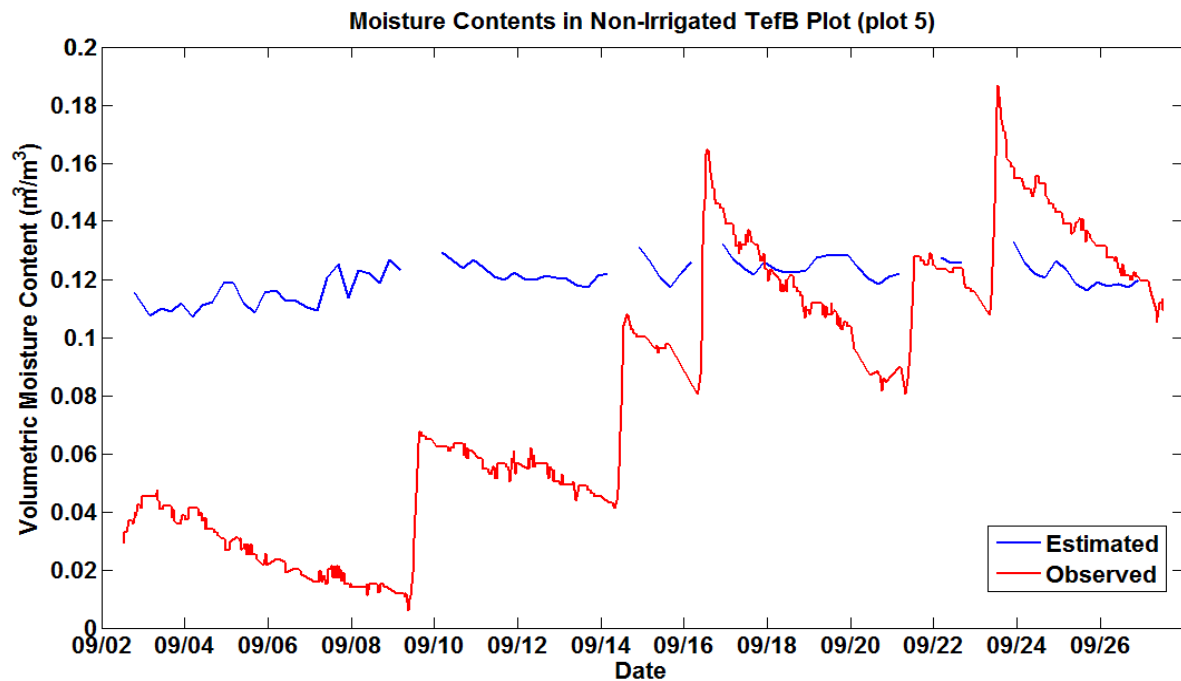


Figure 7.4.3f. Estimated soil moisture in plot 5, a non-irrigated tef plot. The observed measurements come from an EC-5 soil moisture sensor located within the same plot. Note the change in y-scale.

Because soil cores were only collected on one date, not much can be inferred through time from the apparent match of measured soil moisture and estimated soil moisture in figure 7.4.3d. Figures 7.4.3e and 7.4.3f provide the best possible comparison between predicted and observed soil moistures through time, since soil moisture was measured throughout the entire study periods at these locations. The EC-5 soil moisture sensors were positioned vertically from the surface downward. Because of this, the observed measurements cover the top 5 centimeters of soil. Recall that the estimated soil moisture values are from the domain between depths of 5 and 15 centimeters. It therefore makes sense that the observed values in figure 7.4.3f exhibit much more variability and response to irrigation events.

Similar to thermal diffusivity estimates, the overall goal is to provide soil moisture estimates spatially over the field scale. Therefore, soil moisture is presented spatially just as it was in figure 7.4.2 for thermal diffusivity. Just as with that figure, distance is presented on the y-axis, a secondary y-axis delineates plot boundaries, and date is on the x-axis. The same plot numbers that were used for temperature analysis are used here for comparison purposes. Refer to table 7.3.1 for plot number descriptions. The plot numbers that were not modeled are plots 1, 2, 16, 20, and 22. Figure 7.4.3g presents the modeled soil moisture results over the field scale. Note that blue corresponds to higher moisture values.

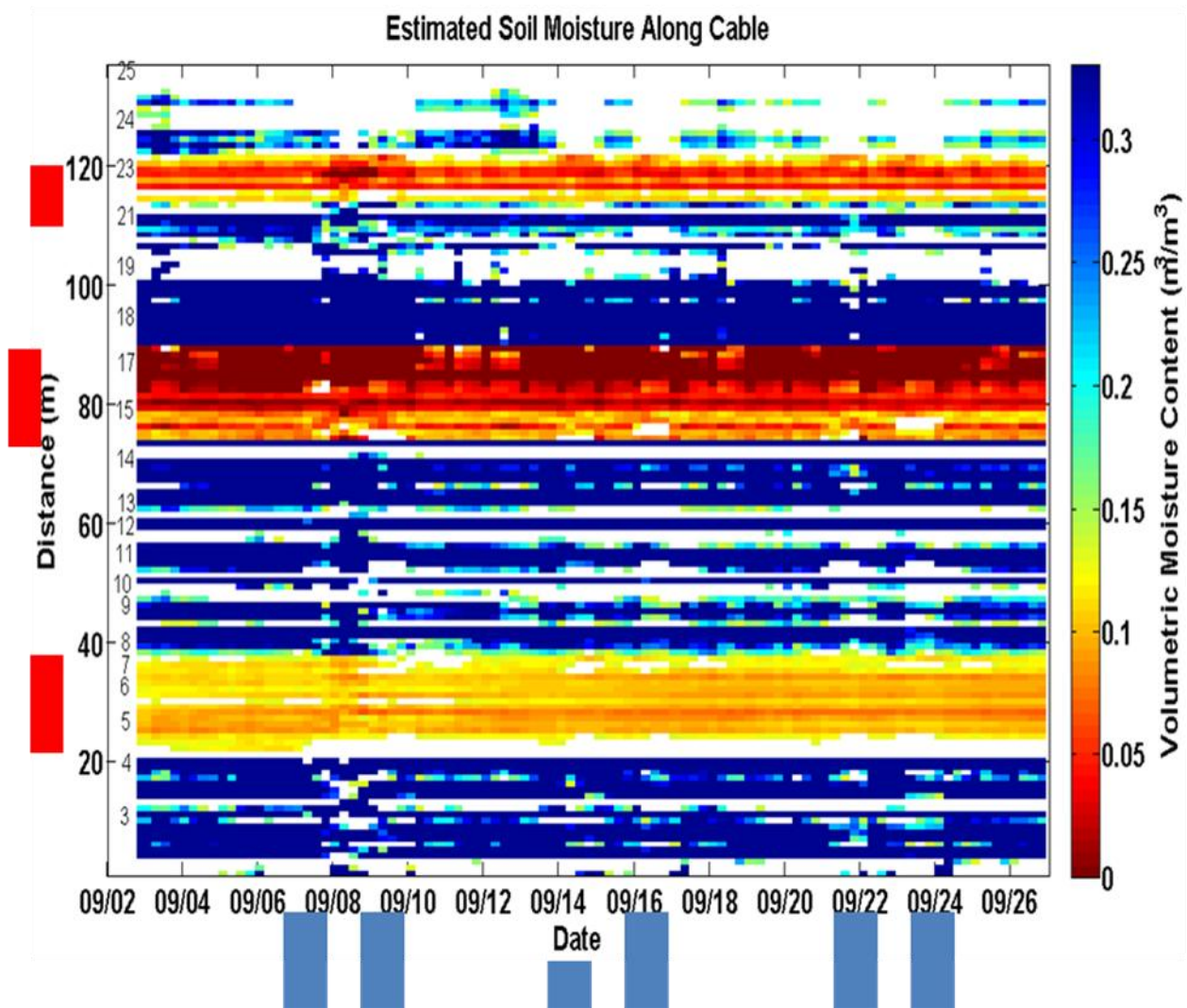


Figure 7.4.3g. Resulting spatial distribution of soil moisture resulting from the trend line equations of figure 8.4.3c being applied to the modeled thermal diffusivity values. Blue rectangles are days with irrigation events and red rectangles delineate plots that received no irrigation.

The non-irrigated sections of the previous figure include meters 21 to 37, 74 to 89, and 114 to 121. These sections are the clearly the driest areas along the cable. From measured values of soil moisture in non-irrigated plots, soil moisture in these plots should be anywhere from 0.02 to 0.18 m^3/m^3 . From measured values of soil moisture in

irrigated plots, soil moisture in these plots should range from 0.10 to 0.30 m³/m³ throughout the study period. The sections of irrigated plots (blue) show lots of heterogeneity in soil moisture. Figure 7.4.3e provides a good example of these irrigated sections, as it exhibits soil moisture values both higher and lower than what is expected, all the while passing through the reasonable range of soil moisture. In non-irrigated sections, soil moisture is fairly constant across time and space.

Another way to present the estimated soil moisture spatially is to provide a figure that is essentially a plan view of the field. The major drawback of such a figure however, is that results can only be displayed for one date. Figure 7.4.3h displays soil moisture data such that all meters within one plot are averaged together, and the estimates throughout the same day are averaged together. In other words, the figure provides one soil moisture value per plot per day. The particular day presented is September 10th, because on this date the previous figures showed agreement between estimated and observed soil moisture contents. Whereas figures 7.4.3d through 7.4.3f provided soil moisture estimates at one point through 25 days, figure 7.4.3h provides soil moisture estimates along the entire length of the cable but only for one day. Many figures similar to 7.4.3h showing results from subsequent dates could be produced and presented in such a way as to show soil moisture progression through time, all while observing the individual plots through a plan view.

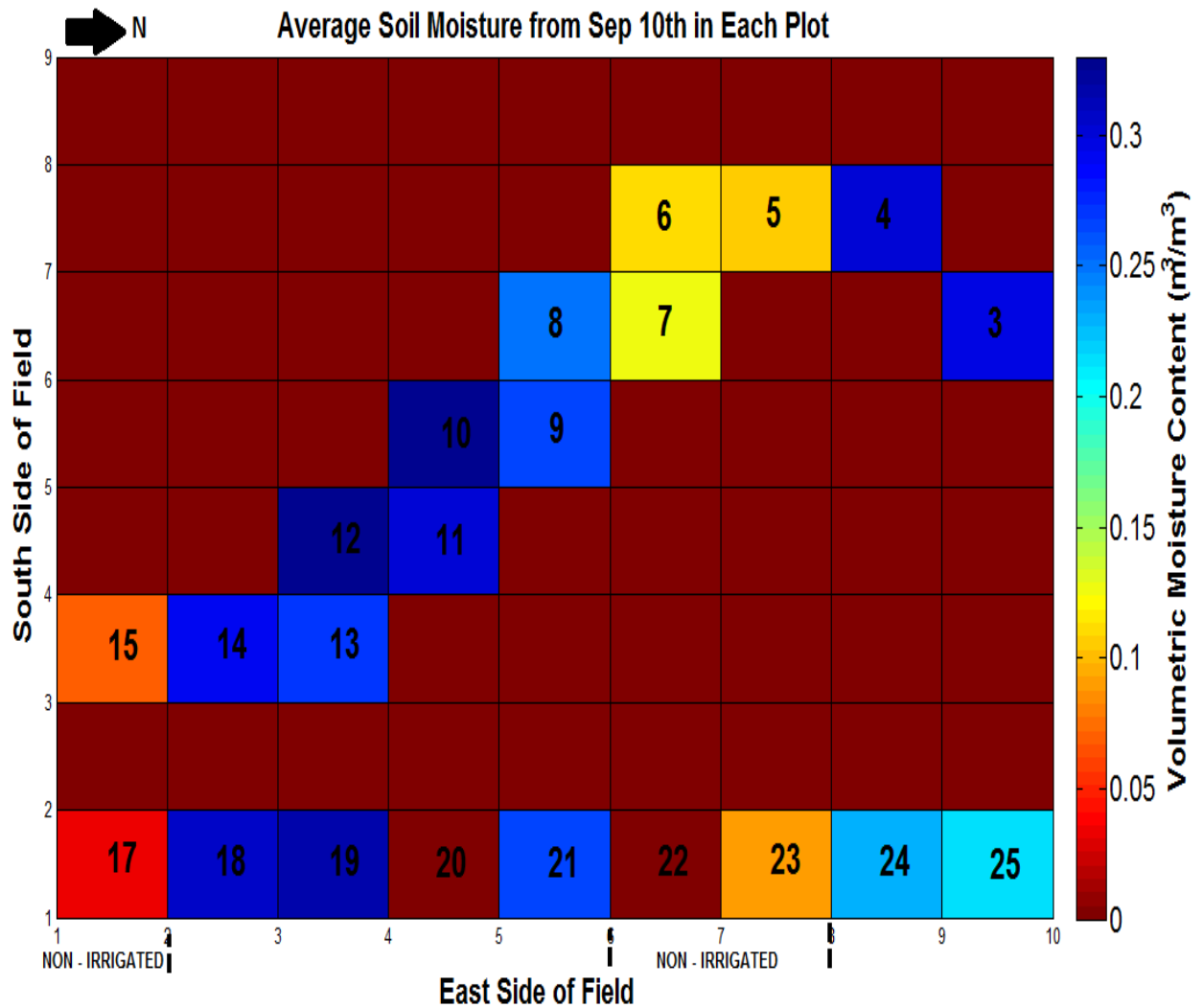


Figure 7.4.3h. Average soil moisture values for each plot during September 10th. Note that plots 20 and 22 were not modeled and so were automatically assigned a value of zero. Non-irrigated rows of crops are delineated.

SECTION 8. DISCUSSION

This section relates study results to each of the three overall project goals as presented in section 4.

8.1 TEMPERATURE ANALYSIS

Goal 1. Effectively use a passive DTS system to analyze the effect that both surface vegetation type and irrigation have on subsurface soil temperatures in an agricultural setting.

8.1.1 Irrigation Effects

The most straightforward analysis of temperature on the spatial scale is presented in figure 7.3.2, in which the daily maximum temperature observed by the top cable is presented. Considering that figure, temperature across time is first analyzed. When looking across time from September 2nd to September 27th, the first and most apparent date of note is September 8th. On this date, it is very clear that the temperatures throughout the entire field are considerably cooler than on the days immediately before and after. Because irrigation occurred on September 7th, it is reasonable to assume that this decrease in subsurface temperature is in response to an increase in soil moisture content. Figure 7.3.1 showing the diurnal signals of temperature at the three cable depths also shows temperature damping occurring on September 8th. However, when looking at

other dates in which irrigation occurred such as the 9th, 14th, 16th, 21st, and 23rd, it becomes clear that this noticeable effect on soil temperature is not caused primarily by irrigation. A quick reference to a plot of air temperature and net radiation as measured by the eddy correlation station reveals that September 8th was a day of low net radiation and low air temperature. Therefore, the apparent decrease in subsurface temperatures of about 4 degrees at 5 centimeters depth occurring on the 8th is more likely due to cloud cover and subsequent lower net radiation than usual.

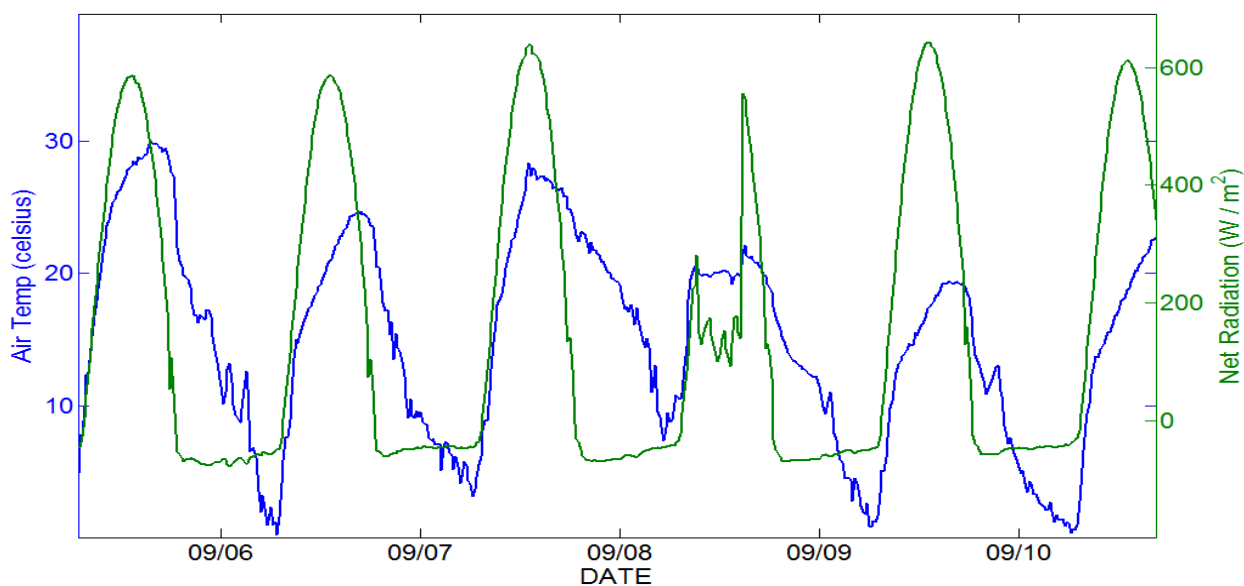


Figure 8.1.1a. The low net radiation and subsequent low air temperatures that occurred on September 8th are the cause of the large subsurface temperature decrease on the same date.

If the large decrease in subsurface temperature that occurred on September 8th was not due to irrigation, then the effect, if any, that irrigation does have on the daily maximum temperature in the shallow subsurface still needs to be determined. By looking

at the same figure again, there is indeed a small but noticeable decrease in the daily maximum temperature of the top cable when irrigation occurs. It is evident that this decrease is not due to ambient weather conditions as it was for September 8th, because the net radiation for these days does not show evidence of cloud cover or decreased air temperature. This effect is noticeable for all of the dates in which irrigation occurred, but for this discussion simply note September 21st and September 23rd, two days in which 0.34 and 0.35 acre feet of water was applied, respectively. It is fairly clear that, compared to the days immediately preceding these dates, the soil temperature at 5 centimeters depth decreases. Interestingly however, the most noticeable temperature decreases during these dates occurs in plots that received no direct irrigation, such as plots 5 and 22. These plots tend to exhibit the highest soil temperature, and it is probable that water from the sprinkler irrigation was blown into these plots. On the 21st and 23rd, the wind velocity over the field averaged 3.2 and 2.7 miles per hour respectively, with gusts reaching up to 14 miles per hour; enough to carry spray irrigation into adjacent plots. Because they exhibit such high soil temperatures and low soil moistures compared to the other plots, the shallow subsurface temperatures in these plots would be rather sensitive to any reception of windblown irrigation. In plots that received irrigation normally, there is no real noticeable effect to the daily maximum soil temperature at a depth of 5 centimeters caused by irrigation events.

Figures 7.3.4 through 7.3.6 show the difference between the daily maximum and daily minimum soil temperatures at depths of 5, 10, and 15 centimeters. These plots were created in an effort to analyze the effect that irrigation would have on the diurnal

temperature signals in the subsurface. The speculation was that introducing water into the soil system would result in a damping of the diurnal temperature signal, much like what happened on the 8th due to cloud cover. As depth increases, there is obviously a much smaller difference between the daily maximums and minimums, but at no depth is there clear evidence of signal damping caused solely by the occurrence of irrigation. On these figures, it appears that irrigation does not have a noticeable effect on the daily maximum temperature of soil for soil that is already relatively wet. However, there is indeed a correlation between irrigation events and dampened temperature signal; the temperature scales on the preceding figures are just too coarse for it to be clearly illustrated. The following figure shows that there is indeed a damping that occurs, as was initially expected.

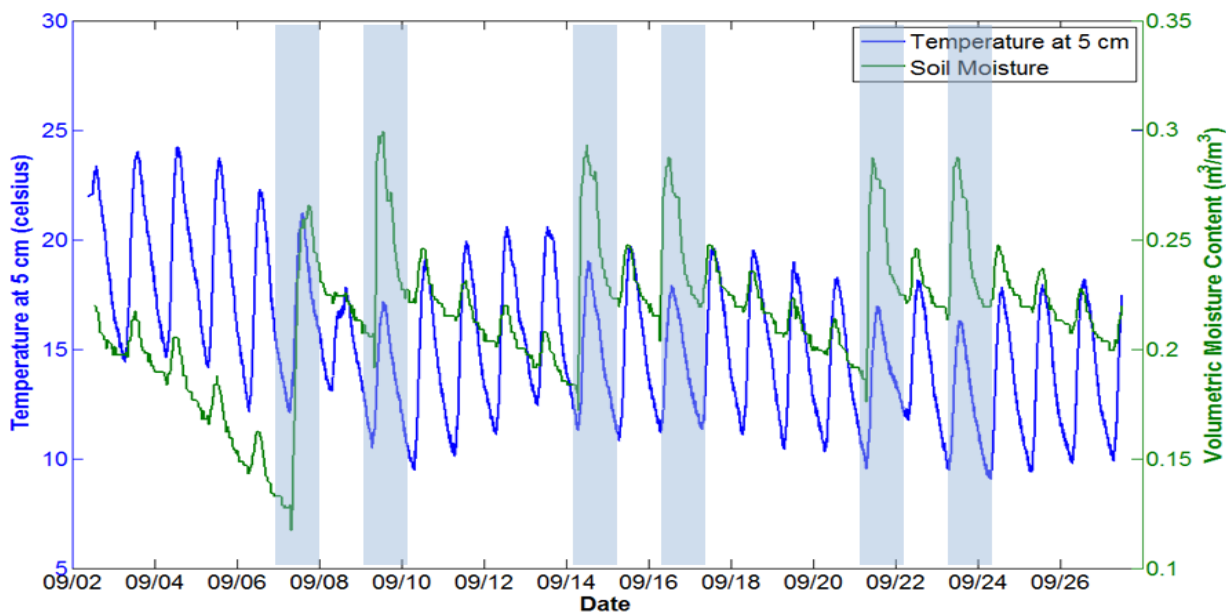


Figure 8.1.1b. Side by side comparison of temperature at a depth of 5 centimeters and moisture content in a plot of Prairie Sandreed which received 100% irrigation. The peaks in soil moisture occur on days of irrigation events, and the diurnal temperature signal is clearly dampened on these dates. Blue bars delineate days of irrigation.

Based upon the preceding figure, it is clear that irrigation events and thus, wetter soil, does in fact decrease the soil temperature in the shallow subsurface. However, this effect is not large, as the maximum daily temperature is only decreased by 1 to 2 °C on the day of the irrigation event. As previously mentioned, this decrease in soil temperature might be so slight because the soil is initially fairly moist (0.20 to 0.25 volumetric moisture contents). The same side by side comparison is performed for a Tef plot in which no direct irrigation occurred.

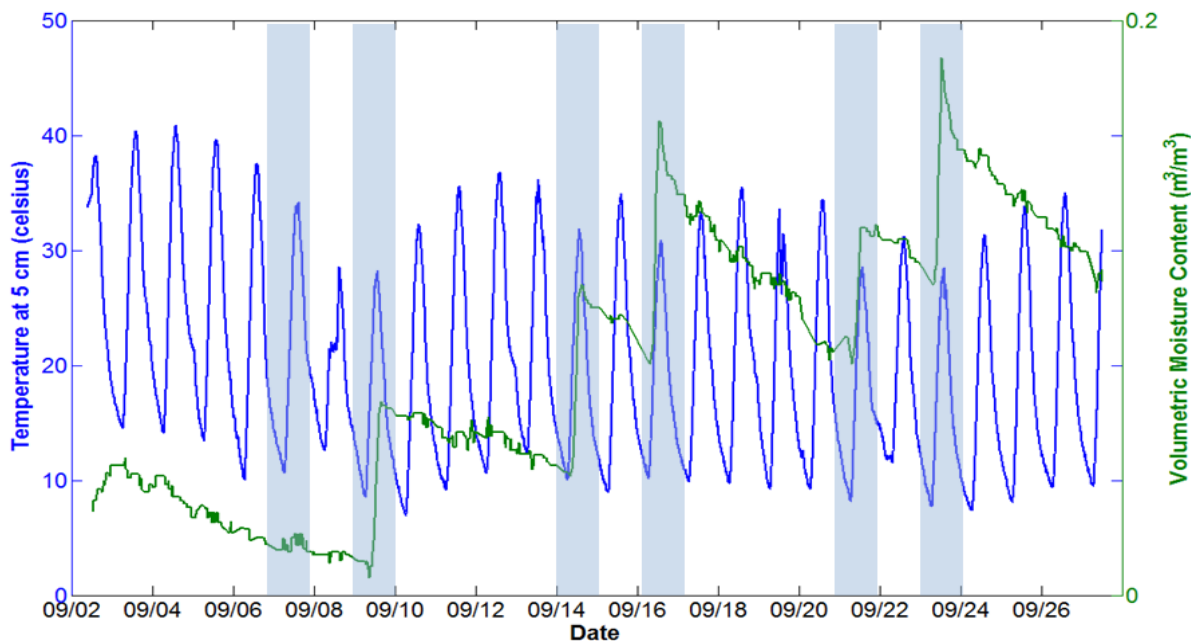


Figure 8.1.1c. Side by side comparison of temperature at a depth of 5 centimeters and moisture content in a plot of TefB which received no direct irrigation. Days in which irrigation occurred in adjacent plots are still delineated. Note the different scales compared to figure 9.1.1b.

Considering that these soil moisture measurements were conducted in a plot that received no irrigation, the first thing to note is that irrigation of adjacent plots clearly hits other plots as well. In regards to the effect irrigation has on soil temperature, the diurnal

temperature signal damping that was observed in figure 8.1.1b is again apparent here. On days in which irrigation events occurred (apparent because of jumps in soil moisture), there is an obvious decrease in maximum temperature at a depth of 5 centimeters. However, because of the much drier condition of this soil, the little bit of water that hits the soil has a much larger damping effect than when the soil was initially wet. Whereas before the background volumetric moisture content was around 0.20 to 0.25 m³/m³ with a corresponding daily maximum temperature decrease of 1 to 2 °C during irrigation events, in this situation the background moisture content ranges from around 0.04 to 0.16 m³/m³ with corresponding daily temperature decrease during days of irrigation of 4 to 5 °C.

This analysis on the effect that irrigation has on temperature signals at depth is important because of the conduction model that is subsequently used to estimate thermal diffusivity. The model works under the simplified assumption that conduction is the primary mode of heat transfer. If conduction was in fact the only heat transfer that occurred, then irrigation would not affect the temperature signals. Because the effect is very small, and is only noticeable at the shallowest depth, this lends validity towards the assumption of conduction as the primary mode of heat transport within the model domain. The conduction model features a domain from a depth of 5 centimeters to a depth of 15 centimeters. If there is only a minimal effect at a depth of 5 centimeters due to irrigation, then the model should work more accurately and for longer time periods than originally believed.

8.1.2 Crop Type Effects

The fiber optic cables buried in the shallow subsurface follow a path through the field that travels beneath 10 different crop types. Figure 7.3.3 provides a direct comparison of subsurface soil temperatures at a depth of 5 centimeters underneath each of these varying crop types. Looking at Figure 7.3.3 it is apparent that there is a large difference in average temperature beneath a crop if irrigation has occurred. For that reason, the mean daily maximum temperature was calculated with only irrigated crops included (for a comparison involving only the crop type variable), and then again with non-irrigated plots included as well. Those plots that did not receive irrigation exhibit much warmer shallow subsurface temperatures than those plots of the same crop type but with irrigation. To analyze just the effect that crop type has on soil temperature, the mean daily maximums from the irrigated plots need to be assessed. The mean temperature values range from Sand bluestem with a mean daily temperature of 17.32 °C to Tef with a mean daily temperature of 22.61 °C. Therefore, under the same irrigation scheme, crop type alone changed the mean daily maximum temperature at a depth of 5 centimeters by 5.29 °C within the field. The most apparent explanation for the difference in soil temperature is as a result of differences in crop height and density. On September 10th, 2010, crop height was measured in the plots. Table 8.1.2 provides measured crop heights, in order of increasing mean daily maximum temperatures at a depth of 5 centimeters.

Average Crop Heights

Crop Type	Average Crop Height (cm)
Sand bluestem	180
Tall Fescue	53
Prairie Sandreed	50
Bluestem	--
Basin Wild Rye	95
Tall Wheatgrass	--
Indian Grass	55
Alfalfa	16
Tef B	47

Table 8.1.2. Average crop height for each crop type, as measured on September 10th, 2010. In order, Sand bluestem exhibited the lowest subsurface temperature and Tef B exhibited the highest. Note that Bluestem and Tall Wheatgrass were not measured.

The fact that Sand bluestem has an average height of 180 centimeters explains why that crop exhibits the lowest soil temperature. Such a tall crop provides the most shade from the sun, as well as a large amount of vegetation to intercept the sun's energy. Referring back to figure 7.3.3, it is clear that the other crops do not exhibit such a difference in daily maximum temperature. As such, there is no clear trend in crop height beyond Sand bluestem, other than when considering the very low height of alfalfa. However, even though alfalfa is a relatively short crop, it tends to be very dense when compared to the grass crops. In addition, the alfalfa was cut and collected on September 13th, 2010. When measured on September 10th, the alfalfa plots averaged a crop height of

only 16 centimeters, and then the crop was cut only 3 days later. It is most likely this mowing of alfalfa that resulted in the higher subsurface temperature and not the short crop height, because alfalfa tends to be a very dense crop.

The other crop type that stands out is tefB. TefB exhibited the highest daily maximum temperature at 5 centimeters depth when both irrigated and non-irrigated crops were considered. However, when looking at the height of the crop compared to the other crops, the height is not significantly shorter than the other crops. When initially plowing the cables into the field, the cable deploying blade tending to rise up during turns. All of the tef plots were located on the sharpest turn that was completed with the plow. Because of this fact, these cables may have elevated during deployment and therefore are most likely closer to the surface. As was seen with the diurnal temperature signals at the three depths, the shallower the cables are buried, the less signal damping occurs and therefore the greater the maximum daily temperature.

Returning to figure 7.3.2, the results showing the daily maximum temperature of the top cable through the various plots over time can again be analyzed, this time for temperature differences caused by crops, as opposed to those differences caused by irrigation. As opposed to looking at temperature across time, looking across the plot numbers at one date now provides the desired temperature comparisons. The temperature data presented in this figure mirrors the mean maximum temperature data presented in the bar graph of figure 7.3.3 for each crop type. It is clear that plots 5 and 6 (both non-irrigated tefB plots), and plots 22 and 23 (a non-irrigated alfalfa plot and a non-irrigated tall fescue plot) are the warmest crop plots. Recall that Plot 16 is simply the location of

the three cables bundled together in a black foam tube. Also evident is that the relation of the subsurface temperatures from plot to plot stays the same throughout the entire field study. In other words, a plot that is warmer than other plots at one date remains warmer than those other plots for all dates. The absolute temperatures may increase or decrease throughout the study duration, but plot temperatures relative to each other stay the same.

This observation holds true for all plots other than for the alfalfa plots, and that is only because the alfalfa was cut on September 13th. The alfalfa plots are plot numbers 22, 24, and 25. The date of mowing (September 13th) is very obvious for these plots as temperatures suddenly increase significantly. Plot 22 is a non-irrigated alfalfa plot, and when mowed on the 13th, the increase in maximum daily temperature at a depth of 5 centimeters was on average 1.01 °C. Plots 24 and 25 are irrigated plots of alfalfa, and after mowing, the average increase in maximum daily temperature at a depth of 5 centimeters was 5.205 °C. The additional 4.195 °C was the result of the soil being at a much higher moisture content. This finding agrees with the work presented by Al-Kayssi *et al.* (1990), in which the diurnal soil temperature signal was monitored under different moisture regimes at different depths in a controlled greenhouse experiment. Al-Kayssi *et al.* (1990) found that for depths ranging from 1 to 20 centimeters, the daily average soil temperature increased significantly with increasing soil moisture content.

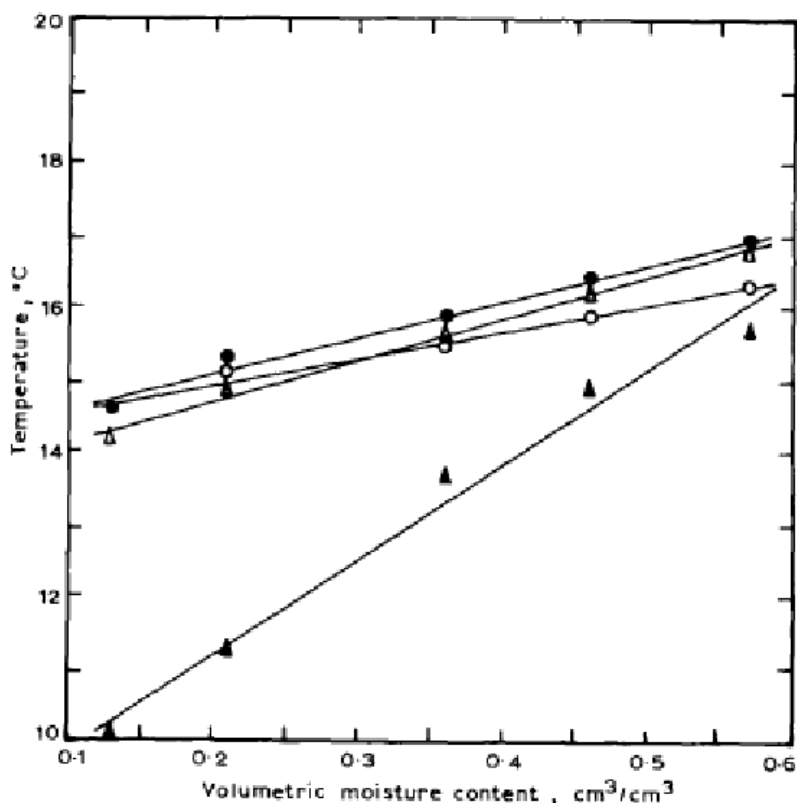


Figure 8.1.2. Data presented by Al-Kayssi *et al.* (1990) relating average daily soil temperature to moisture content for depths of 1 cm (shaded triangles), 5 cm (hollow triangles), 10 cm (hollow circles), and 20 cm (shaded circles).

As soil moisture content increases, the amount of the sun's radiation that gets reflected away from the soil surface (i.e. the surface albedo) decreases (Al-Kayssi *et al.*, 1990). This results in more of the sun's energy being absorbed by the soil surface and propagating downward. This serves to increase soil temperature. The alfalfa plots that were mowed on the 13th nicely demonstrated this phenomenon. The alfalfa was not cut down to the level of bare soil, and surface vegetation also affects the amount of reflectance that occurs, but since mowing should have been the same for all alfalfa plots, soil moisture is the main variable resulting in the difference in temperature increase.

The collection of soil temperature data over such spatial and temporal scales could prove extremely useful for biologists, agronomists, and agriculturalists. Just as with soil moisture sensors, temperature sensors generally measure on the point scale. If high spatial resolution is desired, then a large array of point sensors is often required. The use of distributed temperature sensing via fiber optic cables offers an effective solution to environmental sensing over the field scale, in this case, temperature being the variable assessed. Soil temperature affects physical, chemical, and biological properties of the soil, and these have implications for nutrient transport, nutrient uptake by plants, root growth and physiology, rates and depth of evaporation, presence and activity of soil fauna, and many other important soil processes (Al-Kayssi *et al.*, 1990; Glinski and Lipiec, 1990; Jungk, 1996; Pregitzer and King, 2005). Many of the results presented in this study regarding soil temperature across an agricultural field are data that intuitively make sense and should be expected, but the significance lies in the fact that this data can now be easily quantified over the field scale at high resolution.

8.2 ESTIMATED THERMAL DIFFUSIVITY ANALYSIS

Goal 2. Using temperature data collected via passive DTS technology, estimate thermal properties on the field scale.

This section discussing the estimated thermal diffusivity results will not include discussion on estimates achieved using the Excel finite-difference mesh. Those results

were necessary to present as a means of showing the progression towards estimating soil thermal properties. However, aside from the initial comparison between models, only the MATLAB conduction model was used towards furthering this study. Therefore, discussion will only include results obtained from the conduction MATLAB model.

8.2.1 Estimated Thermal Diffusivity on Point Scale

The overall goal in estimating soil thermal diffusivity using distributed temperature sensing with fiber optic cables is to do so on a spatial and temporal scale not easily achieved with other existing methods. However, although the spatial aspect of thermal diffusivity is very important, it is also equally important to look in detail at the progression through time of thermal diffusivity at one location in space. The most immediate benefit to using DTS technology is that any meter along the entire length of the cable can easily be investigated.

In the results, figures 7.4.2c through 7.4.2e present modeled thermal diffusivity results over time from three individual locations in the field. Figure 7.4.2c, 7.4.2d, and 7.4.2e are results from the middle of an irrigated alfalfa plot, an irrigated Prairie sandreed plot, and a non-irrigated TefB plot respectively. The Prairie sandreed plot and the TefB plots were chosen specifically because those two plots each contained a wireless meteorological station with measured values of soil moisture throughout the study period. The alfalfa plot was chosen because it serves as a good representative crop that is quite different from the other two crops selected, it served as the control crop for separate vegetation studies conducted on site, and was also physically located at the opposite end

of the field. Modeled thermal diffusivity results very well could have been presented from a different crop type for the same effect.

The conduction model in MATLAB assumes that conduction is the only mode of heat transport. This implies that the model is ideal for situations in which there is bare soil, and no active water application. Vegetation and active water application result in evapotranspiration, causing an almost constant flux of water vapor about the canopy layer. Under such agricultural settings during summer months, the latent heat flux due to evapotranspiration is generally the dominant component of the surface energy balance, almost balancing the overall net radiative flux (Arya, 2001). This latent heat flux due to evaporation is generally confined to the top few centimeters of the soil column. Heitman *et al.* (2008) found that while originally occurring at the surface, 6 days after a rainfall, the evaporation zone proceeded 13 mm into the soil column. This was conducted under dry, hot summer conditions in a silty loam. Mayocchi and Bristow (1995) reference DeVries and Philip (1986) in showing an example where all latent heat flux was limited to the top 3 centimeters of the soil column. Considering this fact, the hope was that since the top boundary of the model domain is located at a depth of 5 centimeters, much of these surface and boundary effects would be avoided. Results considered come from days in between irrigation events, and at depth, when conduction would hopefully be the primary mode of heat transfer in the soil. It was expected from the onset that the conduction model that was used would not produce valid results during times of irrigation. That being said, the analysis previously conducted showing an insignificant

response in temperature signal to irrigation events allows for less strict acceptance of the conduction model results.

Times of irrigation should be easily recognized on plots showing the modeled thermal diffusivity results. Recall that irrigation occurred on the 7th, 9th, 14th, 16th, 21st, and 23rd of September. A quick reference to figures 7.4.2c through 7.4.2e shows a pattern of estimated thermal diffusivity on these dates. On these dates, the estimated thermal diffusivity values clearly increase well above the expected thermal diffusivity range. The diffusivity estimates in each of the plots range from around 0.50 to 0.80 mm²/sec during days of non-irrigation. On the days of irrigation however, these values spike up to a minimum of 0.90 mm²/sec and a maximum of 1.30 mm²/sec. On each of the three figures, these spikes are evident and are due to irrigation.

The only exception seems to be when looking for evidence of increased diffusivity values on the 7th and 9th of September. On figures 7.4.2c and 7.4.2e, there is indeed one large extreme value evident, but this occurs on the 8th. The individual peaks do not show up as they do for the other days of irrigation. This is most likely due to the fact that the day of very low net radiation occurred on the 8th, and since the model utilizes a 24 hour window length, this decreased net radiation is incorporated into estimates for both the 7th and the 9th. Because the effect of the cloud cover on 8th was so dramatic (as evidenced earlier in the discussion of temperature analysis), the cumulative effect of the irrigation and the low net radiation appears as the peak on the 8th. In figure 7.4.2e showing modeled diffusivity values in the irrigated prairie sandreed plot, instead of a large peak, there is an extreme low of 0.30 mm²/sec that occurs on September 8th. During

the 8th when net radiation is low, the difference in temperature at the three depths is very small. Figure 8.2.1 was previously presented, but is necessary to illustrate the effect that reduced radiation has on the soil temperature signals.

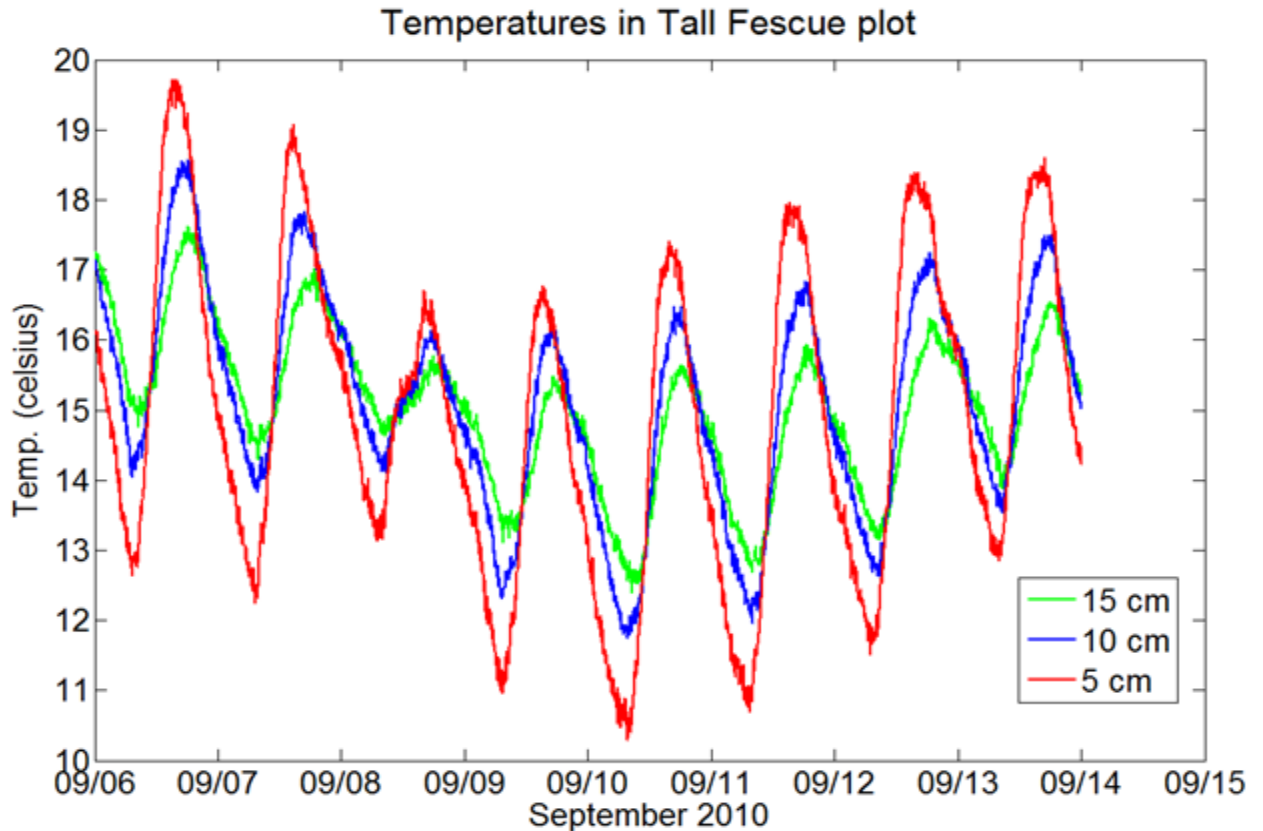


Figure 8.2.1a. On September 8th, reduced net radiation results in a very small difference in soil temperature across the various depths.

When the temperature gradient across the three depths is small, conduction in the soil decreases and the necessary inversion of the conduction equation becomes insensitive. It is clear that the conduction model only works when weather conditions are relatively sunny and clear. This is necessary to ensure significant temperature differences at various soil depths.

Recall that the results presented showing potential damping of temperature signals at depth did not show any overwhelming evidence of damping due to irrigation events. However, although irrigation may not create signal damping to the expected degree, the irrigation events clearly affect diffusivity estimates. This is evident based upon the peaks in thermal diffusivity that occurred during irrigation. Clearly, conduction is not the sole mode of heat transfer, but what causes these peaks still needs to be explained. The underlying (and simplified) equation that propagates the conduction model is the conduction equation in one dimension,

$$\frac{\partial T}{\partial t} = D(\theta) \frac{\partial^2 T}{\partial z^2}, \quad \text{Equation 8.2.1a}$$

where D is thermal diffusivity, T is temperature, t is time, and z is depth. However, in reality, and particularly during times of irrigation, there is also an advective component to heat transfer resulting from the influx of heat energy via incoming water. A more accurate equation to explain heat transfer during irrigation therefore needs to incorporate this advective term.

$$\frac{\partial T}{\partial t} = D(\theta) \frac{\partial^2 T}{\partial z^2} - \bar{v} \frac{\partial T}{\partial z}, \quad \text{Equation 8.2.1b}$$

where \bar{v} is the average linear velocity and $\bar{v} \frac{\partial T}{\partial z}$ represents the average advective flux of heat into the system. However, because this advective component does not exist in the model used, D must increase to compensate for the energy that should be applied to the

advective heat term during times of water influx, explaining why peaks in modeled thermal diffusivity occur during the irrigation events.

Looking at Figures 7.4.2c through 7.4.2e in which estimated thermal diffusivity at one location is provided throughout the entire study period, trends over smaller time frames are difficult to distinguish. Of particular significance is the modeled evolution of diffusivity values between irrigation events. Based off of the developed relationship between thermal diffusivity and soil moisture, it is expected that diffusivity during a drying period would decrease over time in non-irrigated plots (moving down the left side of curve on Figure 7.4.3) and would increase over time in irrigated plots (moving up the right side of curve on Figure 7.4.3). To investigate this, thermal diffusivity over a drying period was modeled using two different window lengths. To be as accurate as possible, windows in which the temperature crossovers occurred were not included (around 11:00 AM and 8:00 PM). Figures 8.2.1b and 8.2.1c therefore provide diffusivity estimates using window lengths of 6 hours (no window shift) from the times of 12:00 AM to 6:00 AM, and then from 12:00 PM to 6:00 PM throughout a drying period. Irrigation occurred on the 16th.

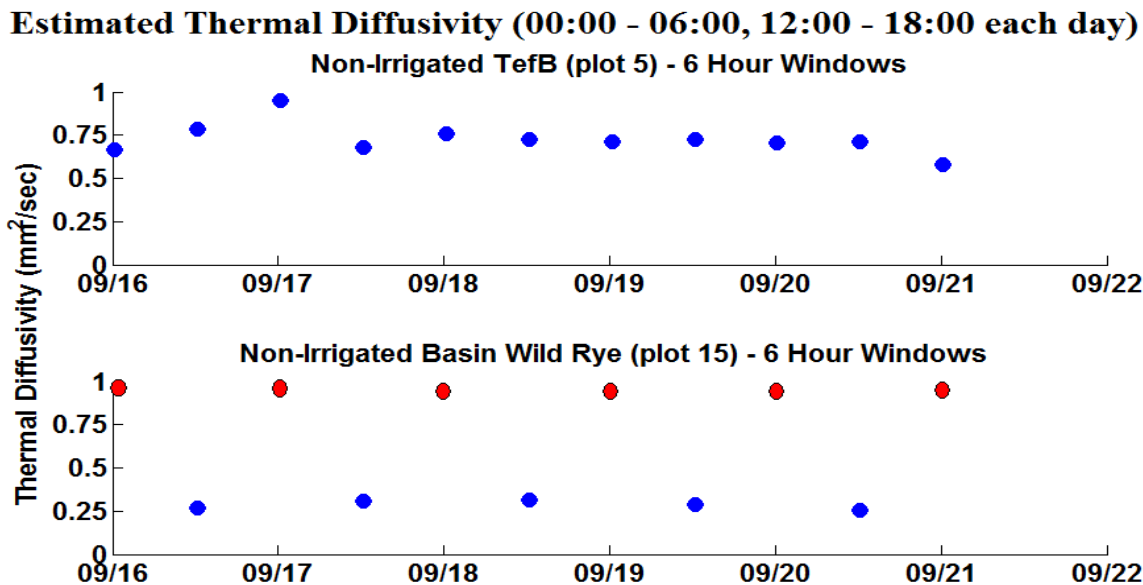


Figure 8.2.1b. Estimated thermal diffusivity during a drying period in two non-irrigated plots. Irrigation occurred on the 16th. Each point is an estimate derived from the following 6 hour time period. The red points represent estimated values off the scale, greatly higher than the reasonable range (not actually estimates of 1 mm²/sec).

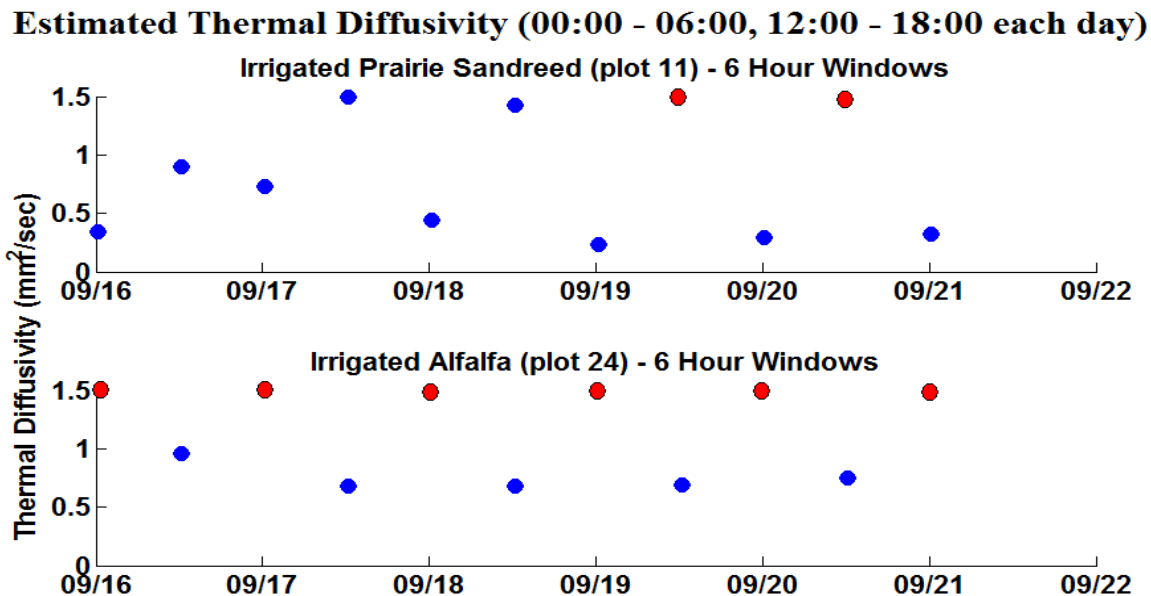


Figure 8.2.1c. Estimated thermal diffusivity during a drying period in two irrigated plots. Irrigation occurred on the 16th. Each point is an estimate derived from the following 6 hour time period. The red points represent estimated values off the scale, greatly higher than the reasonable range (not actually estimates of 1.5 mm²/sec).

Using 6 hour window lengths, and investigating thermal diffusivity estimates over a drying period did not provide the expected trends in diffusivity evolution. The TefB plot in Figure 8.2.1b showed a slight decrease as was expected, but overall, the plots failed to show clear trends. The data was also quite noisy because of the shorter window lengths. The above analysis was completed again over the same time period in hopes of decreasing noise, this time utilizing a 10 hour window frame of 12:00 AM to 10:00 AM each day, again avoiding the times of temperature crossover. These results are provided in Figures 8.2.1d and 8.2.1e.

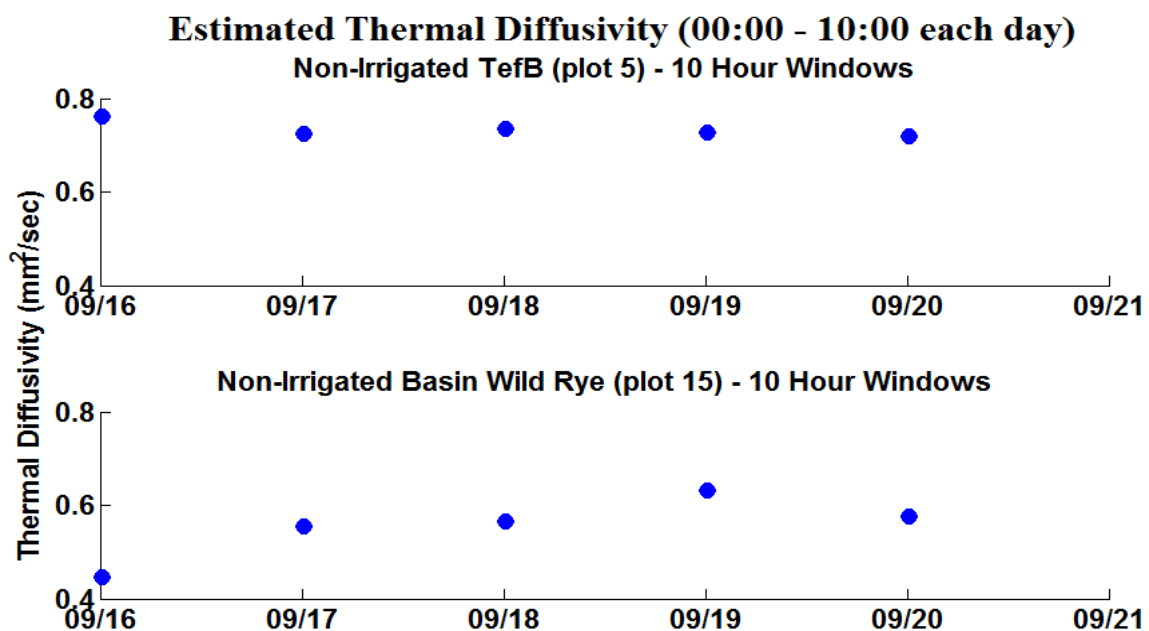


Figure 8.2.1d. Estimated thermal diffusivity during a drying period in two non-irrigated plots. Irrigation occurred on the 16th. Each point is an estimate derived from the following 10 hour time period.

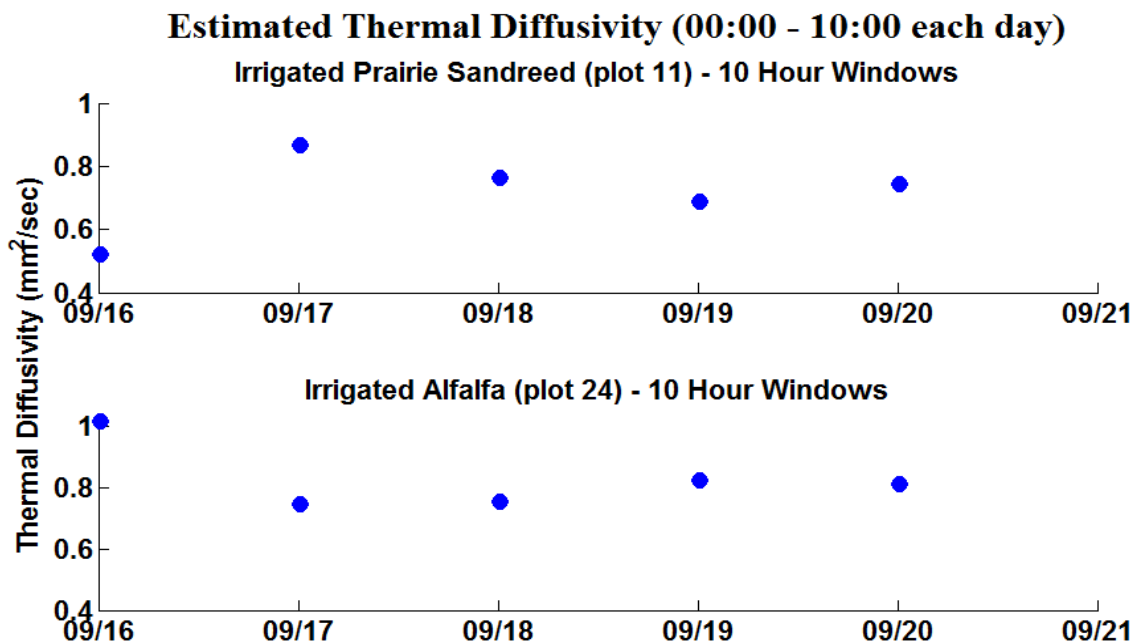


Figure 8.2.1e. Estimated thermal diffusivity during a drying period in two irrigated plots. Irrigation occurred on the 16th. Each point is an estimate derived from the following 10 hour time period.

Using 10 hour window lengths to investigate estimated thermal diffusivity evolution during a drying period provided much less noisy data than when 6 hour windows were used. However, just as with 6 hour window lengths, the expected trend of decreased diffusivity over time for non-irrigated plots and increased diffusivity over time for irrigated plots was not evident.

8.2.2 Estimated Thermal Diffusivity on the Field Scale

Now that thermal diffusivity has been discussed on the point scale, it is important to progress analysis to the field scale. Field scale measurements created with distributed temperature sensing via fiber optic cables are nothing more than a collection of point scale measurements. The difference, when compared to standard means of point scale

measurements, is that the collection of point scale measurements are completed all at the same time, and so do not require the time, energy, labor, or multiple sensors that would be required to achieve measurements over such spatial scales with the standard point scale measurement devices.

Figure 7.4.2f provides thermal diffusivity estimates along the length of the cable and through time. It is from this figure that spatial analysis of thermal diffusivity can be completed. As was discovered when looking at thermal diffusivity estimates at one point in space, thermal diffusivity does not appear to vary over time. That is, when considering one location, the diffusivity stays relatively constant through time.

There is much greater heterogeneity in diffusivity through space than there is through time. Typical values throughout the field range from around 0.3 mm²/sec to 0.9 mm²/sec. There are values that reach up to and beyond 1.0 mm²/sec, but these typically occur during times of irrigation (the peaks that were previously discussed), or most noticeably, in plot 25. Plot 25 is an alfalfa plot at the northern most edge of the field, and was the first plot where cables were installed. Because of this, the cables were not deployed down to proper depths as prescribed in the model (i.e. 5, 10, and 15 centimeters below the surface) because it took a bit of time for the plow to track downward. In terms of the model, this has similar effect to a day of low net radiation, because the difference in temperature between the cables will not be as great as it should be.

An obvious feature from figure 7.4.2f is the very low estimated diffusivity that occurs through time for meters 80 to 100, which correspond to two fescue plots at the

south end of the field. In this region, values are consistently very low and there is a strange pattern of vertical bars of near-zero thermal diffusivity occurring throughout the entire study period. Plot 17 is non-irrigated while plot 18 is irrigated, but both plots have the same vegetation. There is no discernible difference between these two plots, even with the difference in irrigation. Fescue is also the crop type of plots 19 and 23, and yet these plots do not show the same pattern. The top cable through meters 80 to 100 was replaced with a separate piece of Kaiphone cable. Although the attenuation of this replacement cable was different from the rest of the original cable, the temperature from this section did not show any substantial differences when compared to the original cable. The reasoning for these strange diffusivity estimates over this area is unknown.

In the temperature analysis, it became clear that the biggest effect to subsurface temperature signals was from days of low net radiation. Obviously, effects on temperature carry through to very noticeable effects on estimated thermal diffusivity. From just a plot of thermal diffusivity, it is very easy to distinguish the days of low net radiation, as well as days of irrigation. First, consider the day of lowest net radiation, September 8th. Again, the figure of interest is 7.4.2f. On the 8th, there is a very clear disturbance in diffusivity estimates that is seen along the entire cable. Some of the values during this date increase sharply, while others decrease equally sharply. As previously noted, days of low net radiation cause the difference in temperature at depth to greatly decrease. In addition, the difference in temperature with respect to time sometimes decreases and sometimes increases under such conditions. Mathematically speaking, the

values of the $\frac{\partial T}{\partial t}$ and $\frac{\partial^2 T}{\partial z^2}$ terms of the conduction equation vary much differently during cloudy days than they do during sunny days when soil temperature gradients are larger and more consistent. Because the model only has the simplified conduction equation with which to work, these variances make convergence difficult and therefore, the remaining thermal diffusivity term of the conduction equation D is forced to vary unnaturally to account for changes in the other terms. The conduction model does not work under such conditions, and it is easy to see why these results are best disregarded. Although not to the same extent, irrigation events are also quite noticeable when looking at modeled thermal diffusivity across time and space. Recall that irrigation occurred on the 7th, 9th, 14th, 16th, 21st, and 23rd. On these dates, there is a very clear increase in thermal diffusivity across the entire field. This increase is noticeable even in plots that did not receive irrigation. As mentioned, a fair amount of irrigation may have blown onto plots even though they were not actively intended for irrigation. Because the plots were so dry initially, this windblown irrigation was enough to affect modeled thermal diffusivity.

With thermal diffusivity estimated along the cable and through time, it is now possible to relate estimates to the derived relationship between thermal diffusivity and soil moisture.

8.3 ESTIMATED SOIL MOISTURE ANALYSIS

Goal 3. Using estimated thermal properties, predict soil moisture on the field scale.

The first subsection will discuss soil moisture estimates at single locations and the second subsection will discuss results of soil moisture estimates on the field scale.

8.3.1 Estimated Soil Moisture on Point Scale

It was only possible to obtain soil moisture estimates once a relationship between thermal diffusivity and soil moisture was obtained. Figure 7.4.3a provides the comparison of this relationship between that derived from the Campbell model and that derived from measured values on soil cores collected from the field. The magnitude of the thermal diffusivity values matched very well, as did much of the relationship. The only difference occurred under dry conditions. The peak dividing the dry side of the curve from the wet side of the curve occurred under wetter conditions for the measured values. The peak occurs at a moisture content of $0.11 \text{ m}^3/\text{m}^3$ for the Campbell model, but at $0.14 \text{ m}^3/\text{m}^3$ for the measured values. Although this difference is small, it results in different soil moisture estimates depending upon the relationship used. This is explained simply by the different equations defining the trend lines that fit the curves. Because the shape of the relationships, as well as the magnitude of the values were very similar, the discrepancy was accounted for by shifting the Campbell model by a moisture content of $0.03 \text{ m}^3/\text{m}^3$, as can be seen in figure 7.4.3b.

Figure 7.4.3e and 7.4.3f present estimated soil moisture values against observed values. It is clear in figure 7.4.3f, in which soil moistures are presented for a non-irrigated plot, that the estimated values seem more moderate than the observed values of soil moisture. This is because they come from the model domain representing depths of 5 to 15 centimeters. The observed moisture contents come from soil moisture sensors covering only the top 5 centimeters of soil closest to the surface. At greater depths there is much less variability in water content than there is near the surface.

In figure 7.4.3f, which provides moisture results in a non-irrigated plot of tef, the peaks in soil moisture that occur due to irrigation result in diffusivity values above the allowable range, and are thus unusable soil moisture estimates. However, in figure 7.4.3e, which provides moisture results for an irrigated prairie sandreed plot, it appears as though there is a lag in soil moisture peaks between the observed and modeled results. Estimated soil moistures reach maximum values a few hours prior to the maximum value in observed soil moisture near the surface. However, in reality the irrigation events and coinciding peaks in observed soil moisture again result in unusable soil moisture estimates. The peaks that are present in the estimated soil moisture results are actually caused by the low values of thermal diffusivity that occur directly before each of the irrigation events. If any lag were to exist, one would think that the estimated soil moisture from greater depths would lag behind the observed near-surface soil moisture.

Figure 7.4.3d provides estimated soil moisture content within an alfalfa plot, along with the location of soil moisture measured from a soil core taken on September

10th. The following figures provide similar results for the location of other soil cores taken on the 10th.

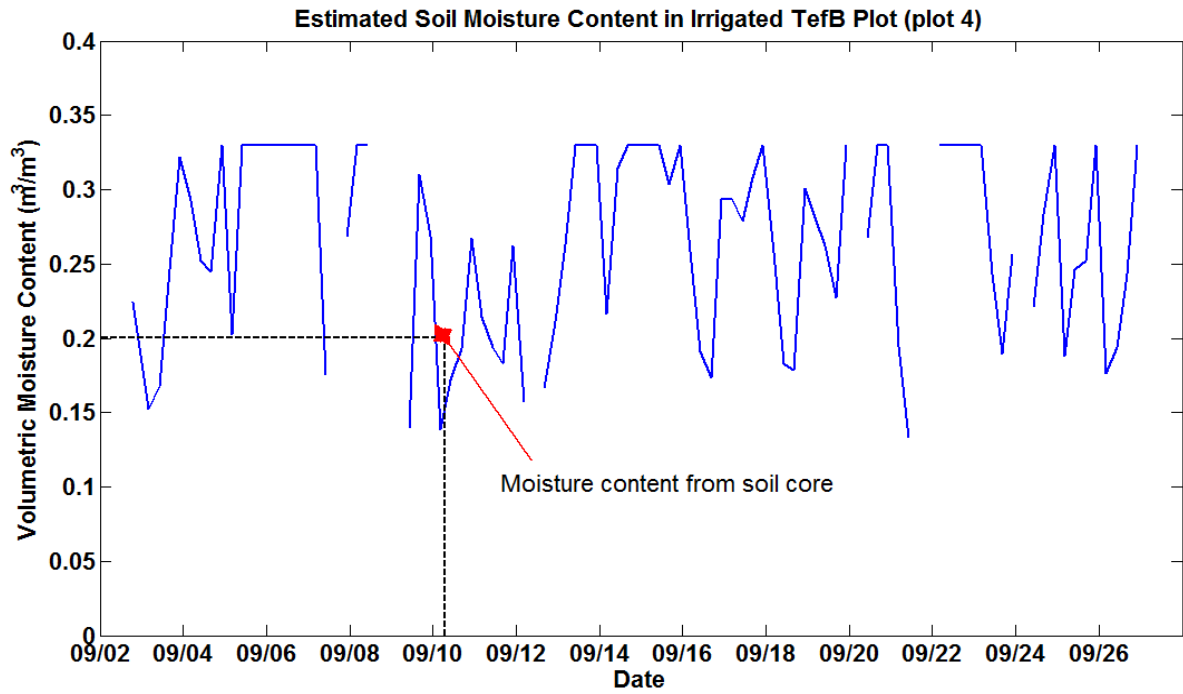


Figure 8.3.1a. Estimated soil moisture content in plot 4, an irrigated TefB plot. The red star denotes a moisture content measured via gravimetric method on September 10th.

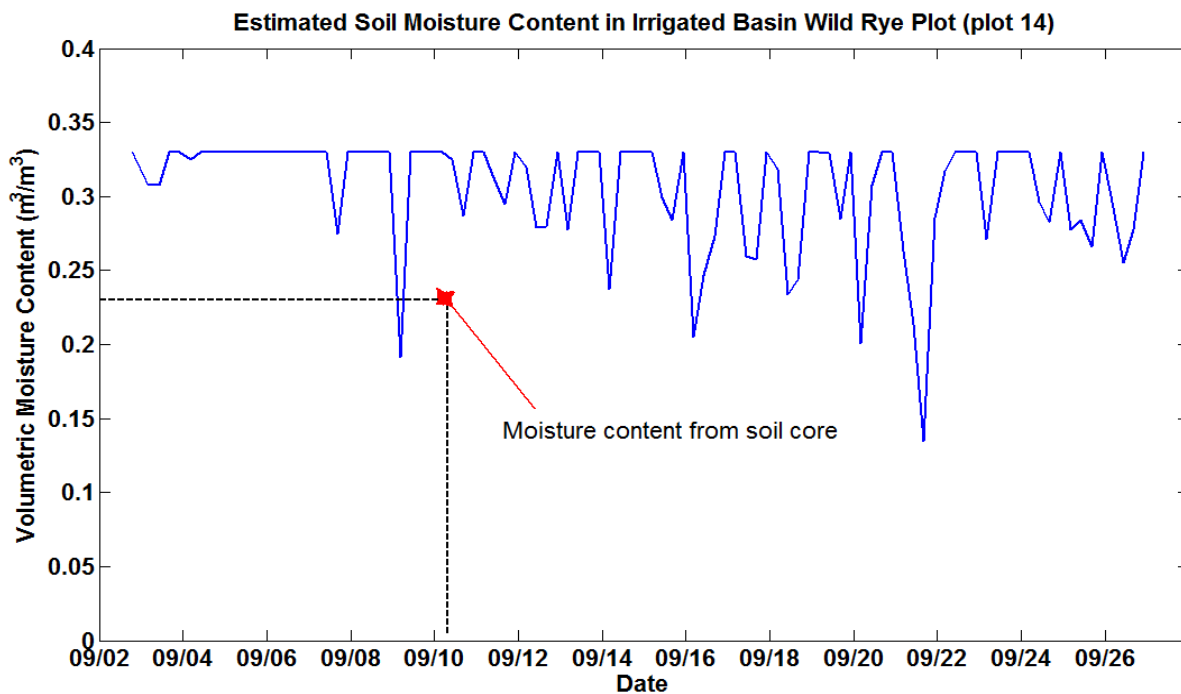


Figure 8.3.1b. Estimated soil moisture content in plot 14, an irrigated Basin Wild Rye plot. The red star denotes a moisture content measured via gravimetric method on September 10th.

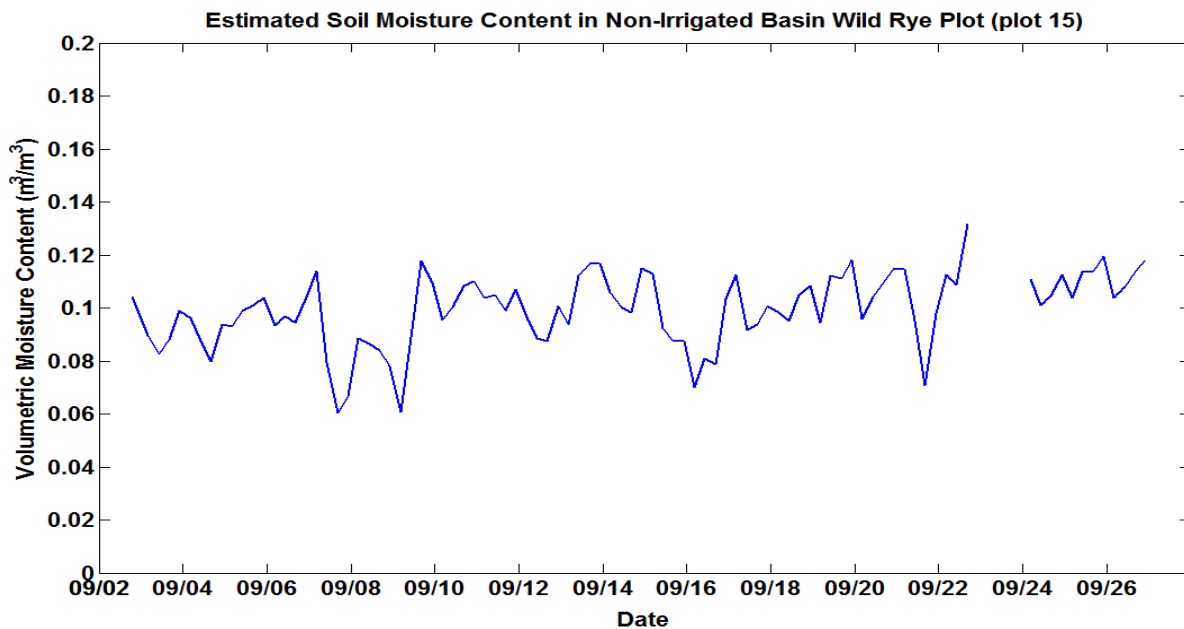


Figure 8.3.1c. Estimated soil moisture content in plot 15, a non-irrigated Basin Wild Rye plot. Note the difference in estimated moisture contents between this figure and figure 8.3.1b, an irrigated Basin Wild Rye plot.

The moisture contents determined via the gravimetric method from cores taken on September 10th match the estimated results fairly well. More soil cores collected during the study period would improve this comparison between modeled results and measured moisture contents through time. What is clearly seen is that the estimated soil moistures in irrigated plots are larger than those from non-irrigated plots. This in itself is valuable. Although the accuracy of these estimates cannot be determined, it can qualitatively be stated whether one location is wetter or drier than another location. However, one of the downsides to using this method to estimate soil moisture is that some prior knowledge in regards to the wetness of the soil is necessary. This is because one needs to know which side of the thermal conductivity – soil moisture curve to consider. Otherwise, the situation of non-uniqueness is encountered.

Figures 7.4.3e and 7.4.3f provide observed soil moisture measurements throughout the entire study in one location. From the irrigated plot, figure 7.4.3e, it is apparent that the estimated data can be used to tell when soil moisture increases rapidly and is at its greatest. In terms of accurately providing soil moisture contents throughout the study duration however, it seems as though the soil moisture results are much too noisy for this to be possible when on the wet side of the curve. Considering data from the non-irrigated plot, figure 7.4.3f, the results between modeled and observed moisture contents match fairly well. The observed soil moisture values range from very dry conditions ($0.02 \text{ m}^3/\text{m}^3$) to $0.18 \text{ m}^3/\text{m}^3$, while the estimated soil moisture contents stay fairly consistent at $0.12 \text{ m}^3/\text{m}^3$ throughout the 25-day period. As previously mentioned, the observed moisture contents are from the top few centimeters of the soil column, while

estimated values are from an average depth of 10 centimeters. One would expect the deeper moisture contents to be somewhere around the average of those from higher in the soil column, as well as being less noisy. This is exactly what is observed within this non-irrigated plot.

Wetter plots result in noisier data because the more moisture that is present in the soil, the more likely it is that conductive heat transport is accounting for less and less of the heat transfer that is taking place. The model used assumes that conduction is the primary mode of heat transfer. Therefore, in wetter soils when this conduction assumption is less valid, noisier results are being produced.

8.3.2 Estimated Soil Moisture on the Field Scale

Compiling the modeled soil moisture results from each location and presenting them through time yields figure 7.4.3g. This figure provides soil moisture estimates along the length of the cable through the entire 25-day study period. For ease of comparison, this figure is presented again, with the modeled results of thermal diffusivity presented directly before it.

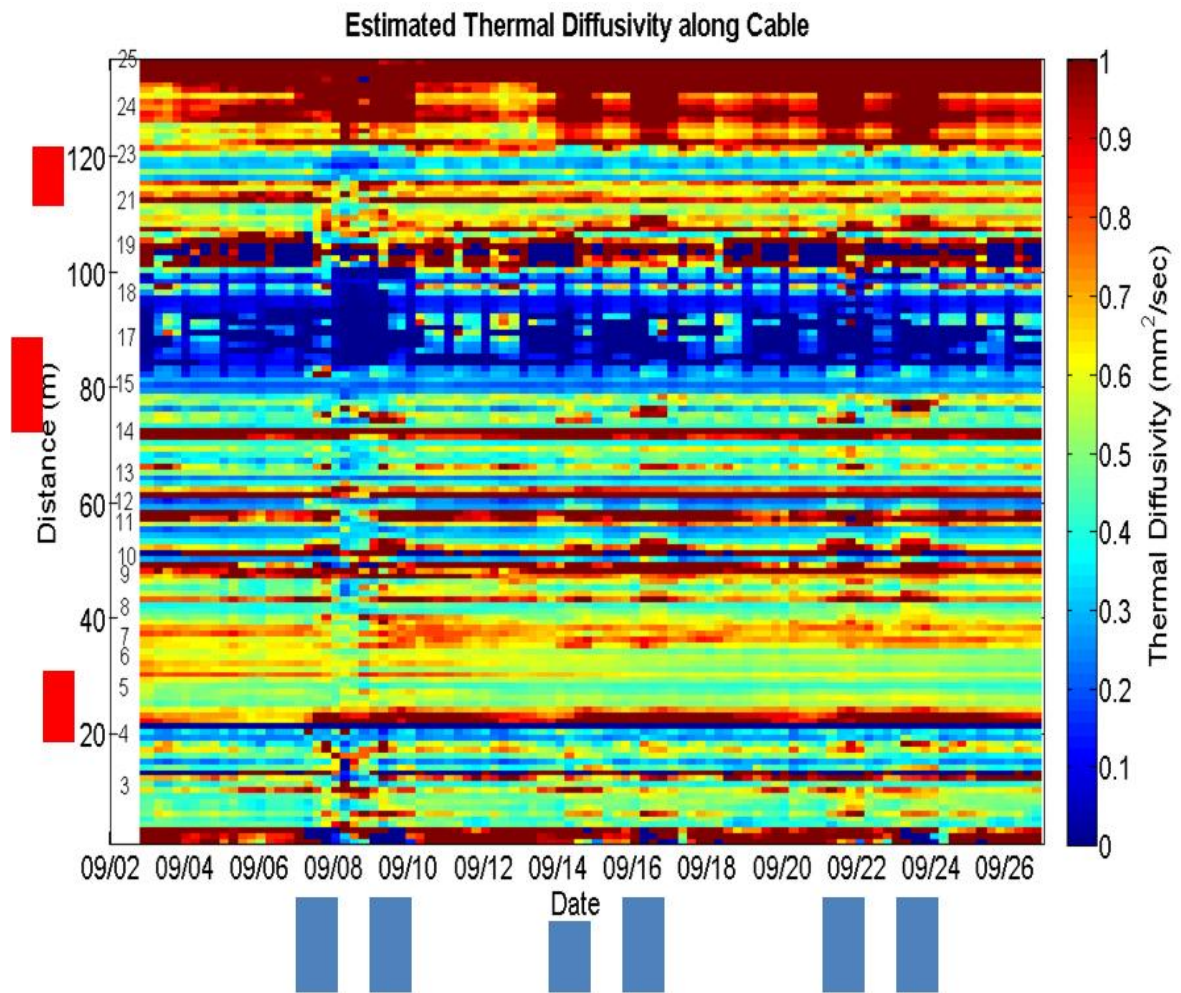


Figure 8.3.2a. Modeled results of thermal diffusivity through space and time.

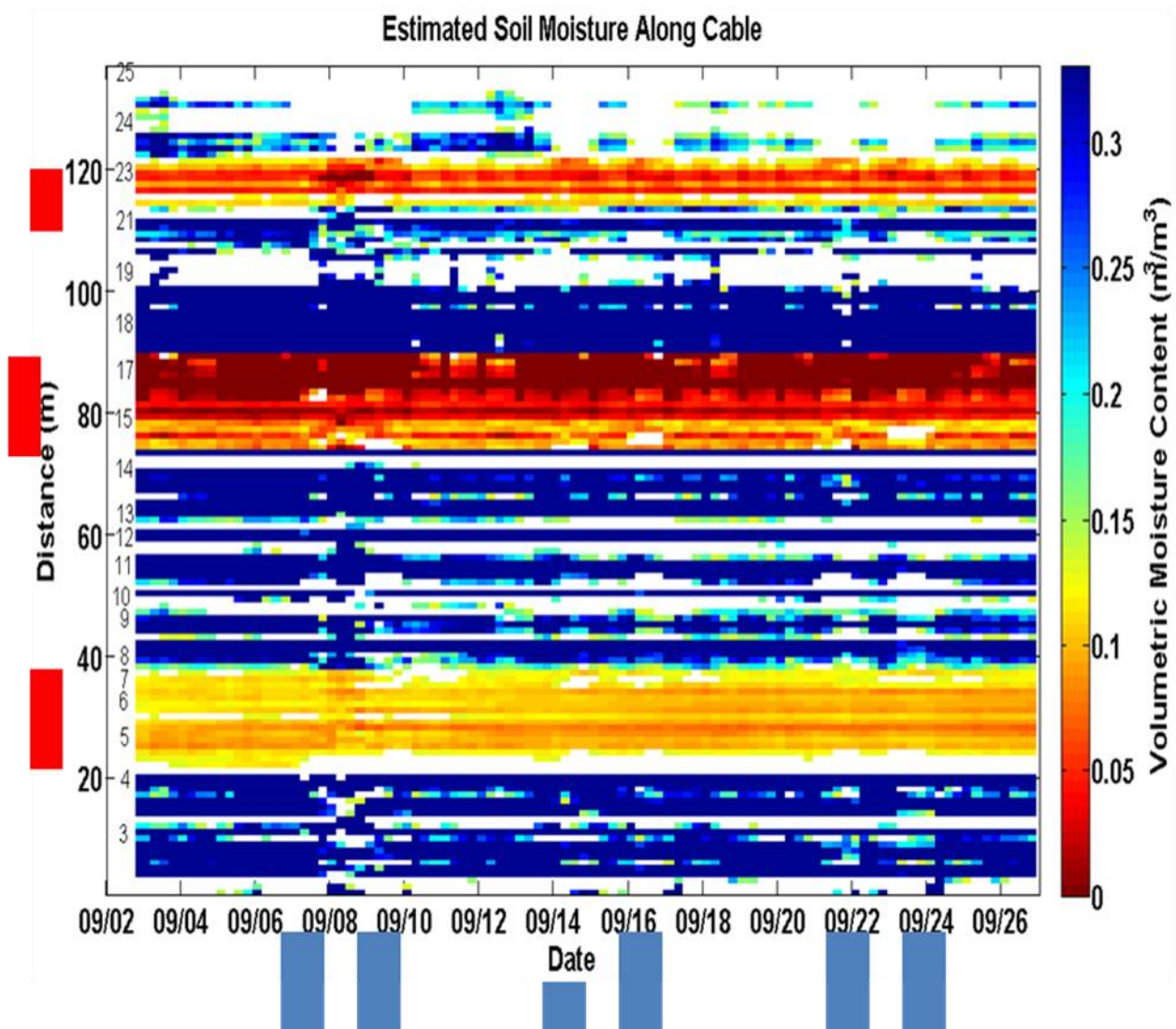


Figure 8.3.2b. Resulting spatial distribution of modeled soil moisture through space and time. Note that blue corresponds to higher values of water content.

Recall that the non-irrigated sections of the previous figure include meters 21 to 37, 74 to 89, and 114 to 121. It is very apparent that the estimated soil moisture in these non-irrigated areas is much lower than in the irrigated areas. Because it was known that these areas were non-irrigated, the equation for the dry side of the curve could be applied. Assuming one did not initially know if a soil was irrigated or non-irrigated, and therefore

applied equations from both sides of the curve, the following table presents the resulting estimated moisture contents for hypothetical thermal diffusivity values.

Moisture Estimates using Both Sides of Thermal Diffusivity – Soil Moisture Curve

D (mm ² /sec)	θ (m ³ /m ³) using “Dry Equation”	θ (m ³ /m ³) using “Wet Equation”
0.25	0.035	0.330
0.30	0.046	0.330
0.35	0.060	0.330
0.40	0.072	0.330
0.45	0.083	0.330
0.50	0.093	0.330
0.55	0.102	0.330
0.60	0.110	0.293
0.65	0.117	0.231
0.70	0.124	0.182
0.75	0.130	0.143
0.80	0.136	0.113
0.85	---	---

Table 8.5.2. Hypothetical thermal diffusivity values and corresponding soil moisture contents using the equations from both sides of the thermal diffusivity – soil moisture relationship. Above 0.80 mm²/sec, soil moisture estimates are not carried out.

Table 8.5.2 illustrates that it is indeed very critical to have prior knowledge as to whether the soil of interest is wet or dry. Given the same thermal diffusivity, resulting soil moisture estimates are very different depending on which side of the curve is used.

In addition, the previous table also serves to illustrate another large problem with this method as a whole. Under wet conditions (right side of the developed curves) thermal diffusivity is very insensitive to changes in moisture content. Soil moisture varies considerably over just a small change in thermal diffusivity in this wet range. This is evident when looking at the moisture results derived from the wet side of the curve (third column of the previous table). Soil moisture varies from 0.113 to 0.330 m^3/m^3 over a change in thermal diffusivity of only 0.25 mm^2/sec . This makes it very difficult to accurately predict soil moisture under wet conditions, since a slightly different modeled thermal diffusivity can produce very different soil moisture estimates.

An interesting aspect of this two-equation approach to estimating soil moisture is that it results in adjacent meters within the field having drastically different soil moisture contents. This occurs on the boundaries between irrigated plots and non-irrigated plots. In the field, these boundaries were not measured for soil moisture contents, but it is highly unlikely that there exists such a defined boundary where on one side the moisture content is 0.10 m^3/m^3 , and on the other side the moisture content is at saturation levels, as is seen in various locations in the modeled results.

It is worth reiterating that some prior knowledge in soil moisture conditions is absolutely necessary if estimates in soil moisture are to be completed. Because it was known which plots received irrigation and which did not, it was safe to apply a particular equation relating thermal diffusivity and soil moisture to those plots. Without knowing if a soil was relatively wet or dry, the non-uniqueness evident in the relationship between diffusivity and soil moisture would pose a much larger problem.

SECTION 9. CONCLUSIONS

9.1 CONCLUDING REMARKS and RECOMMENDATIONS

The use of distributed temperature sensing via fiber optic cables lends itself very well towards environmental monitoring in an agricultural setting. The soil type plays a very large role in determining how deep cables can actually be deployed, as 15 centimeters was very close to the maximum depth achievable in the rocky soils of this field site. The depths reached in this study served the purpose very well, as it is these shallow subsurface depths that are most important for overall crop production. This is especially true in arid environments, where irrigation is vital to crop growth, and the top 20 centimeters is where the most variability in soil moisture occurs.

A multi-cable deployment, such as the one used here, is necessary if one is to avoid as many problems with this technique as possible. For example, having 3 cables allows for leniency in the absolute depth of deployment. More important than absolute depth is the relative depth between each cable location. This is necessary for deployment within the ground because it is very difficult to obtain the same absolute depth during installation, especially given tough, rocky soils. Another benefit to the multi-cable setup is that it takes away the need for surface temperature measurements. If one cable is used, then another temperature measurement must be taken from somewhere in order to provide a temperature gradient for modeling purposes. Most often, this additional temperature measurement is taken from somewhere along the surface. Being able to avoid such surface measurements avoids many of the complex processes that occur at or

near the surface including surface turbulences due to vegetation and additional advective heat transport that occurs through evaporation. Trying to measure or predict heat or moisture variables in the shallow subsurface will always be very difficult due to the complex interactions between temperature, heat and water, and also the inherent heterogeneity that exists within soil. In addition, all of these variables are very temporally dependent. Multiple cables buried at depth at least allows for some minimization of these surface effects.

This study has shown that temperatures in the shallow subsurface can be very easily studied and analyzed under various conditions on the field scale and through time. As temperature plays a vital role in many crop growth processes, this is very important information for crop producers. Once installed, passive DTS allows for very easy measurement on scales very difficult to achieve using other methods.

A simplified model of heat transport assuming that conduction is the primary transfer process gains validity as the depth of the studied area increases. Again, this is because of the complex surface effects that result in other modes of heat transfer. Although it was shown that water input did not have an overwhelming effect on subsurface temperature signals, this would not necessarily hold true in more humid, wetter environments where more water is present in the soil system for longer durations of time. This study very effectively showed the high variability in thermal properties that exist on the field scale.

A model taking advective heat transport into account would greatly improve thermal diffusivity estimates in an irrigated, agricultural setting. Future studies would benefit greatly from inclusion of advective heat transport within the inversion model. Recall that when advection is included, the basic heat transport equation becomes

$$\frac{\partial T}{\partial t} = D(\theta) \frac{\partial^2 T}{\partial z^2} - v \frac{\partial T}{\partial z} , \quad \text{Equation 9.1.1}$$

where v is the average linear velocity of the moving water phase (cm/sec). To incorporate this term into the model, the linear velocity of incoming water (via irrigation) needs to be measurable through time. To determine the average linear velocity of water, v , within the pores, the water flux into the soil, q , must be divided by water content, θ :

$$v = q / \theta . \quad \text{Equation 9.1.2}$$

With detailed knowledge of irrigation events including the total volume of water applied, total duration of water applications, timing of applications, and the total area of the plots that were irrigated during each event, v could be roughly estimated through time.

Accurately estimating soil moisture based from soil thermal properties is difficult to achieve because of the many interrelated processes involved. A slight under or overestimate in thermal properties will result in a larger discrepancy in soil moisture estimation. Still, reasonable soil moisture estimates were achieved when compared to observed soil moisture values. The largest fault of this study is in the lack of more intensive soil moisture measurements during the study period. Safe assumptions regarding the accuracy of estimated soil moisture values can only be reasonably made

within the two plots which contained EC-5 soil moisture sensors for the entire study period. It is safe to assume that passive DTS can successfully be used to determine if a soil location is wetter or drier compared to another location. It also seems evident that soil moisture estimation is much more accurate in dry conditions, with much noisier data being produced in wet soil. Given the results achieved here, it would be difficult to rely on the actual estimated soil moisture content provided for a particular location of interest.

In all, passive DTS lends itself very well and is useful for the analysis of soil temperature over space and time. Once installed, this method provides temperature data across these scales much easier than do other existing methods. Estimated soil thermal properties can be used in conjunction with these temperature measurements to provide soil heat flux estimates through space and time. Passive DTS also shows changes in soil thermal properties as a result of corresponding soil moisture levels. However, at this point, accurate quantitative estimates of soil moisture on the field scale cannot be made utilizing passive DTS as it was for this study.

9.2 FUTURE STUDY

This study has shown great promise towards using passive DTS technology to estimate thermal properties and soil moisture on a spatial and temporal scale. However, the complexity associated with cables buried underneath a patchwork of various crop types receiving varying degrees of irrigation makes the full potential of this method difficult to achieve. A simpler experimental setup should be created to refine the associated heat transfer modeling and soil moisture estimation using fiber optic cables.

Once the method is closer to being perfected, then it could be reapplied to real-world situations such as in the agricultural field used in this study.

If another attempt was made at using passive DTS as a standalone technology to estimate soil moisture through space and time, a very useful and invaluable experiment would be to excavate a ditch many meters in length. The ditch should then be entirely filled with a uniform sand of known properties. A multi-cable installation can then be easily achieved, and both relative and absolute depths of the buried cables known with certainty. At the same depth as the buried cables, soil moisture sensors should be installed throughout the length of the ditch, as close together as logistically possible. By directly applying controlled volumes of water to precise areas of the cable, the effect of irrigation could also be studied.

This setup would greatly enhance the ability to effectively model and estimate thermal properties and soil moisture in the subsurface. It would allow for very complex natural processes to be simplified as much as possible, and for these processes to be effectively measured under controlled conditions. If accurate soil moisture estimation using passive DTS was not achievable under such conditions, then it could be stated with finality that the method alone simply does not provide the desired results. If successful and accurate moisture estimates were achieved, then the experiment could be once again conducted under more natural conditions, this time with much more knowledge and understanding of all processes involved.

However, it is this researcher's strong recommendation that future studies involving the use of passive DTS to estimate soil moisture be done in conjunction with other methods, specifically active DTS. The results obtained from preliminary active DTS experiments (such as Saydi *et al.*, 2009) show great promise in terms of obtaining reliable quantitative soil moisture estimates. Because the active method requires an active source of energy, it can only be completed at discrete time intervals. Soil moisture estimates can be obtained during these active measurements, and then passive DTS can be used when the active measurements are not being taken. Passive DTS would effectively serve to temporally connect the discrete moisture measurements obtained during each active heat pulse. In addition, this would tend towards more accurate soil moisture estimates via the passive method, since the preceding active measurements would serve to initially locate the soil upon the thermal conductivity – soil moisture relationship curve.

A combined passive and active DTS method is already underway near Marena, Oklahoma, at an in situ sensor testbed for current and emerging soil moisture technologies. This is part of a SMAP (Soil Moisture Active Passive) test validation site which is in coordination with the NASA Terrestrial Hydrology Program, USDA-ARS, and Oklahoma State University. Initial installment and data processing of this DTS experiment was and is conducted by Susan Steele-Dunne and Christine Hatch.

SECTION 10. REFERENCES

- Al-Kayssi, A.W., A.A. Al-Karaghoul, A.M. Hasson, and S.A. Beker, (1990). Influence of Soil Moisture Content on Soil Temperature and Heat Storage under Greenhouse Conditions, *Journal of Engineering Agricultural Resources*, 45, 45:241-252.
- Arya, S.P. (2001). *Introduction to Micrometeorology*. Second Edition. International Geophysics Series, vol. 79, Academic Press, San Diego, California.
- Assouline, S., K. Narkis, S.W. Tyler, I. Lunati, M.B. Parlange, and J.S. Selkerm (2010). On the diurnal soil water content dynamics during evaporation using dielectric methods, *Vadose Zone Journal*, 9, doi:10.2136/vzj2009.0109.
- ASTM (1987). Standard test methods for moisture, ash, and organic matter of peat and other organic soils. American Society for Testing and Materials D 2974.
- Behaegel, M., P. Sailhac, and G. Marquis (2007). On the use of surface and ground temperature data to recover soil water content information, *Journal of Applied Geophysics*, 62, doi:10.1016/j.jappgeo.2006.11.005.
- Bogena, H.R., J.A. Huisman, C. Oberdorster, and H. Vereecken (2007). Evaluation of a low-cost soil water content sensor for wireless network applications, *Journal of Hydrology*, 344, doi:10.1016/j.jhydrol.2007.06.032.
- Bradford, J.H. (2008). Measuring water content heterogeneity using multifold GPR with reflection tomography, *Vadose Zone Journal*, 7, 7:184-193.
- Cahill, A.T and M.B. Parlange (1998), On water vapor transport in field soils, *Water Resources Research*, 34, 34:4:731-739.
- Campbell, G.S. (1985), *Developments in Soil Science 14: Soil Physics with BASIC Transport Models for Soil – Plant Systems*. Elsevier. Amsterdam.
- Chung, S.O. and R. Horton (1987). Soil heat and water flow with a partial surface mulch, *Water Resources Research*, 23, doi:10.1029/WR023i012p02175.
- Daily, W., A. Ramirez, D. LaBrecque, and J. Nitao (1992). Electrical resistivity tomography of vadose water movement, *Water Resources Research*, 28, 28:1429-1422.
- Decagon Devices (2008). KD2 Pro Thermal Properties Analyzer, Operator's Manual, Version 10, Pullman, Washington.

- Desilets, D., M. Zreda, and T.P.A Ferre (2010), Nature's neutron probe: Land surface hydrology at an elusive scale with cosmic rays, *Water Resources Research*, 46, doi:10.1029/2009WR008726.
- deVries, D.A. (1952), A nonstationary method for determining thermal conductivity of soil in situ, *Soil Science*, 73, 73:83-89.
- deVries, D.A. (1963), Thermal properties of soils, *Physics of Plant Environment*, North Holland Publishing Co., Amsterdam.
- deVries, D.A. and J.R. Philip (1986), Soil heat flux, thermal conductivity, and null-alignment method, *Soil Science Society of America Journal*, 50, 50:12-18.
- Engman, E.T. and N. Chauhan (1995). Status of microwave soil moisture measurements with remote sensing, *Remote Sensing Environment*, 51, 51:189-198.
- Evelt, S.R. (2003), Soil water measurement by neutron thermalization, *Encyclopedia of Water Sciences*, pp 889-893, Marcel Dekker, Inc., New York.
- Evelt, S.R., and G.W. Parkin (2005), Advances in soil water content sensing: the continuing maturation of technology and theory, *Vadose Zone Journal*, 4, doi:10.2136/vzj2005.0099.
- Glinksi, J. and J. Lipiec (1990). *Soil physical conditions and plant roots*. CRC Press, Boca Raton, Florida.
- Greenwood, D.J., K. Zhang, H.W. Hilton, and A.J. Thompson (2009), Opportunities for improving irrigation efficiency with quantitative models, soil water sensors and wireless technology, *Journal of Agricultural Science*, 148, doi:10.1017/S0021859609990487.
- Hausner, M.B (2010), Estimating in situ integrated soil moisture content using fiber-optic distributed temperature sensing (DTS) measurements in the field, M. Sc. Thesis, University of Nevada, Reno, 124 pp.
- Heitman, J.L., J.M. Basinger, G.J. Kluitenberg, J.M. Ham, J.M. Frank, and P.L. Barnes (2003). Field evaluation of the dual-probe heat-pulse method for measuring soil water content, *Vadose Zone Journal*, 2, 2:552-560.
- Heitman, J.L., R. Horton, T.J. Sauer and T.M. DeSutter (2008), Sensible heat observations reveal soil-water evaporation dynamics, *Journal of Hydrometeorology*, doi:10.1175/2007JHM.

- Hillel, D (2004). *Introduction to Environmental Soil Physics*. Academic Press, San Diego, California.
- Hoes, O.A.C., R.P.S. Schilperoort, W.M.J. Luxemburg, F.H.L.R. Clemens, and N.C. van de Giesen (2009), Locating illicit connections in storm water sewers using fiber-optic distributed temperature sensing, *Water Research*, 43, doi:10.1016/j.watres.2009.08.020.
- Horai, Ki-iti and G. Simmons (1969), Thermal conductivity of rock-forming minerals, *Earth and Planetary Science Letters*, 6, 6:359-368.
- Jackson, T.J. (1993). Measuring surface soil moisture using passive micromave remote sensing, *Hydrological Processes*, 7, 7:139-152.
- Jackson, T.J., J. Schmugge, and E.T. Engman (1996). Remote sensing applications to hydrology: soil moisture, *Hydrological Sciences Journal*, 41.
- Johansen, O. (1977). Thermal conductivities of soils. Ph.D thesis. University of Trondheim, Norway. Draft translation. U.S. Army Corp of Engineers. Hanover, New Hampshire.
- Jury, W.A., and R. Horton (2004), *Soil Physics (6th Edition)*. John Wiley & Sons, Inc., Hoboken, New Jersey.
- Kachanoski, R.G., E.G. Gregorich, and I.J. van Wesenbeek (1988). Estimating spatial variations of soil water content using noncontacting electromagnetic inductive methods, *Canadian Journal of Soil Science*, 68, 68:715-722.
- Kaiphone Technology Company (2012).
[http://www.flexibletube.com/en/2_2333/manufacture/
 Armored_Fiber_Optic_Patch_Cord_id55087.html](http://www.flexibletube.com/en/2_2333/manufacture/Armored_Fiber_Optic_Patch_Cord_id55087.html).
- Kizito, F., C.S. Campbell, G.S. Campbell, D.R. Cobos, B.L. Teare, B. Carter, and J.W. Hopmans (2008), Frequency, electrical conductivity and temperature analysis of a low-cost capacitance soil moisture sensor, *Journal of Hydrology*, 352, doi:10.1016/j.jhydrol.2008.01.021.
- Knight, H.J., W. Jin, and G.J. Kluitenberg (2007). Sensitivity of the dual-probe heat-pulse method to spatial variations in heat capacity and water content, *Vadose Zone Journal*, 6, doi:10.2136/vzj2006.0170.
- Ledieu, J., P. de Ridder, P. de Clerck, and S. Dautrebande (1986), A method of measuring soil moisture by time-domain reflectometry, *Journal of Hydrology*, 88.

- Lu, N., G.H. Ristow, and W.J. Likos (2000), The accuracy of hydrometer analysis for fine-grained clay particles, *Geotechnical Testing Journal*, 23, 23:487-495.
- Mayocchi, C.L. and K.L. Bristow (1995), Soil surface heat flux: some general comments and questions on measurements, *Agricultural and Forest Meteorology*, 75, 75:43-50.
- Michot, D., Y. Benderitter, A. Dorigny, B. Nicoullaud, D. King, and A. Tabbagh (2003), Spatial and temporal monitoring of soil water content with an irrigated corn crop cover using surface electrical resistivity tomography, *Water Resources Research*, 39, doi:10.1029/2002WR001581.
- Miller, W.W., E.M. Carroll-Moore, E. Leger, J. Davison, S.W. Tyler, M. Hausner, P.S.J. Verburg, Z. Johnson, R.G. Qualls, G. Wilson, and K.L. Dean (2010). Project C: Plant, Water, and Soil Interactions. Walker Report. Walker Basin Project. Nevada.
- Mills, A.F. (1999). *Heat Transfer*, pp 221-222. Prentice Hall. New Jersey.
- Mohanty, B.P., W.M. Klittich, R. Horton, and M.T. van Genuchten (1995), Spatio-temporal variability of soil temperature within three land areas exposed to different tillage systems, *Soil Science Society of America Journal*, 59, 59:752-759.
- Mori, Y., J.W. Hopmans, A.P. Mortenson, and G.J. Kluitenberg (2003), Multi-functional heat pulse probe for the simultaneous measurement of soil water content, solute concentration, and heat transport parameters, *Vadose Zone Journal*, 2, 2:561-571.
- Mori, Y., J.W. Hopmans, A.P. Mortenson, and G.J. Kluitenberg (2005), Estimation of vadose zone water flux from multi-functional heat pulse probe measurements, *Soil Science Society of American Journal*, 69, doi:10.2136/sssaj2004.0174.
- Parlange, M.B., A.T. Cahill, D.R. Nielsen, J.W. Hopmans, and O. Wendroth (1998), Review of heat and water movement in field soils, *Soil and Tillage Research*, 47, 47:5-10.
- Pregitzer, K.S. and J.S. King (2005). Effects of soil temperature on nutrient uptake, *Ecological Studies*, 181. Springer-Verlag, Berlin.
- Rawls, W.J., D.L. Brakensiek, and K.E. Saxton (1982), Estimation of Soil Water Properties, *Transactions of the American Society of Agricultural Engineers*, 21, 21:1316-1320.

- Ren, T., Z. Ju, Y. Gong, and R. Horton (2003). Development of thermo-time domain reflectometry for vadose zone measurements, *Vadose Zone Journal*, 2, doi: 10.2136/vzj2003.5440.
- Reynolds, S.G. (1970), The gravimetric method of soil moisture determination, a study of equipment and methodological problems, *Journal of Hydrology*, 11.
- Robinson, D.A., C.S. Campbell, J.W. Hopmans, B.K. Hornbuckle, S.B. Jones, R. Knight, F. Ogden, J. Selker, and O. Wendroth (2008), Soil moisture measurement for ecological and hydrological watershed-scale observatories: a review, *Vadose Zone Journal*, 7, doi:10.2136/vzj2007.0143.
- Robinson, D.A., S.B. Jones, J.M. Wraith, D. Or, and S.P. Friedman (2003), A review of advances in dielectric and electrical conductivity measurement in soils using time domain reflectometry, *Vadose Zone Journal*, 2, doi:10.2136/vzj2003.4440.
- Roth, T.R., M.C. Westhoff, H. Huwald, J.A. Huff, J.F. Rubin, G. Barrenetxea, M. Vetterli, A. Parriaux, J.S. Selker, and M.B. Parlange (2010), Stream temperature response to three vegetation scenarios by use of a distributed temperature validated model, *Environmental Science Technology*, 44, 44:2072-2078.
- Sayde, C., C. Gregory, M.G. Rodriguez, N. Tufillaro, S. Tyler, N. van de Giesen, M. English, R. Cuenca, and J.S. Selker (2009), Feasibility of soil moisture monitoring with heated fiber optics, *Water Resources Research*, 46, W06201, doi:10.1029/2009wr007846.
- Scanlon, B.R., J.G. Paine, and R.S. Goldsmith (1999), Evaluation of Electromagnetic Induction as a Reconnaissance Technique to Characterize Unsaturated Flow in an Arid Setting, *Ground Water*, 37, doi:10.1111/j.1745-6584.
- Selker, J.S., L. Thevenaz, H. Huwald, A. Mallet, W. Luxemburg, N. van de Giesen, M. Stejskal, J. Zeman, M. Westhoff and M.B. Parlange (2006), Distributed fiber-optic temperature sensing for hydrologic systems, *Water Resources Research*, 42, W12202.
- Singha, K., F. D. Day-Lewis, and S. Moysey (2007), Accounting for tomographic resolution in estimating hydrologic properties from geophysical data, *Geophysical Monograph Series 171*, American Geophysical Union, 10.1029/171GM16.
- Steele-Dunne, S.C., M.M. Rutten, D.M. Krzeminska, M. Hausner, S.W. Tyler, J.S. Selker, T.A. Bogaard, and N.C. van de Giesen (2009), Feasibility of soil moisture estimation using passive distributed temperature sensing, *Water Resources Research*, 46, W03534, doi:10.1029/2009WR008272.2009.

- Sun, Ne-Zheng (1994). *Inverse Problems in Groundwater Modeling*. Kluwer Academic Publishers, Dordrecht, The Netherlands.
- Topp, G.C., J.L. Davis, and A.P. Annan (1980), Electromagnetic determination of soil water content: measurements in coaxial transmission lines, *Water Resource Research*, 16, 16:574-582.
- Tyler, S.W., J.S. Selker, M.B. Hausner, C.E. Hatch, T. Torgerson, C.E. Thodal, and S.G. Schladow (2009), Environmental temperature sensing using Raman spectra DTS fiber-optic methods, *Water Resources Research*, 45, W00d23, doi:10.1029/2008WR007052.
- Tyler, S.W., S.A. Burak, J.P. McNamara, A. Lamontagne, J.S. Selker, and J. Dozier (2008), Spatially distributed temperatures at the base of two mountain snowpacks measured with fiber-optic sensors, *Journal of Glaciology*, 54.
- Waite W.F., L.Y. Gilbert, W.J. Winters, and D.H. Mason (2006), Estimating thermal diffusivity and specific heat from needle probe thermal conductivity data. *Review of Scientific Instruments*, 77.
- Walker, J.P., G.R. Willgoose, and J.D. Kalma (2004), In situ measurement of soil moisture: a comparison of techniques, *Journal of Hydrology*, 293, doi:10.1016/j.jhydrol.2004.01.008.
- Weast, R.C. (1986). *CRC Handbook of Chemistry and Physics 67th edition*. CRC Press, Boca Raton, Florida.
- Westhoff, M.C., H.H.G. Savenije, W.M.J. Luxemburg, G.S. Stelling, N.C. van de Giesen, J.S. Selker, L. Pfister, and S. Uhlenbrook (2007). A distributed stream temperature model using high resolution temperature observations, *Hydrological Earth Systems Sciences*, 11, 11:1469-1480.
- Young, M.H., G.S. Campbell, and J. Yin (2008). Correcting dual-probe heat-pulse readings for changes in ambient temperature, *Vadose Zone Journal*, 7, doi:10.2136/vzj2007.0015.
- Zhou, Q.Y., J. Shimada, and A. Sato (2001). Three dimensional spatial and temporal monitoring of soil water content using electrical resistivity tomography, *Water Resources Research*, 37, 37:273-285.
- Zreda, M., D. Desilets, T.P.A. Ferre, and R.L. Scott (2008), Measuring soil moisture content non-invasively at intermediate spatial scale using cosmic-ray neutrons, *Geophysical Research Letters*, 35, doi:10.1029/2008GL035655.